Advances in Colloid and Interface Science 344 (2025) 103601

Contents lists available at ScienceDirect

Advances in Colloid and Interface Science

journal homepage: www.elsevier.com/locate/cis

# Droplet microfluidics, colloidal assembly and nanoscale processing: Synergistic control and properties of colloid-based photonic microobjects

Yuandu Hu [a,b,c,*], Arezoo Ardekani [d], Jintao Zhu [e,*], Yajiang Yang [e], Juan Pérez-Mercader [f]

[a] Department of Materials Science and Engineering, School of Physics Science and Engineering, Beijing Jiaotong University, Beijing 100044, China
[b] Guangdong Provincial Key Laboratory of Technique and Equipment for Macromolecular Advanced Manufacturing, South China University of Technology, Guangzhou 510641, China
[c] Key Laboratory of Advanced Materials of Ministry of Education, Department of Chemical Engineering, Tsinghua University, Beijing 100084, China
[d] Key Laboratory of Materials Chemistry for Energy Conversion and Storage (HUST) of Ministry of Education School of Chemistry and Chemical Engineering, Huazhong University of Science and Technology (HUST), Wuhan 430074, China
[e] Department of Mathematics, School of Mechanical Engineering, Purdue University, 585 Purdue Mall, West Lafayette, IN 47907-2088, United States
[f] Department of Earth and Planetary Sciences, and Origins of Life Initiative, Harvard University, Cambridge, MA 02138, United States

ARTICLE INFO

*Keywords:*
Photonic microobjects
Microfluidics
Colloidal building blocks
Post-processing strategies
Diverse microstructures
Photonic performances

ABSTRACT

Colloidal photonic crystals have drawn wide attention in a number of realms due to their manyapplications. Photonic microobjects can be processed by a combination of droplet-based microfluidics and the subsequent different post-processing approaches in a precisely controlled manner in terms of compositions, geometries, and functionalities, offering a wide range of properties for the resulting products. In this review, we provide a summary of colloidal-based photonic microobjects that have evolved from droplets produced by microfluidic devices with different configurations and designs. The colloidal building blocks can be either inert or responsive to external stimuli, which impart the colloidal photonic microobjects with tunable properties. By leveraging a number of post-processing strategies, including evaporation of solvents from the droplet templates, external field-guided assembly, selective sputter coating, controlled etching, osmosis regulating, etc., the obtained photonic microobjects eventually possessed diverse microstructures with different fashions, featuring the photonic microobjects with demanded photonic performances in sub-microscale or can be further organized for bulk applications. Finally, we analyze the challenges and present outlooks on future development trends regarding the construction of colloid-based photonic microobjects, including current issues, critical needs, and promising emerging photonic applications. Also, we propose some emerging scientific questions and engineering limitations may be worthy of exploration based on the combination of microfluidics processing, colloidal assembly, and post-treatments.

## 1. Introduction

Photonic crystals are periodic nanostructures that can affect and manipulate photons' behaviors in a similar fashion to how semiconductors could precisely tune the behaviors of electrons [1]. Photonic phenomena can be traced back to a long story. In 1887, Lord Rayleigh studied a type of one -dimensional photonic crystal and predicted the existence of high reflectivity of light of a specific wavelength range, which later became known as a stopband [2]. In the 1960s, Luck and Hiltner et al. respectively reported ordered structures from uniform-sized latex showing refraction phenomena and studied their refraction properties [3,4]. In 1979, Clark and Hurd et al. reported the crystals' formation and destruction of single colloidal crystal structures under external fields (such as shearing force, etc.) [5]. A few years later, the concept of photonic crystal was formally brought up by Yablonovitch and John et al. when they extended the study to solid ordered three-dimensional photonic structure [1,6]. Since then, research articles about the construction of photonic structures with diverse applications have exponentially increased [7–14].

Due to their wide applications in a number of realms, such as photonic computers, sensing, biomimetics, diagnosis, novel pigments, and optical/electron devices, etc., photonic structures have attracted a large

* Corresponding authors at: Department of Materials Science and Engineering, School of Physics Science and Engineering, Beijing Jiaotong University, Beijing 100044, China.
*E-mail addresses:* huyd@bjtu.edu.cn (Y. Hu), jtzhu@mail.hust.edu.cn (J. Zhu).

https://doi.org/10.1016/j.cis.2025.103601
Received in revised form 14 May 2025;
Available online 17 July 2025

amount of research attention [7,9,10,15–25]. In general, the construction of photonic crystal structures was mainly realized through two routes: one is the so-called top-down method, which can create periodic nanostructures on substrates coated with photoresists using precise processing tools and techniques, such as e-beam, nano imprint lithography, electrochemical etching, and film deposition [15,26,27]. This approach normally has some drawbacks, such as requiring expensive instruments and skillful instrument operators, or it can only construct limited duplicated layers [28]; another is the bottom-up approach, namely, the periodic ordered structures of photonic crystals were obtained through the self-assembly of amphiphilic block copolymers, colloids, and cholesteric liquid crystals (CLCs) [28–39]. Compared to the top-down approach, photonic structures formed from the bottom-up assembly are much more facile to achieve and considerably less expensive, making it much more affordable for an ordinary laboratory [40]. In terms of the building blocks for self-assembly, photonic crystal from self-assembly of block copolymers requires the formation of microdomains of block copolymers with enough repeating units to form microdomains with thickness up to 100 nm. Despite the fact that the self-assembly of ultrahigh-molecular-weight block copolymers can be beneficial for generating sophisticated engineering of crystal lattices and resulting in better control for photonic waves, e.g., topologically protected photon propagation including Weyl photonic crystals, it requires block copolymers with precision architectures and high molecular weight, which in turn makes it difficult to be self-assembled into ordered structures due to the increased viscosity of the polymer melts or polymer solution. As a result, this would significantly extend the annealing cycle [12,41–43]. Moreover, the synthesis of such amphiphilic block copolymers with precise structures is much more complicated than that of the synthesis of colloidal particles (CPs) [29,35,36,44]. Despite homopolymer-based microobjects also displaying structural colors even though they don't have any periodic nanostructures, it requires the microobjects with curved interfaces to leverage the synergistic effect of total internal reflection and optical interference [45–48]. Although photonic microobjects formed from the assembly of cholesteric liquid crystals (CLCs) have also been reported, the color saturations of these photonic microobjects remain to be improved [49,50]. Therefore, owing to their facile designable merits and convenient synthesis process, different colloids have been the most widely and intensively investigated building blocks for the construction of photonic structures via the self-assembly approach [9,10,28,34,51–62]. Since the end of last decade, there has been an enormous amount of research papers focusing on the fundamental theories and experimental characterizations of photonic structures formed from colloidal self-assembly [10,16,63–69]. In terms of the 'hardness' of colloidal building blocks for the construction of photonic structures, there are generally two categories of CPs employed: one is the nondeformable 'rigid' CPs under normal conditions, such as monodispersed $SiO_2$, metallic oxide colloids (i.e., $TiO_2$, $\gamma$-$Fe_2O_3$, $Fe_3O_4$, or the relevant compound colloids), metallic colloids (such as Au) with high refractive index, polymer colloids (i.e., polystyrene (PS), poly(methyl acrylate) (PMMA), ligin colloids, or polymer-based high refractive index colloids, such as fluorinated polymethacrylate poly(1H,1H-heptafluorobutyl methacrylate) (PFBMA)) [9,16,69–81]. For example, Pusey and Megen reported the phase behaviors of 'hard' or 'near hard' colloidal suspensions and studied the phase behaviors of the relationship between the states of fluid, crystal, and glassy and the concentrations of CPs [82,83]; the other is the deformable 'soft' colloids, such as thermoresponsive poly(N-isopropyl acrylamide) (pNIPAAm)-based or poly(ethylene glycol) (PEG) and the derivatives-based gel particles, or colloids with partial deformability under ordinary conditions (i.e., room temperature), such as PS-pNIPAAm or Au-pNIPAAm core-shell CPs with a rigid core [84–88]. In particular, photonic structures based on soft colloids have gained wide attention [10,89–94]. Despite numerous articles about the construction of bulk photonic structures through diverse conventional methods that have been reported, colloid-based photonic microobjects are also significantly impacting this field [95–99]. Various methods have been used to manufacture photonic microobjects, among which producing colloid-based photonic microobjects through microfluidics in a precise manner is crucially important in many fields [72,95,97,98,100–108]. However, a systematicreview regarding the construction and tuning of the properties and shapes of photonic microobjects is still missing. In light of this, this review is particularly focused on the construction, shaping, and tuning of colloid-based photonic microobjects through droplet-based microfluidics, given that this technique allows researchers to control the resultant photonic microobjects in a precise and on-demand fashion [109–112]. In this review, we summarize the development of colloidal photonic microobjects that are shaped and regulated by a combination of droplet-based microfluidics and a variety of other approaches, specifically elaborating on the advances in the aspects of photonic microspheres with isotropic properties, spherical photonic microobjects with anisotropic photonic properties, structurally anisotropic photonic microobjects, microcapsules, and fully inverse opal microparticles. In addition, future research directions about microfluidics-assisted preparation of colloid-based photonic microobjects and the relevant scientific questions regarding the structural and property regulation of these microobjects are also discussed.

As a powerful tool, microfluidics has been comprehensively developed in the past two decades and can be used to precisely handle very tiny amounts of liquid ($10^{-9}$–$10^{-18}$ L) to construct microobjects with different kinds of structures and functionalities [113–117]. Droplet microfluidics and the corresponding microobjects can lead to the resulting microobjects with very narrow size distributions (coefficient of variation (C.V.) $< 5$ %), facile tunable size, and precisely controllable droplet structure [115,116,118–121]. This technique typically allows researchers to produce photonic microobjects with sizes ranging from a few ($> 2$) microns to hundreds of microns depending on several factors, including the types of building blocks used, the formation mechanisms, and also the flow rates of different phases used [122–124]. This technique could also impart the microobjects with unique advantages in terms of conducting research from a statistical point of view [125]. In the past two decades, the preparation of photonic microobjects by combining microfluidic techniques and colloidal assembly has attracted intensive research attention [126–129]. Since the preparation of colloidal photonic structures using a co-flow microfluidic chip was firstly reported by Yang's group, droplet microfluidics has been widely used for the construction, shaping, and assisted regulating of colloidal photonic microstructures and their relevant properties [125,130]. A number of research groups, including Yang and Kim, Weitz, Kanai, Gu, Zhao, Chen, Zhu et al., all have respectively made considerable contributions in the realms of design and generation of photonic microstructures based on microfluidic platforms [109,110,131–133]. Regarding the packing densities of the CPs, there are two types of photonic structures: close-packed and non-close-packed colloidal photonic structures. The close-packed opal structure from monodispersed spherical CPs has been the most intensively studied architecture due to the fact that it is the simplest form of colloidal crystal [134,135]. So, we start our discussion with the opal-structured photonic microspheres in this review and roll out the summary of photonic microobjects in diverse forms. However, one common point of these photonic microobjects is that all of them involve the utilization of a microfluidics platform in the construction steps. We then elaborate on our discussions from the point of view of the colloid-based microobjects with different structures and how the structures and the corresponding photonic properties of the microobjects were regulated by different means.

## 2. Colloid-based photonic microspheres with isotropic properties

### 2.1. Opal photonic microspheres with close-packed structure

Following Yang's work, Gu's group and Luo's group respectively

reported the fabrication of uniform-sized colloidal photonic microbeads with diameters ranging from tens of micrometers to several millimeters through different droplet-generating apparatus [131,136]. For the typical flow-focusing droplet-producing device in Gu's report, as illustrated in Fig. 1a, they utilized a polydimethylsiloxane (KF-96, 10 cSt) oil containing surfactant and an aqueous suspension of monodispersed (polydisperse index below 5 %) PMMA CPs (diameters ranging from 195 nm to 268 nm, 1.77 wt%) as the outer phase (OP) and inner phase (IP) to produce uniform-sized water-in-oil (W/O) droplet templates. The diameters of the droplets were controlled by the flow rate ratios of the two phases since their compositions were fixed. For a given flow rate of the IP, the larger flow rate of the OP can lead to larger shear force and result in smaller diameters of the droplets. The sizes of the resultant colloidal crystal microspheres obtained from the evaporation of colloidal-containing droplets are normally smaller than that of the initial droplet templates; this was due to solvent evaporation-induced shrinkage of the droplets. In those cases, the sizes of the microobjects were mainly determined by two factors: the initial concentrations of the CPs and the initial diameters of the droplets. For a fixed concentration of initial CPs' suspension, the larger size of the initial droplets resulted in a relatively larger size of the final photonic microobjects. Alternatively, for a fixed size of the initial droplet templates, the higher the concentration of the initial CPs' suspension, the larger the size of the resultant photonic microobjects, and vice versa. This is because the densest packing of colloids within a sphere occupies a maximum volume fraction of ~74 % and with an FFC structure [137,138]. In an alternative experiment in Luo's report, a mixture of n-butyl alcohol/n-octyl alcohol with surfactant Span 85 and an aqueous suspension of monodispersed PS CPs (diameters of 200 nm and 260 nm, 1 wt%) were used as the OP and IP, respectively. The addition of surfactant Span 85 not only decreased the interfacial tension between the two phases but also favored the formation of monodisperse droplets and prevented the droplets from experiencing coalescence, eventually yielding monodisperse photonic microobjects. The generated monodispersed droplets with average diameters from 55 μm to 500 μm [136]. For a typical two-phase microfluidic experiment in a T-junction microfluidic device, the diameter of the resultant droplet is expressed as $d = (1.5 \pm 0.1)Ca^{0.4\pm0.05}w$, $Ca$ and $w$ are the capillary number and width of the microfluidic channel. This is based on the prerequisites of $d \ll w$ [139]. The capillary number $Ca$ can be expressed as $Ca = \frac{\mu U}{\gamma}$, where $\mu$, $U$ and $\gamma$ are the viscosity of the OP, the droplet's velocity at the T-junction, and the interfacial tension between the two phases, respectively. Once those produced droplets were collected in a Teflon dish, solvent evaporation (or extraction) started to take place. Eventually, PMMA (or PS) CPs within the individual droplets stacked into close-packed opal structures both on the surface and interior of the resultant microspheres (Fig. 1b-c). The reflection spectra of the microspheres can be controlled by the diameters of the CPs. For an FCC structure and (111) plane parallel to the substrate, the diffraction peak of the (111) plane is determined by Bragg's law: $N\lambda = 2d_{111}\sqrt{\left(n_{eff}^2 - \sin^2\theta\right)}$, where $N$ represents the diffraction order, $d_{111}$ is the layer lattice spacing for the (111) plane, $n_{eff}$ is the effective refractive index, and $\theta$ is the incident angle [140]. The $n_{eff}$ can be expressed as: $n_{eff} = \sqrt{\left(n_p^2\varphi + n_m^2(1-\varphi)\right)}$, where $n_p$ and $n_m$ are the refractive indices of the CP and the filling medium (can be air or any other liquids) among the CPs, $\varphi$ is the total volume fraction of the colloid particles. Though the drying of the droplets can result in close-packed photonic crystal structures, the interaction among the CPs is dominantly contributed by the van der Waals forces among CPs. This interaction is weak and can be readily destructed upon external vibration when the photonic microspheres are subject to analyses or even purification procedures [141]. In light of this, Gu et al. produced photonic crystal beads with relatively more stable mechanical properties than those of the above-mentioned PMMA-based colloidal crystal microbeads. A T-junction microfluidic device was used in their synthesis steps [141]. Instead of using the polymer-based (PMMA/PS) CPs as building blocks, monodispersed $SiO_2$ colloids were used as building blocks in the study. Once the close-packed opal structure photonic beads formed upon complete evaporation of solvent, calcination was introduced to treat the beads at 700 °C and 110°C, respectively, to generate 'necks' between neighboring silica CPs, which could consequently improve the mechanical stability of the

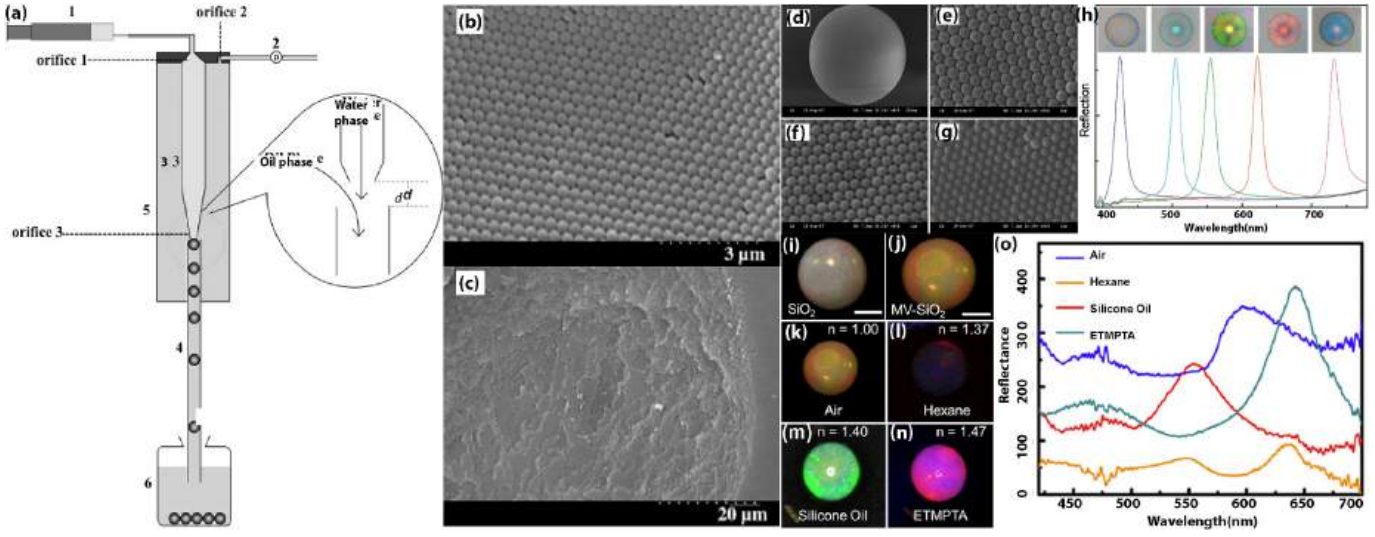


**Fig. 1.** (a) Schematic figure of a microfluidic device used to opal structure colloidal crystal microbeads using PMMA CPs as building blocks. (b)-(c) Scanning Electronic Microscopy (SEM) images of the surface and inner part of the photonic microsphere [131]. Reprinted from ref. 131 with permission from Wiley, copyright 2006. (d) SEM image of a colloidal crystal microbead using monodispersed $SiO_2$ Cs as the building blocks [141]. (e)-(g). SEM image of the surface of the microsphere before (d) and after (e) calcination at 700 °C and the surface of the microsphere was calcinated at 1100 °C (g). (h). Reflection spectra and their corresponding appearances of colloidal crystal microspheres using different diameters of $SiO_2$ CPs [141]. Reprinted from ref. 141 with permission from the American Chemistry Society, copyright 2008 (i)-(j). Optical microscopy (OM) images of colloidal crystal microspheres formed from the assembly of $SiO_2$ CPs (i) and MV-modified $SiO_2$ CPs (j), respectively. (k)-(n) OM images of MV-modified $SiO_2$ CP-based colloidal crystal microspheres in different media: air (k); hexane (l); silicone oil (m); ETMPTA (n). (o) Reflection spectra of the MV-modified $SiO_2$ CPs-based photonic crystal microspheres in different media [143]. Reprinted from ref. 143 with permission from the American Chemistry Society, copyright 2019.

resulting photonic crystal beads despite the anti-cracking capability of the photonic microspheres being much higher than that of the colloidal photonic film (as shown in Fig. 1d-g) [141]. This calcination strategy was further used to develop inverse-opal structures using a mixture of binary CPs, such as monodispersed PS colloids building blocks with relatively larger diameters and ultrafine $SiO_2$ nanoparticles (NPs; 5 nm, nanoparticles refer to the particles with sizes <100 nm) as the matrix materials [142]. The structural colors and reflection spectra of the resulting photonic microspheres can be tuned by using $SiO_2$ CPs with different diameters from 200 nm to 295 nm (as shown in Fig. 1h). The high temperature in the calcination process decomposed the PS colloidal building blocks, leaving behind the silica matrix and yielding fully inverse opal photonic microspheres that will be discussed in section 5 of this paper. Furthermore, to improve the color saturation of the opal-structured photonic crystal microspheres based on the assembly of CPs, Yu and Chen et al. reported the fabrication of photonic microspheres via microfluidics. In their study, methyl viologen (MV)-functionalized $SiO_2$ colloids were used as the building blocks of the photonic structures [143]. The methyl viologen (MV) moieties were functionalized on the surface of the CPs via silane chemistry and acted as the light-absorbing groups. The resulting microspheres based on MV-functionalized $SiO_2$ colloids displayed a much darker appearance when compared with that of the microspheres based on bare $SiO_2$ colloids (as shown in Fig. 1i-j). This was because of the light-absorbing properties of the MV moieties. Moreover, the microspheres based on MV-functionalized $SiO_2$ colloids display distinctive colors when the voids of the microspheres are filled with different media. Specifically, the microspheres exhibited bright red, dark red, bright green, and bright pink when exposed to air, hexane, silicone oil, and trimethylolpropane ethoxylate triacrylate resin (ETMPTA or ETPTA) solution, respectively (as shown in Fig. 1k-n). And the microspheres in the liquid media all showed higher saturation than in air. Correspondingly, the peak values of the reflection spectra are located at different positions due to the different refractive indexes of the ambient media (as shown in Fig. 1o). In particular, the reflection spectra of the microsphere in hexane and ETPTA both exhibited a redshift when compared with that of the microsphere in air, while that of the microsphere in the silicone oil uniquely showed a blueshift. These phenomena were due to the close refractive index between the silicone oil ($n$ = 1.405) and the MV-functionalized $SiO_2$ colloids, which resulted in the microsphere being more transparent and enabled the light to travel deep inside the microsphere rather than a few outer layers of the microsphere in other cases. As a result, the reflection peak at 550 nm originated from other scattering planes instead of the (111) plane. It was noteworthy to mention that the emergence of two reflection peaks when the microsphere was immersed in hexane. This was due to the close refractive indices between hexane (1.37) and the MV-functionalized $SiO_2$ colloids (1.39). This strategy can also be used to fabricate photonic microparticles using hollow silica CPs as the building blocks [59]. The microparticles can be subsequently used for barcodes.

In addition to the construction of opal-structured photonic microobjects using simple composition-based CPs, such as $SiO_2$ or PMMA CPs, Chen et al. reported the construction of photonic microobjects via microfluidics by using hybrid CPs as the building blocks. Specifically, core-shell CPs with CdTe nanocrystals (NCs, ~ 4.3 nm) entrapped, where the core-shell colloids were composed of a polystyrene-*co*-acrylic acid (PS-co-PAAc) core part and a polyhydroxy ethyl methacrylate-*co*-polyacrylic acid (PHEMA-*co*-PAAc) shell part (as shown in Fig. 2) [144]. Once droplets of an aqueous suspension of the hybrid latexes were produced from a T-junction microfluidic device and collected into a container, water evaporation from the droplets started to occur. The droplets eventually evolved into photonic supraballs containing close-packed CPs upon complete evaporation of the solvent (as shown in Fig. 2a-b). By selecting the hybrid CPs with different diameters from

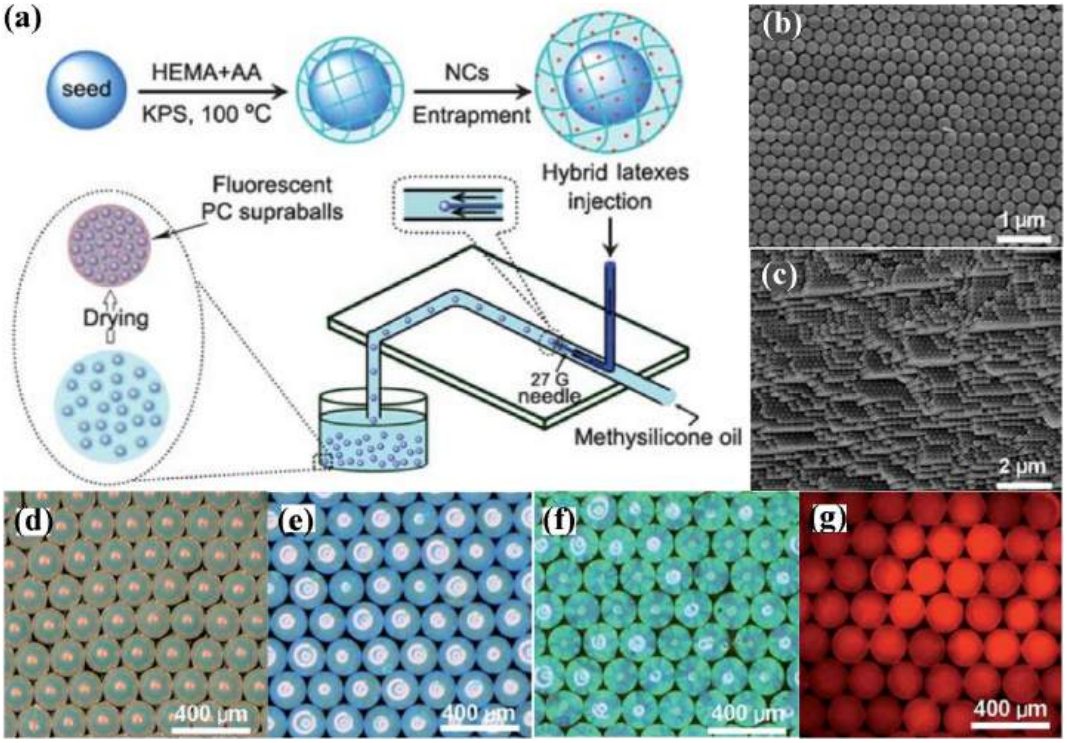


**Fig. 2.** (a) The illustration figure shows the roadmap for the construction of hybrid CPs based photonic supraballs. Top: synthetic route of the preparation of NCs entrapped hybrid CPs. Bottom: Microfluidics fabrication of hybrid CPs-based photonic supraballs. (b) SEM image of the surface of a supra formed from assembly of the hybrid CPs with a diameter of 260 nm. (c) Cross-section SEM image of a supraball formed from the hybrid CPs with a diameter of 190 nm. (d)-(f) OM images of photonic suprapballs formed from CPs with different diameters. (g) Fluorescence microscopy (FM) image shows the supraballs displaying a red color when being illuminated with blue light at a wavelength of 450 nm [144]. Reprinted from ref. 144 with permission from the Royal Society of Chemistry, copyright 2010. (For interpretation of the references to color in this figure legend, the reader is referred to the web version of this article.)

260 nm to 230 nm to 190 nm, the resulting supraballs displayed red, green, and blue hues, respectively (as shown in Fig. 2d-f). Meanwhile, due to the entrapment of NCs in the hybrid CPs, the supraballs also displayed fluorescence properties (as shown in Fig. 2g). The supraballs also exhibited pH value-dependent fluorescence intensity change due to the responsivity of the PHEMA-co-PAAc shell, which allowed the fluorescence NCs to freely pass through the shell part of the CPs under alkaline conditions [145].

The use of pH-responsive colloidal building blocks to regulate the fluorescence characteristics of photonic supraparticles is a well-established concept. However, there has been a pressing need to explore how ambient environmental factors can be harnessed to govern the assembly of these CPs, with their inherent stimulus-responsive properties, and in turn, influence their resulting photonic properties. In light of this, José Paulo S. Farinha et al. studied the assembled microstructures and the corresponding photonic properties of pH-responsive colloids within a confined space [146]. pH value and temperature of the ambient environment were leveraged to tune the microstructures and photonic properties of the resulting supraparticles. To statistically study the populational behaviors of the supraparticles, droplets of aqueous dispersion of PS@PMMA-co-AAc core-shell CPs were firstly produced from a PDMS-based microfluidic device with a T-junction configuration (as shown in Fig. 3a) and were subsequently evaporated at 50 °C in a hexadecane oil solution containing 5 wt% of span 80. Due to their pH-responsive property, the CPs within a droplet eventually assembled into a spherical supraparticle with a close-packed FCC structure and a supraparticle with amorphous structures when the initial pH values of the colloidal dispersions were above and below the pKa of the pAAc block, respectively (Fig. 3b-c). In addition to the utilization of pH values to regulate the assembled microstructures, the temperature field was also leveraged to regulate the assembled structures of the supraparticles. The colloidal supraparticles gradually transitioned from a close-packed FCC state to an amorphous state when the incubation temperature varied from 50 °C (Fig. 3d) to 60 °C (Fig. 3e) to 65 °C (Fig. 3f), while the initial pH value of the colloidal dispersions was set to 6.2 (close to the pKa value of pAAc). These transition trends also apply to the supraparticles formed from the assembly of CPs with different diameters.

In addition to endowing conventional colloidal photonic particles with fluorescence properties via functionalizing colloidal building blocks with semiconductor NPs, such as CdS and others, there has been growing interest in harnessing the photoluminescence quantum yields (PLQY) and cost-effectiveness of perovskite nanocrystals (NCs) for the fabrication of novel photonic microstructures. These microstructures were envisioned and employed for innovative applications in areas like anticounterfeiting and information security. Zhao et al. reported the preparation of photonic microspheres integrated with $CsPbBr_2I$ NCs. Instead of using a conventional two-step approach, such as preparing CPs with NCs first and then assembling the CPs into a photonic structure, they adopted a different strategy, where $SiO_2$ colloid-based photonic microspheres were firstly constructed by a conventional route and followed with post-deposition of $CsPbBr_2I$ NCs into the voids among the $SiO_2$ colloids in an organic solution (as shown in Fig. 4a-b) [147]. Through this operation, the perovskite NCs were successfully loaded in the voids among the $SiO_2$ colloids, as can be verified by SEM characterizations and energy dispersive spectrum (as shown in Fig. 4b-c). Not only can the structural colors of the resulting microspheresbe tuned by using different diameters of $SiO_2$ colloidal building blocks, but also the fluorescence properties of the microspheres can be regulated by the composition of the perovskite solutions (as shown in Fig. 4d-e). More importantly, the perovskite NCs can undergo a conformational change when exposed to water-rich conditions, leading to the quenching of their fluorescence signal (as shown in Fig. 4f), where the photonic microsphere displayed a strong fluorescence signal under dry conditions. In contrast, the signal vanished after wetting. This special property can be further utilized to construct information-hidden materials. For example, a typical Yin-yang pattern can be constructed by using two different fluorescence colors of photonic microsphere arrays (as illustrated in

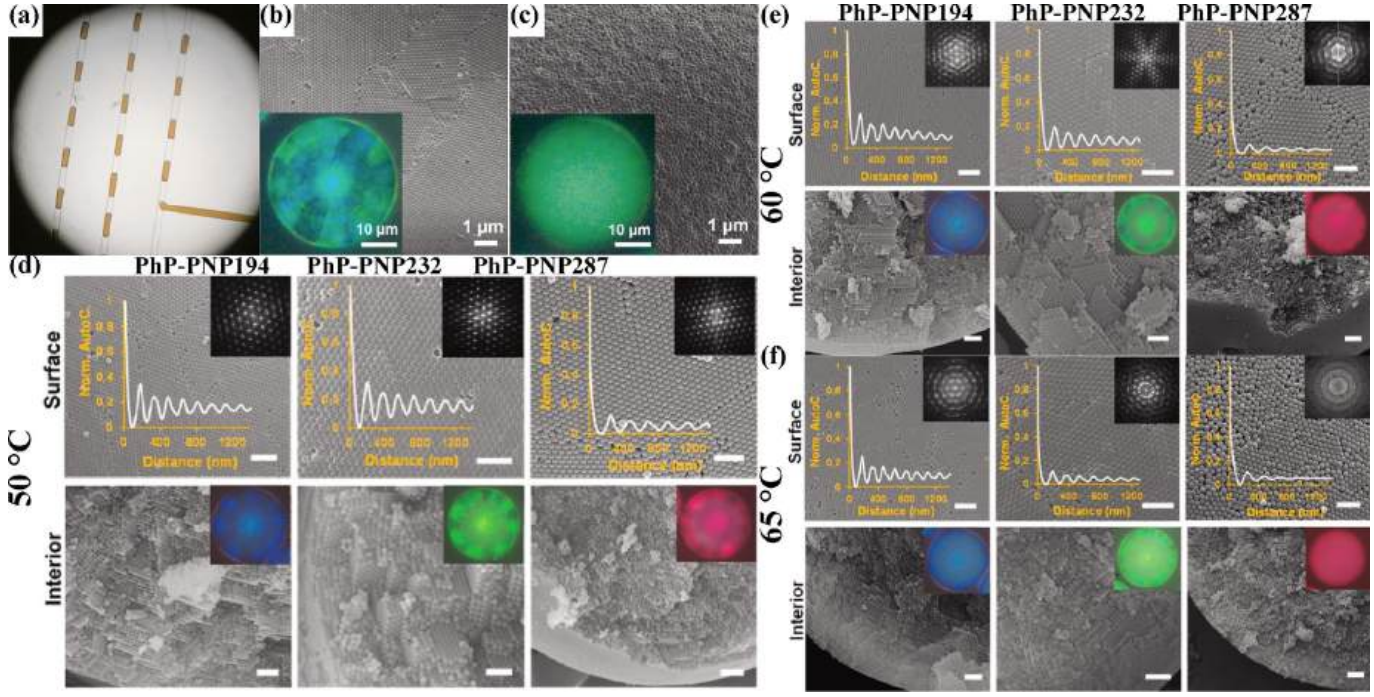


**Fig. 3.** (a) Microscopy image of droplets of colloidal particle dispersion inside a T-junction microfluidic device. (b)-(c) SEM images of FCC packing of PNPs inside the supraparticle (b) and an amorphous supraparticle (c) with random close-packing of the PNPs. The inset figures in the left bottom panel of b-c show the corresponding photonic properties under OM. (d)-(f)SEM images of the surface and interior part of the colloidal photonic microparticles formed from the assembly of CPs with different diameters from 194 nm (left column), 232 nm (middle column), and 287 nm (right column) under different temperatures: 50 °C (d), 60 °C (e), and 65 °C (f) [146]. Reprinted from ref. 146 with permission from Elsevier, copyright 2022.

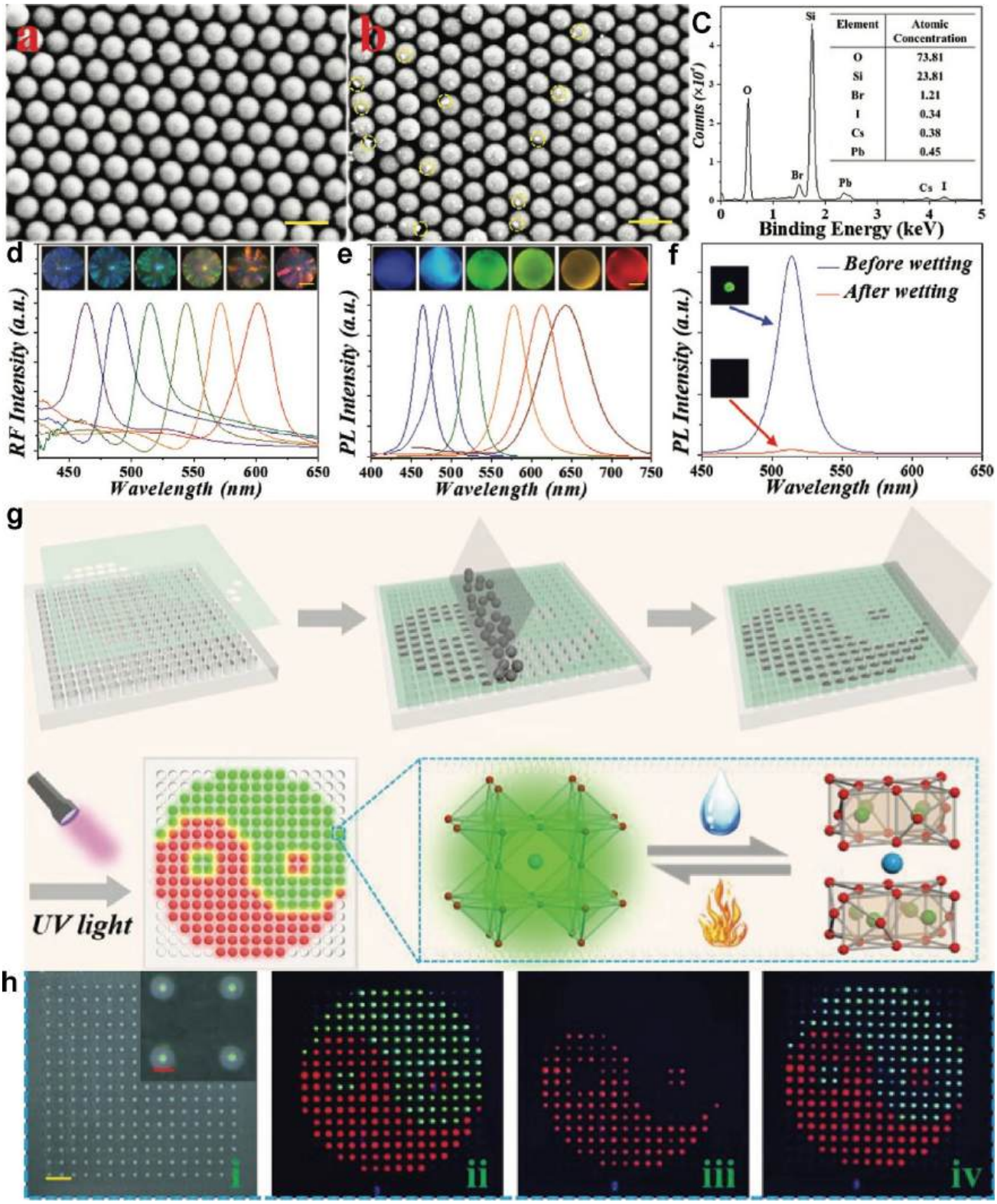


**Fig. 4.** (a) SEM image of silica colloids on a photonic microsphere; (b) SEM image of silica colloids deposited with $CsPbBr_2I$ NCs on a photonic microsphere. (c). Element analysis of the nanocrystal-deposited silica colloids. (d) Reflection spectra of different colors of photonic microspheres formed from the assembly of bare silica colloids and their corresponding OM images. (e) Reflection spectra of different colors of photonic microspheres formed from the assembly of $CsPbBr_2I$ NCs loaded silica colloids and their corresponding OM images. (f) Reflection spectra of the $CsPbBr_2I$ NCs-loaded photonic microsphere before and after wetting. (g) The schematic figure shows the preparation process and hydrochromic phenomenon of PNs-integrated photonic microsphere arrays. (h) Encryption of a QR code by using the PNs-integrated photonic crystal microsphere arrays. (i)-(ii) OM (i) and fluorescence microscopy (ii) images of the array. (iii)-(iv) FM images of the array after wetting (iii) and redrying (iv) [147]. Reprinted from ref. 147 with permission from Wiley, copyright 2022.

Fig. 4g). The pattern displayed different information under wet and dry conditions (as illustrated in Fig. 4h).

While the colloidal photonic microballs from a single type of CP have been demonstrated and their optical properties have been studied, the question regarding how the intrinsic structures of the microballs and the confining effects affect the optical properties of the microballs remains perplexing to scientists. Despite Dijkstra et al. studying the impact of the spherical confining effect on NPs with diameters at around 12 nm, the NPs at this size range are below the threshold that could modulate the light in the visible light spectrum range [148]. In light of this, Vogel and Aizenberg et al. systematically investigated a seriess of factors, including sizes of the colloidal building blocks, confining effects, and curvatures of the microballs on the optical properties of the opal-structured photonic microballs. The photonic microballs were prepared by using negatively charged monodispersed PS CPs as the building blocks via a PDMS-based microfluidic device (as shown in Fig. 5a-c) [149]. The resultant CP-based microballs have diverse diameters, ranging from 15 μm to 100 μm, but with monodispersed size distributions. The diameters of the monodispersed PS CPs were 180 nm, 225 nm, and 250 nm, respectively, leading to the resulting microballs with structural colors varing from blue to green to pink (as shown in Fig. 5d). It was discovered that the intensity of the Bragg reflection peak from the microball reached a saturated value when the diameter of the microball was 50 μm and beyond (as shown in Fig. 5e-f). Moreover, linear PEG (polyethylene glycol)-modified Au NPs (~ 12 nm in diameter) were utilized as the scattering light absorbers in the microballs and can successfully suppress the scattering effects (as shown in Fig. 5g-h). Grating diffraction patterns were also observed when CPs with diameters at 400 nm or beyond were used as the building blocks and likely originated from the secondary diffraction as well. Further studies revealed that the grating diffraction patterns arose from the periodic arrangement of colloids at the surfaces of the microballs (as shown in Fig. 5i-n).

In most scenarios, the resulting colloidal photonic supraparticles, termed as photonic balls, that were formed from the assembly of CPs normally possessed isotropic photonic properties due to their layer-like interior structure [150]. However, the formation of colloidal clusters upon evaporation from the droplet templates was governed by several factors, particularly at low temperature conditions and the extremely low evaporation rate [101,151]. The synergistic effect from the evaporation of emulsion droplet templates could result in the colloidal supraparticles with anisotropic photonic properties. Despite emulsion droplets normally evolving into colloidal clusters with spherical shapes, how a variety of factors, including solvent evaporation rate and the numbers of CPs within individual droplet templates, particularly discrete numbers of colloids confined within the droplet template, affect the localized structures on the surface of the colloidal clusters has never been systematically exploited from an experimental perspective [152]. Vogel et al. leveraged the microfluidics-fabricated droplets containing monodispersed PS CPs and investigated their assembled structures of the colloidal clusters [153]. By controlling the evaporation rates and temperatures, statistically tuning the surface structures of the colloidal clusters formed from the evaporation of colloid-containing droplets could be achieved. Four major colloid clusters with increased orders were obtained in the experimental studies (as shown in Fig. 6a-d). It was discovered that a slow evaporation rate favored the formation of icosahedral clusters to a fraction of up to 75 % in total (as shown in Fig. 6e-f). Although the surface geometries can be clearly characterized by SEM, characterization of the detailed inner structure of the photonic microballs without destructing the integrity of the colloidal clusters was still difficult to achieve, particularly for clusters with larger diameters, for instance, colloidal clusters with diameters above a few micrometers. In specific, it was remaining a big hurdle to unlock the information of the inner structures using conventional instruments, such as small-angle X-ray scattering, SEM, TEM, and FIBs (focused ion beams). Although cutting-edge tools, i.e., 3D X-ray microscopy, may reveal the secrets beneath the layers of close-packed colloids, it is time-consuming and sophisticated. In order to overcome the shortcomings, Vogel et al. developed a straightforward method to uncover the underlying details

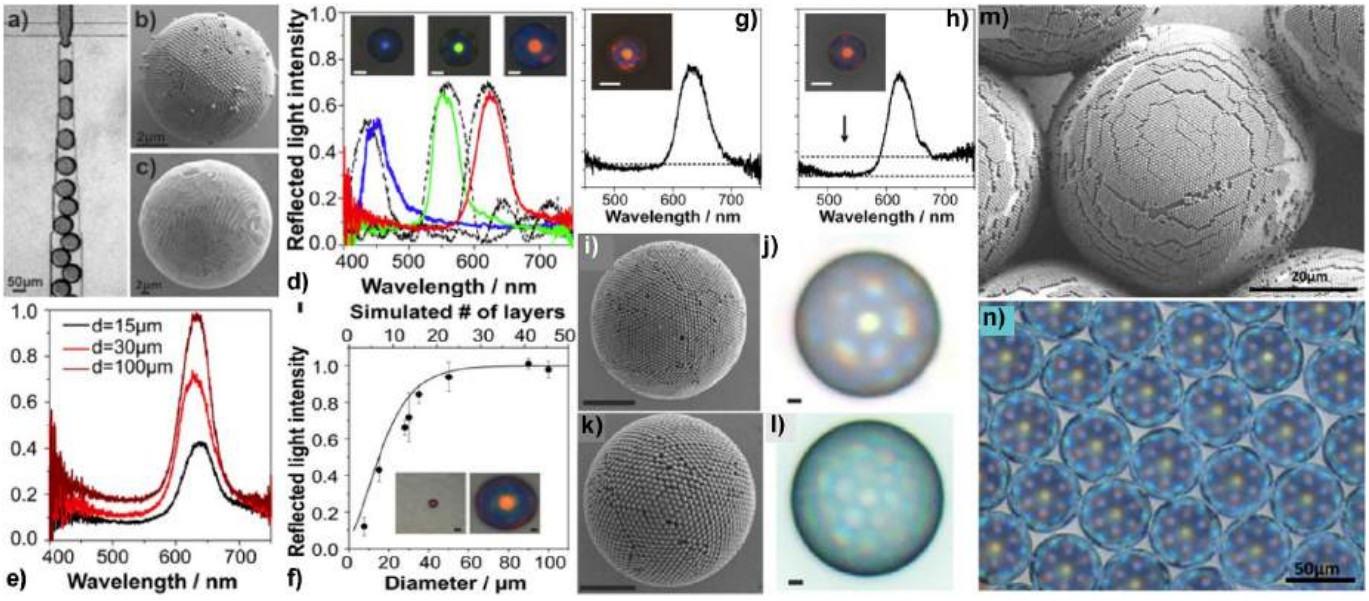


**Fig. 5.** (a) OM images of microfluidic fabrication of $SiO_2$ CPs-based photonic crystal microballs. (b)-(c) SEM images of two microballs with diameters of 8 μm and 30 μm, respectively. Both microballs were formed from the assembly of $SiO_2$ CPs with a diameter of 250 nm. (d) Solid line: reflection spectra of the microballs with different structural colors; dotted line: 1D simulations (dotted lines) of light reflection at stacked (111) planes within the microballs. (e) Reflection spectrum intensity of the photonic microballs with different diameters. (f) Plot of the reflection intensities of the balls as a function of ball diameters. (g)-(h) Comparison of reflection spectra of photonic microballs without (g) and with (h) the addition of Au NP absorbers. (i)-(j) SEM image of photonic microball formed from the packing of 610 nm $SiO_2$ colloids and the corresponding OM image (diffraction pattern). (k)-(l) SEM image of photonic microball formed from the packing of 1060 nm $SiO_2$ colloids and the corresponding OM image (diffraction pattern). (m). SEM image of a monolayer of close-packed 610 nm colloids deposited on the surface of a 50 μm photonic microball to mimic the periodic arrangement of the colloids at the surface of a photonic microball. (n) OM image of grating patterns from 3D photonic microballs [149]. Reprinted from ref. 149 with permission from the National Academy of Sciences of the USA, copyright 2015.

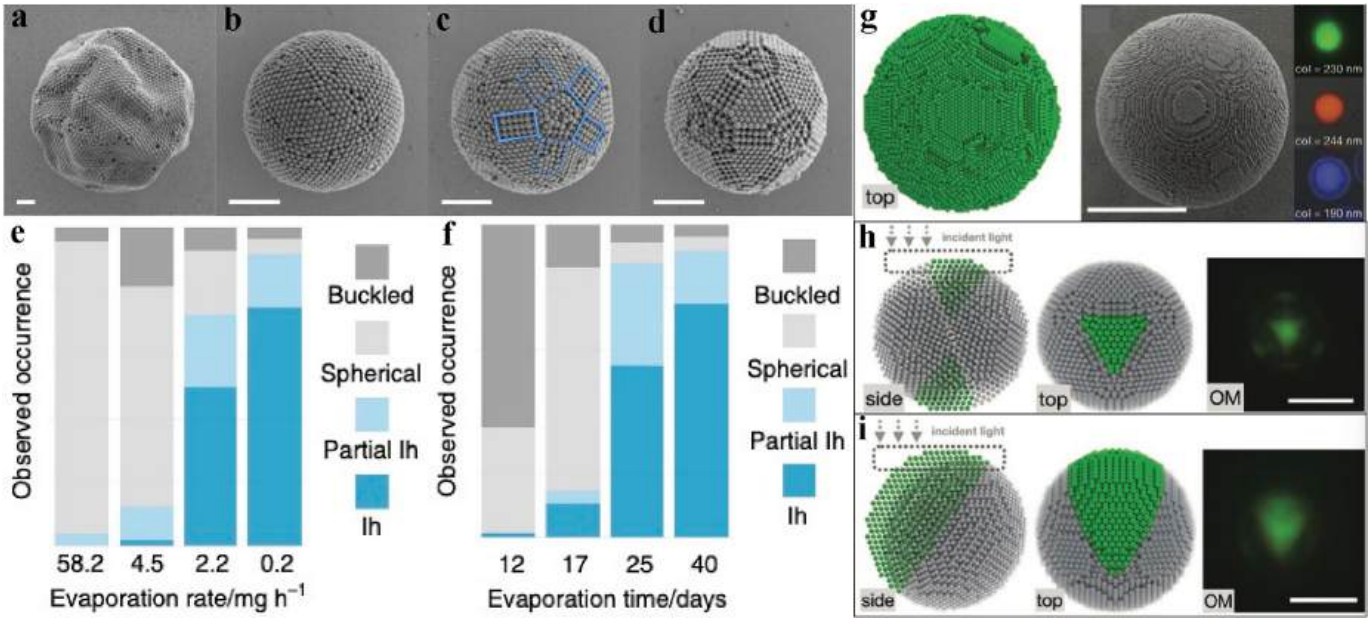


**Fig. 6.** (a)-(d) SEM images of four colloidal clusters with different morphologies formed from the evaporation of droplets of PS CPs under different evaporation conditions. (e)-(f) Statistical plots of percentage of colloidal superstructures with different geometries as a fraction of evaporation rate (e) and percentage of colloidal superstructures with different evaporation periods (f) [153]. Reprinted from ref. 153 with permission from Springer Nature, copyright 2018. (g) Left: View of the simulated cluster along one incident light direction. Middle: Experimental characterization of colloidal clusters oriented in the incident light direction corresponding to the simulated model. Right: OM images of the colloidal clusters formed from different diameters of PS CPs. (h). Appearance of structural color under one illumination scenario from side (left) and top (middle) views and the corresponding structural color from top view (right). (i) Appearance of structural color under one illumination scenario from side (left) and top (middle) views and the corresponding structural color (right) from top view under OM observation [154]. Reprinted from ref. 154 with permission from Wiley, copyright 2020.

beneath layers of CPs of the assembled colloidal crystal particles [154]. They presented a method to infer the internal cluster structures from structural colors of the clusters in a low-cost and versatile fashion. Three kinds of clusters have been used as examples to test the versatility of this method. All of the three kinds of clusters' structural colors were in good agreement with their corresponding structure models. For example, the FCC clusters (Fig. 6g), decahedral colloidal clusters (Fig. 6h), and icosahedral colloidal clusters (Fig. 6i) respectively show different structural color patterns when the incident light was illuminated from the different orientations. The similar phenomena were also observed in studies by Ohnuki et al., in which cases the colloidal photonic microballs were constructed by conventional methods [155,156].

The construction of opal photonic microspheres was normally achieved by evaporation-induced crystallization of CPs confined in emulsion droplets [157]. To obtain photonic microspheres with high color saturation, single-crystalline structure within the photonic microspheres was highly demanded. However, it had been a challenge to produce such a kind of single-crystalline structure in a short timeframe due to the evaporation rate, which can be vary among different droplet templates [158]. To address this challenge, Kim et al. introduced an approach to achieve the production of single-crystalline photonic microsphere arrays by mixing two different types of droplets together: colloid-containing droplets and salt solution-containing droplets (as illustrated in Fig. 7a). Each colloids-containing droplet was surrounded by approximately the same numbers of salt droplets, and consequently the colloid-containing droplets and salt-containing droplets respectively experienced size decrease and expansion (as shown in Fig. 7b-c). Through this design, the rate of CPs' enrichment under evaporation can be kept at a relatively low variation level. As a result, the majority of the resulting photonic supraballs with single crystalline structure were achieved (as shown in Fig. 7d). Meanwhile, photonic supraballs with polycrystal, partial single crystal, and single crystal structures were obtained in the same batch (as shown in Fig. 7e-g). Moreover, the colloids' enrichment rate can be controlled by the concentrations of salt or the mixing ratio of the two different droplets. Therefore, the droplet templates incubated under different conditions resulted in superball mixtures with different compositions. Specifically, the percentage of the photonic superballs can be regulated by the incubation conditions (as shown in Fig. 7h-k). In other words, this approach may not be able to achieve superballs with completely pure photonic structure. Furthermore, the authors also investigated how the thermodynamics and kinetics affected the assembled superstructure from finite numbers of hard PS CPs confined within the droplet templates. They concluded that thermodynamics predicts both stable icosahedral clusters and stable decahedral cluster, while kinetic generally favor icosahedral clusters [159].

An extensive amount of research attention has been paid to constructing photonic microobjects through the assembly of spherical CPs [91,160]. This is because spherical CPs are easy to develop, have high availability, and have a tendency to form close-packed ordered structures [20]. Research attempts on the construction of photonic structures using nonspherical CPs have also achieved [161]. Nevertheless, photonic microobjects using polyhedral particles as the building blocks have been stagnated for quite a while [162]. Two obstacles were attributed to the lack of development of such kinds of photonic structures: on the one hand, the CPs are too small to produce the Bragg diffraction in the visible wavelength range [163]; on the other hand, the CPs, particularly for metallic CPs, are too heavy, leading to the sedimentation effect dominating the process and possibly failing to form stable photonic structures. In light of this, Vogel et al. reported the fabrication of supraparticles using colloidal polyhedral metal-organic framework (MOF) particles as building blocks, as MOF particles have attracted wide application attention in diverse fields [164]. The photonic supraparticles were formed from confining assembly of MOF CPs within droplets that were produced from microfluidics [20]. Due to their ideal size range (~200 nm to 400 nm), low density, and capabilities for facile surface functionalization, the MOF CPs can be self-assembled into three-dimensional ordered supraparticles with photonic properties, displaying different structural colors. Four different geometries of MOF particles,

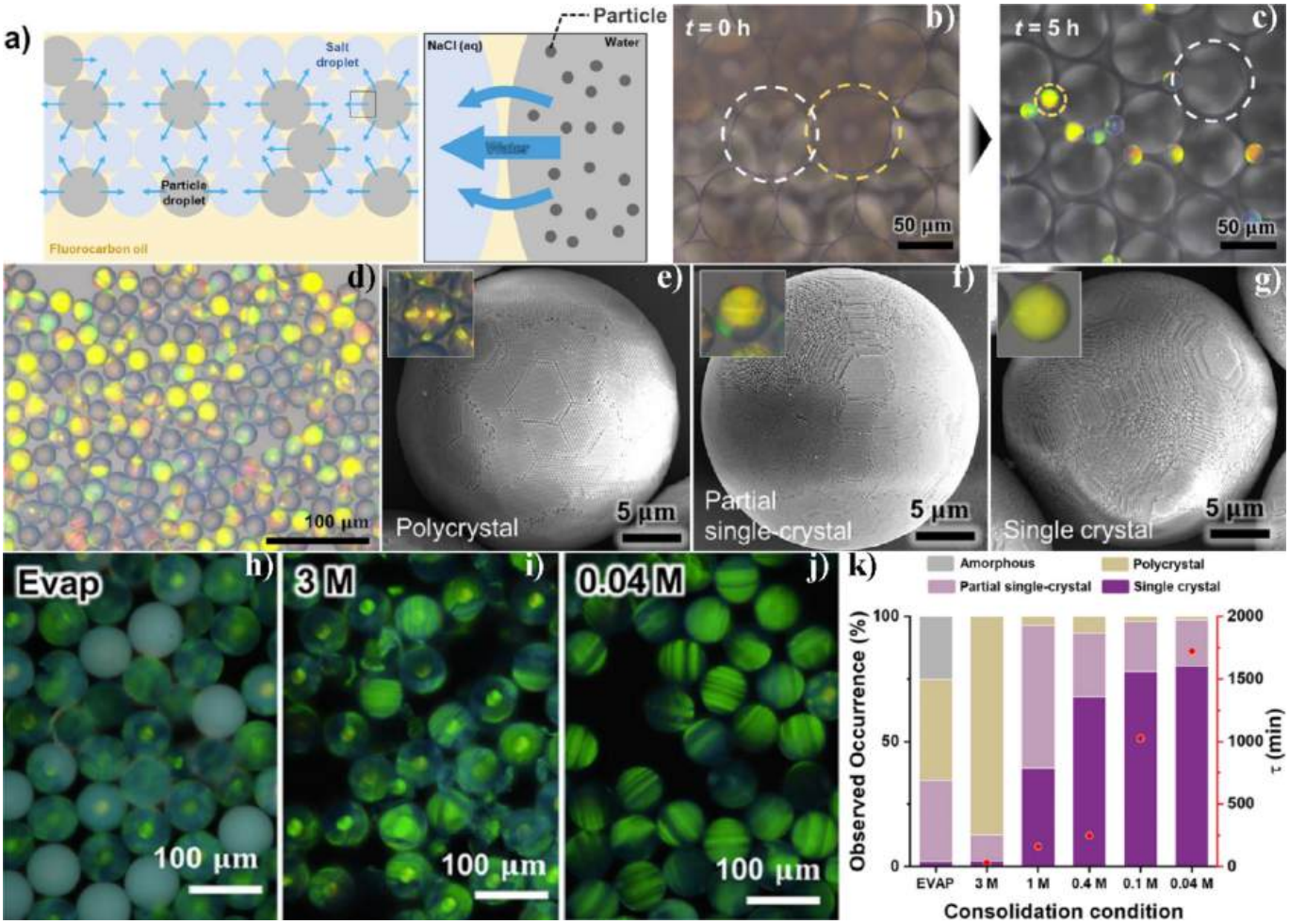


**Fig. 7.** (a) The illustration figure shows the production of photonic supraballs using the droplet-to-droplet extraction method. (b) OM images of two different kinds of droplet mixtures just after production and 5 h of incubation. (c) OM image (reflection mode) of the photonic superballs. (e-f) SEM images of the photonic superballs with different crystal structures. (g)-(j) OM images of green-colored photonic superballs incubated under different conditions. (k) The plot shows the relationship among the percentage of the photonic superballs with different crystal structures, observation time, and the consolidation conditions [158]. Reprinted from ref. 158 with permission from the American Chemistry Society, copyright 2023. (For interpretation of the references to color in this figure legend, the reader is referred to the web version of this article.)

including cubic zeolitic imidazolate framework-8 (C-ZIF-8), truncated rhombic dodecahedral TRD-ZIF-8, perfect rhombic dodecahedral RD-ZIF-8, and octahedral Universiteteti Oslo-66 (O-UiO-66) particles, were used to construct the photonic supraparticles (as shown in Fig. 8a). The resultant supraparticles displayed a flawless spherical shape (as shown in Fig. 8b) and corresponding structural colors (bottom left inset figures in Fig. 8b). The reflection spectra were well coordinated with the corresponding structural colors (as shown in Fig. 8c). In addition, cross-section images indicate that the polyhedral CPs in all four types of supraparticles assembled into onion-like structures from the surface toward the center of the supraparticles (as shown in Fig. 8d). More importantly, the supraparticles formed from the evaporation of droplets displayed angle-dependent structural colors. The droplets were prepared by the hand-shaking method using different shapes of primary particles with similar sizes. This was due to the interference of light reflected at the onion-like layers dominating the coloration mechanism (as shown in Fig. 8e). This angle-dependent phenomenon was further verified by the corresponding reflection spectra in Fig. 8f; specifically, the reflection spectra peaks exhibited different values when viewing from different angles. This angle-dependent feature was contrary to that of photonic microcapsules using spherical CPs as the colloidal building blocks in the report by Kim et al. [165] This difference was likely because different geometries of colloidal building blocks were used in the two cases. However, the supraparticles still lacked strong mechanical stability due to there being no strong interactions (i.e., covalent bonds) among CPs, which may need to be addressed in further applications.

Despite a number of studies having reported the production of photonic microballs with high color saturations by adding color saturation additives, such as Au NPs or others [149,166]. However, the plasmonic properties from Au NPs can alter the hue and saturation of the resulting photonic structures. Therefore, it was highly demanded to develop additives for saturation enhancement in aqueous dispersions of CPs for co-assembly with minimum impact on color brightness and hue value of the resulting photonic structures. Eumelanin NPs possess very low toxicity and can act as efficient light absorbers in biological systems [167]. Therefore, it caught the attention of researchers for color saturation enhancement in colloidal photonic systems [168]. Kim et al. emulsified an aqueous suspension of the mixture of 250 nm PS CPs and ~ 4.1 nm eumelanin NPs through a microfluidic approach [169]. The droplets were subjected to a series of microstructural evolutions from single-crystalline array towards polycrystalline array formation in the enrichment processes (as illustrated and shown in Fig. 9a-e). In addition to the eumelanin NPs, much larger NPs, such as ~92 nm polydopamine (PD) NPs, were also used as additives for colloidal photonic supraparticle systems. For example, José Farinha et al. investigated how the addition of PD NPs affects polymer CP-based colloidal photonic systems

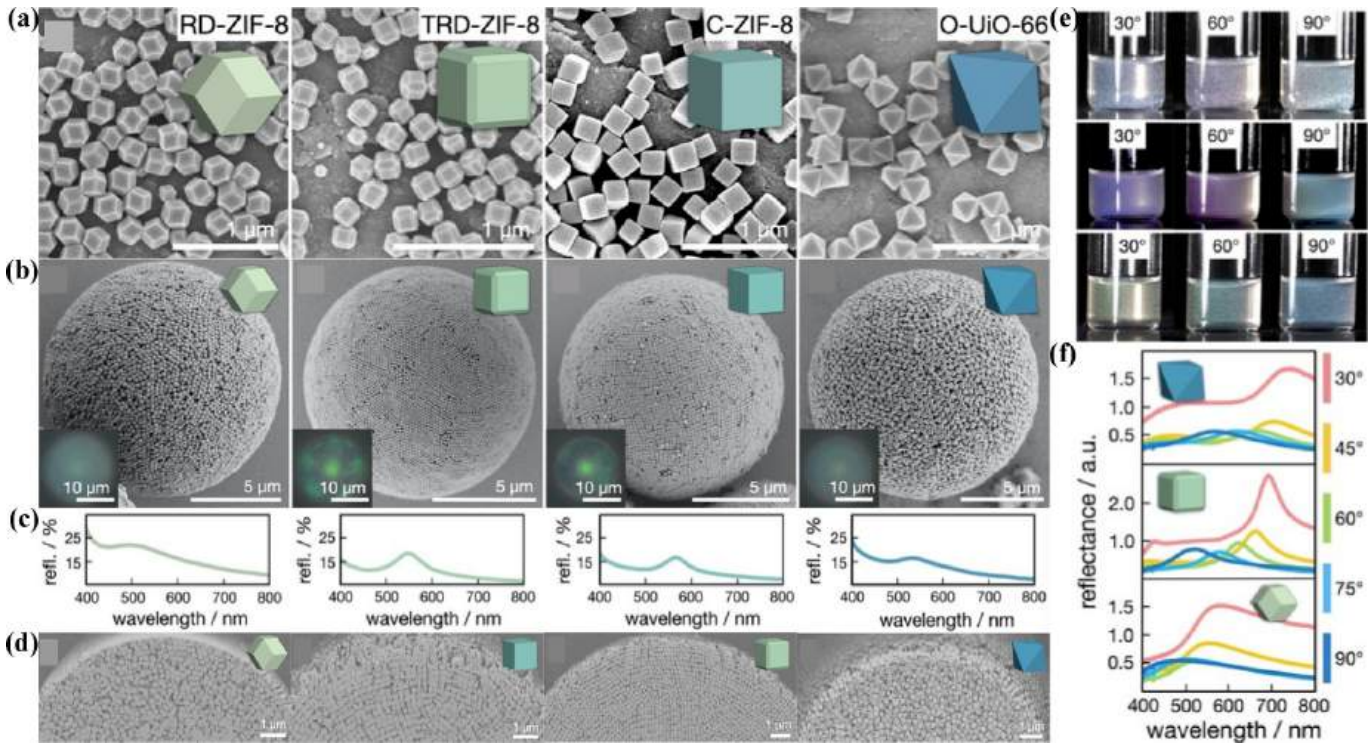


**Fig. 8.** (a) SEM images of four different types of polyhedral CPs. (b) SEM images of supraparticles formed from the assembly of four different types of CPs within droplet templates that were produced from microfluidics. Inset figures at the bottom left of each figure show the OM images of the corresponding supraparticles. (c) Reflection spectra of the supraparticles in (b). (d) Focused ion beam (FIB) cross-section images of the supraparticles in (b). (e–f) Angle-dependent phenomenon (e) of three different types of supraparticles with the same size but consisting of different CPs and their corresponding reflection spectra (f) at different angles. Supraparticles in (e) were formed from the assembly of octahedron (top panel), truncated rhombic dodecahedron (middle panel), and rhombic dodecahedron (bottom panel) CPs, respectively [20]. Reprinted from ref. 20 with permission from Wiley, copyright 2022.

[170]. Droplets of aqueous suspensions of PS@PMMA-co-AAc CPs with or without PD NPs (TEM images and chemical structures of PS@PMMA-co-AAc CPs and PD NPs were shown in Fig. 9f-g) were firstly fabricated through a microfluidic device and subsequently subjected to solvent evaporation. It turned out that the supraparticles evolved from the droplets containing PD NPs, showing only short-range order, non-iridescent and vivid colors with high color saturation (as shown in Fig. 9h). This was due to the fact that the addition of PD NPs disrupted the long-range order of the structure and absorbed the diffuse scattering resulting from the structural disorder. Further study indicated that the increase in disorder became more notable when the PS@PMMA-co-AAc CPs had diameters beyond a certain value, for example, 223 nm. The distribution of PD NPs in a random fashion contributed to the resulting photonic supraparticles with a more homogeneous coloration and more saturated hues (as shown in Fig. 9i).

### 2.2. Opal photonic microspheres with nonclose-packed structure

#### 2.2.1. Nonresponsive photonic microobjects with nonclose-packed structure

Instead of simply packing CPs together to form colloid-based photonic structures, photocurable polymer precursor (matrix) suspensions of monodispersed CPs with photonic properties were also developed for further construction of photonic microobjects. Precisely controlling the volume fraction of CPs in the suspensions could enable the suspension with photonic properties. Preparation of bulk photonic structures based on these suspensions has been extensively studied [10,16,69]. The CPs particles in the resultant photonic structures have been proved to be non-close-packed structures [166]. Those photonic suspensions can be further emulsified using microfluidics to generate monodispersed photonic droplets, which can be subsequently cured via UV light irradiation either in situ or at the post-collecting step to immobilize the photonic structure in a thermal treatment-free manner. Yang et al. have reported the optofluidic fabrication of monodispersed photonic microballs by using $SiO_2$ CPs (diameter of 145 nm, 152 nm, and 190 nm) as the building blocks and photocurable ETPTA resin as the matrix material, respectively (as shown in Fig. 10a-b) [109]. Given the nonvolatile nature of the resin suspension, the diameters of the resultant microballs were slightly smaller than or almost the same as that of the droplet templates, given that the curing process could lead to the shrinking of droplet templates. The microballs displayed vivid colors when dispersed in aqueous solutions (as shown in Fig. 10c). SEM images also revealed that the microballs formed from different volume fractions of $SiO_2$ CPs, showing different lattice spacings between the CPs.

#### 2.2.2. Stimulus-responsive photonic microspheres with nonclose-packed structure

*2.2.2.1. Photonic microspheres using stimulus-responsive colloids as the building blocks.* Despite photonic microobjects being able to be featured with different structural colors, each color composition normally requires one batch synthesis, leading to the complexity of the fabrication process. To overcome this drawback, Kwon and Yin et al. leveraged a real-time optofluidic synthesis strategy to prepare magnetochromatic hydrogel photonic microspheres. Poly(ethylene glycol) diacrylate (PEGDA) suspension of magnetic CPs (~160 nm in diameter) and mineral oil were used as the disperse and continuous phases, respectively. After producing droplets (~72 μm in diameter) of photonic suspension from the microfluidic channel of a T-junction microfluidic device (as shown in Fig. 11a), a magnetic field was applied over the droplets in situ, and UV light irradiation was exerted on the droplets simultaneously. This magnetic field could align the arrangement of the magnetic CPs inside the droplets to modulate the structural colors of the droplets (as shown in Fig. 11b-c). Subsequently, the droplets were cured by UV light

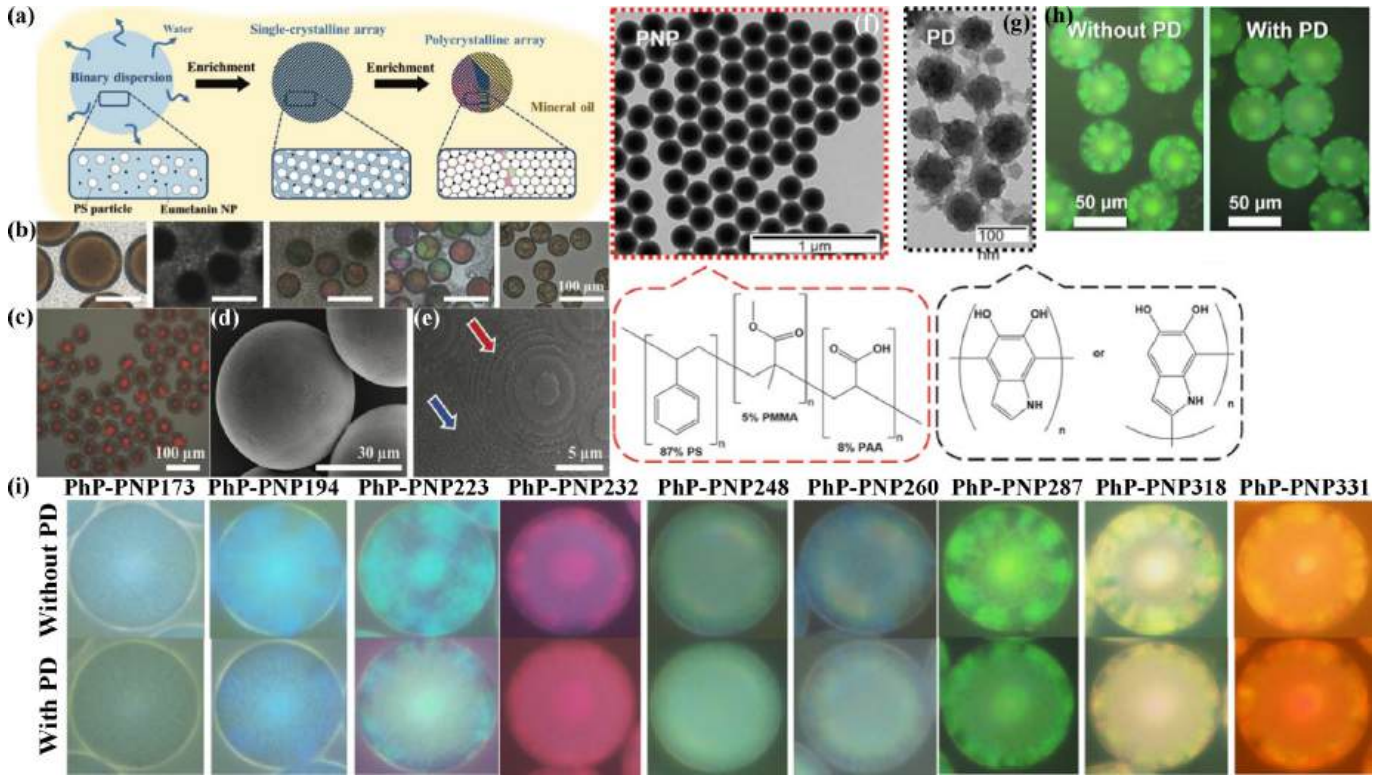


**Fig. 9.** (a) The illustration figure shows the evolution of droplets containing binary particles: PS CPs and eumelanin NPs. The binary particles inside the droplets gradually evolved into a single-crystalline array upon the enrichment process and continue to evolve into a polycrystalline array upon further enrichment in mineral oil. (b) OM images showing the evolution of the microspheres at different stages. (c) OM image of red-colored photonic supraballs [169]. Reprinted from ref. 169 with permission from Wiley, copyright 2022. (d) SEM image of the surface of photonic balls. (e) Enlarged SEM image of the photonic supraball showing hexagonal arrays on concentric step edges. (f)-(g) TEM images of PS@PMMA-co-PAAc CPs and PD NPs (top row) and their corresponding chemical structures (bottom row). (h) Reflection mode OM images of green-colored photonic balls without (left) and with (right) the addition of PD NPs. (i) Reflection mode OM images of different color photonic balls formed from the assembly of the PS@PMMA-co-AAc (PhP-PNP) CPs with different diameters varied from 173 nm to 331 nm. The top and bottom rows respectively show the different-colored balls without and with the addition of PD NPs [170]. Reprinted from ref. 170 with permission from the American Chemistry Society, copyright 2021. (For interpretation of the references to color in this figure legend, the reader is referred to the web version of this article.)

exposure after proper alignment of CPs under the magnetic field. Through this operation, photonic microspheres with different modulated structural colors could be synthesized in one batch (as shown in Fig. 11d) [171]. Fig. 11e-f show the OM images of the resulting microspheres under transmission (e) and reflection (f) modes, respectively. The structural colors of the resulting microspheres can be modulated by the magnetic field during the synthesis process. Specifically, the microspheres displayed randomly orientations and random colors while no magnetic field was applied to the microspheres (as shown in Fig. 11g). The microspheres all exhibited a green hue when the same magnetic field (120 G) was imposed on the direction parallel to the view axis (as shown in Fig. 11h). Moreover, when a dynamical magnetic field, for example, the magnetic field was flipped between 170 G and 430 G with equal time duration within a single synthesis process, was imposed on the droplets, the individual microsphere showed either a green or blue hue depending on the magnetic field magnitude at the moment of its photopolymerization.

*2.2.2.2. Photonic microobjects using stimulus-responsive matrix materials.* Stimulus-responsive properties could impart photonic materials with unique characteristics, therefore broadening their applications. It is highly demanded that photonic microobjects can be endowed with stimulus-responsive properties. Despite the utilization of magnetic CPs as building blocks of photonic suspension or the addition of carbon black (CB) NPs (~23 nm) into photonic suspensions that could endow the resultant photonic microobjects with electro- or magnetic-responsiveness, the stimulus-responsive properties were monotonous [171,172]. An alternative approach was introduced to construct stimulus-responsive photonic microobjects by using stimulus-responsive matrix materials to immobilize CPs with or without stimulus-responsive properties. Those stimulus-responsive matrix materials can be either polymer hydrogels or mechano-responsive polymers, such as elastomers. Kanai and Weitz et al. reported the fabrication of thermoresponsive photonic hydrogel microspheres assisted by droplet microfluidics [132]. An aqueous suspension of mixtures, including highly charged PS CPs, NIPAAm monomers, crosslinker BIS, and photoinitiator, was injected into a glass capillary-based microfluidic device to generate monodispersed droplets (as illustrated in Fig. 12a). The aqueous suspension was preassembled and featured with photonic properties, leading to the resultant droplets with photonic characteristics. The PS CPs inside the droplets were immediately immobilized upon the UV light irradiation due to the polymerization and crosslinking of NIPAAm monomers, and consequently colloidal photonic hydrogel microspheres with thermoresponsive properties were obtained (as shown in Fig. 12b-d) [132]. In addition to the thermoresponsive photonic microspheres, Chen et al. reported the fabrication of humidity-responsive hydrogel photonic supraballs via microfluidics combined with post-UV irradiation-induced polymerization [173]. An aqueous suspension containing monodispersed PS CPs, acrylamide, BIS, and photoinitiator and a silicone oil solution with surfactant were used as the dispersed phase and continuous phase, respectively (as shown in Fig. 12e). Monodispersed droplets were produced from a PDMS-based microfluidic device and collected in a container to incubate the aqueous suspension at 20 °C for 10 h to partially evaporate water. After a certain amount of solvent evaporation, the droplets gradually exhibited structural colors due to the self-organization of PS CPs (as shown in Fig. 12f). The

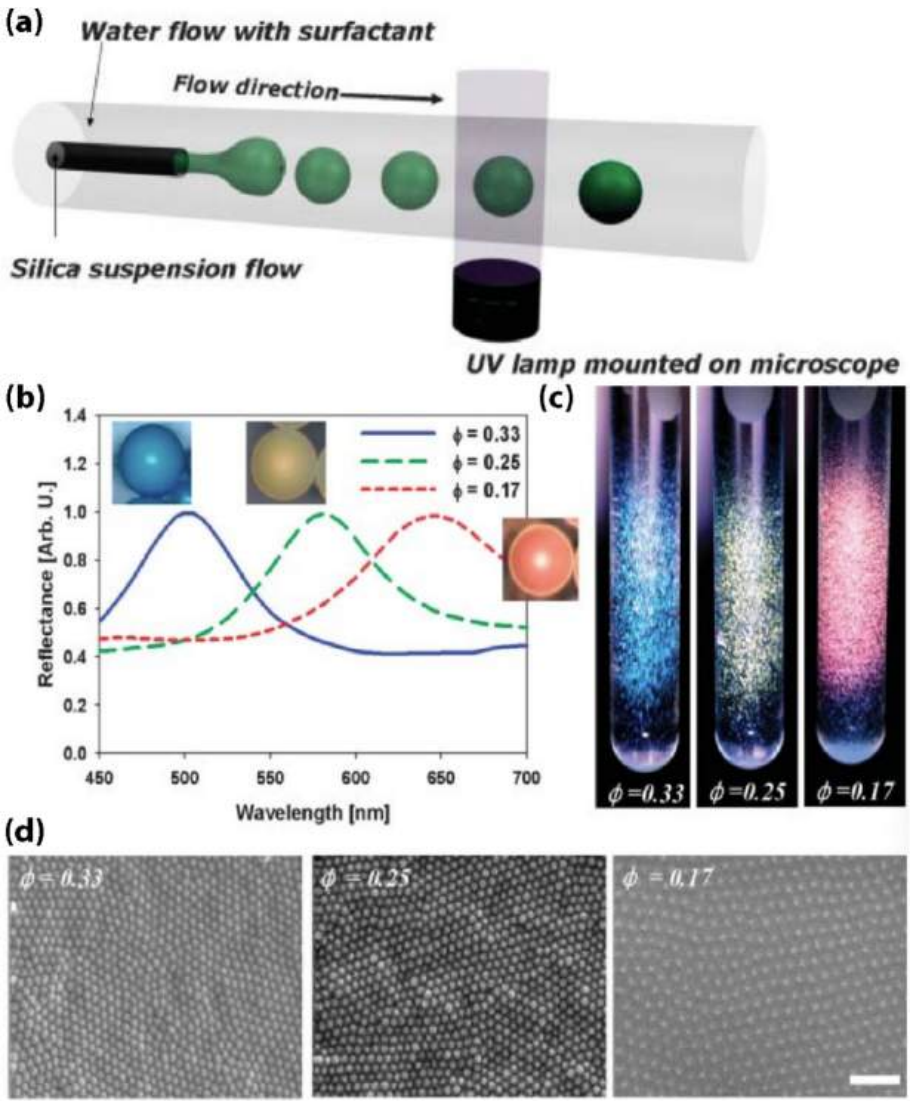


**Fig. 10.** (a) Illustration figure showing microfluidics generation of photonic microballs. Monodispersed photonic droplets containing photocurable resin ETPTA suspension of $SiO_2$ CPs were first produced at the tip of the microfluidic device and subsequently photocured to form the photonic microballs. (b). Microfluidics-fabricated photonic crystal microballs with different structural colors from blue and orange to red and their corresponding reflection spectra. The microballs use different volume fractions (0.33, 0.25, and 0.17) of photocurable resin ETPTA suspension of $SiO_2$ CPs. (c) Different colors of the photonic microballs' suspensions show vivid structural colors. (d) SEM images of the surfaces of the microballs indicated the microballs formed from different volume fractions of $SiO_2$ CPs showing different lattice spacings. [109]Reprinted from ref. 109 with permission from Wiley, copyright 2008. (For interpretation of the references to color in this figure legend, the reader is referred to the web version of this article.)

droplets were subsequently transformed into pAAm-based hydrogel photonic supraballs when subjected to UV light irradiation. The resultant supraballs showed reversible color change with humidity variations due to the pAAm-based hydrogel skeleton's humidity responsive property (as shown in Fig. 12g) [173,174]. Chu et al. adapted the similar approach and prepared thermochromic photonic microspheres using $Fe_3O_4$@PVP CPs and a mixture of NIPAAm and AM as the colloidal building blocks and matrix material, respectively [122].

Despite environment-responsive photonic microbeads having been constructed, sometimes it is also demanded to build photonic micro-objects with some other properties, such as mechanochromic properties. In this context, Kim et al. prepared photonic suspension using $SiO_2$ CPs as building blocks and photopolymerizable poly(ethylene glycol) phenyl ether acrylate (PEGPEA) resin precursor as the matrix material (as illustrated in Fig. 13a). To enhance the color saturations, polydopamine (PDA, ~ 100 nm) CPs were also added to the photonic suspension (as illustrated in Fig. 13b), which was subsequently emulsified by a silicone oil solution in a glass-capillary-based microfluidic device. Therefore, uniform photonic droplets were generated (as illustrated in Fig. 13c-d) and were subsequently transformed into photonic microbeads upon UV light irradiation. Therefore, microbeads with RGB structural colors can be obtained by varying the initial concentrations of $SiO_2$ CPs (as shown in Fig. 13f-h). The microbeads featured with a mechanochromic property due to the elastic nature of the polymerized PEGPEA resin [175]. These elastic photonic microspheres from the O/W emulsion droplets with high color saturation require pre-addition of light - absorbing additives, such as PDA NPs. In light of this, an alternative way with free addition of light absorbing materials was also developed to prepare photonic microspheres with high color saturation. In this manner, O/O emulsion droplets were used as the templates rather than the O/W emulsion droplet templates [176]. The PEGPEA suspension of $SiO_2$ CPs (volume fraction of 33 %) was used as the dispersed phase, while PEGPEA-saturated silicone oil solution was used as the continuous phase for microfluidics experiments to match the refractive index between the microbeads and the medium (as shown in Fig. 13i). This refractive index match between the microbeads and the medium eventually led to the

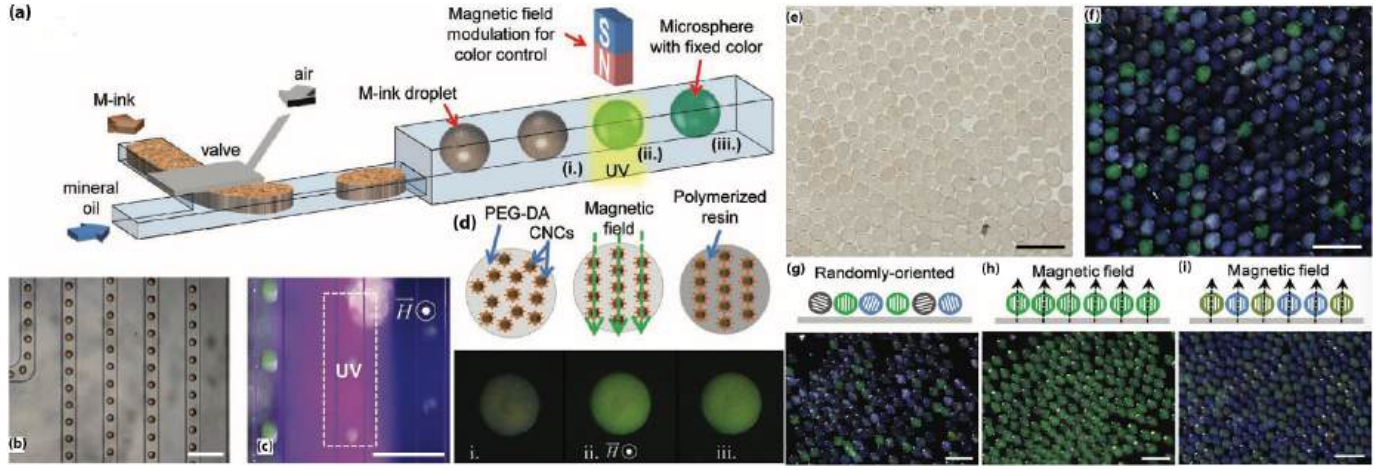


**Fig. 11.** (a) The schematic figure shows the on-chip microfluidics fabrication of hydrogel-based photonic microparticles with magneto-responsive properties. (b) OM image of the droplets inside the channel of the microfluidic device. (c) OM image of the magnetic tuning of the structural colors of the droplets and UV irradiation area (the dot-square region). (d) The illustration figure shows the step-wise view of the synthesis process. (d) OM image (transmission mode) of the resulting photonic hydrogel microspheres. (e)-(f) OM image (g, transmission mode) and OM image (h, reflection mode) of the resulting photonic hydrogel microspheres. (g)-(i) Illustration figures of the different orientations of the microspheres under different types of magnetic field effects and the OM images of the resulting microspheres [171]. Reprinted from ref. 171 with permission from Wiley, copyright 2011.

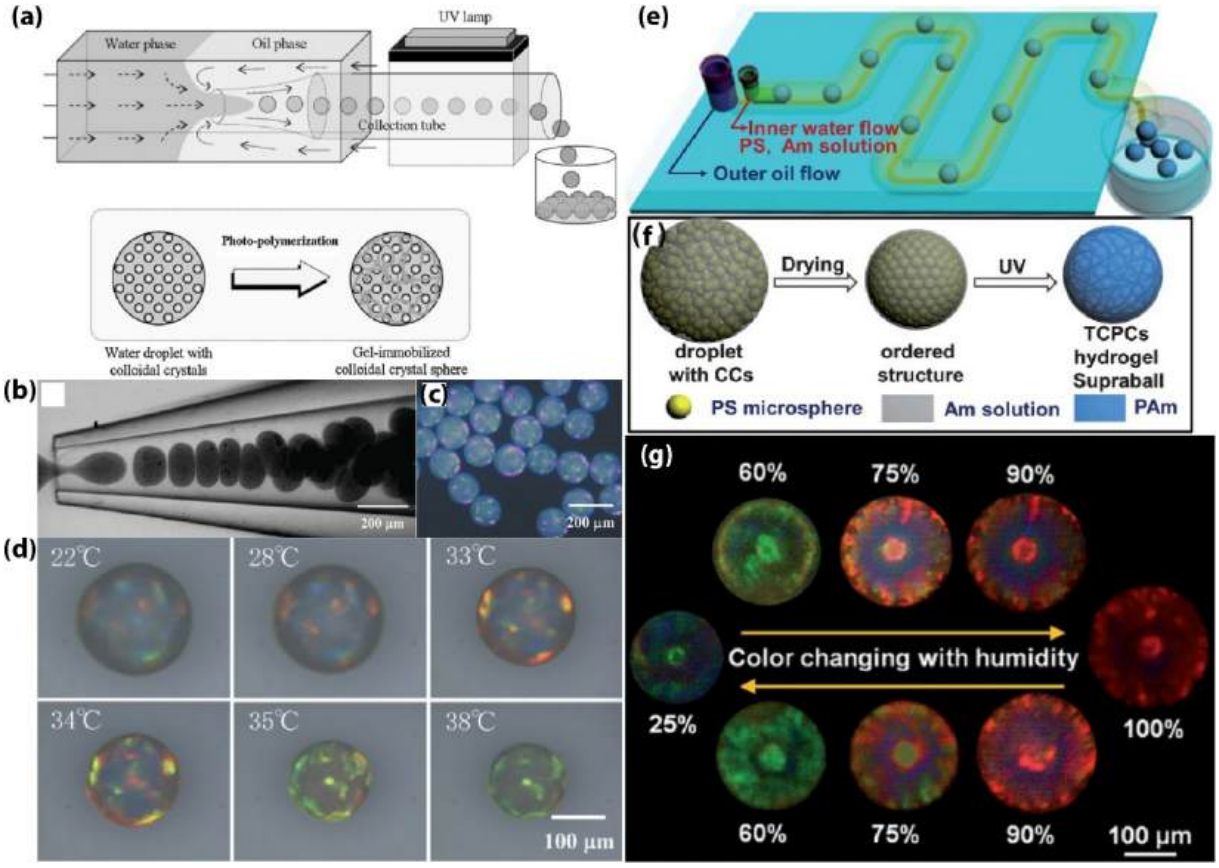


**Fig. 12.** (a) The illustration figure shows the microfluidics fabrication of pNIPAAm hydrogel-based photonic crystal microspheres using charged PS NPs and photocurable NIPAAm monomers as building blocks and matrix materials, respectively. (b)-(c) OM image of the microfluidics process and the resulting photonic hydrogel beads (c). (d) OM images show the thermoresponsive behavior of the photonic hydrogel beads [132]. Reprinted from ref. 132 with permission from Wiley, copyright 2010. (e). Illustration figure shows the fabrication of monodispersed droplets of aqueous suspension of PS CPs, precursor reagents for hydrogel matrix, through a PDMS-based microfluidic. (f) Cartoon figure shows the evolution of colloid-containing droplets, the evolution into colloidal crystal arrays, and the subsequent formation of colloidal crystal hydrogel microspheres by a UV-mediated crosslinking process. (g) OM images show the reversible color change of the colloidal crystal hydrogel microsphere upon the stimulus of humidity [173]. Reprinted from ref. 173 with permission from the Royal Society of Chemistry, copyright 2013.

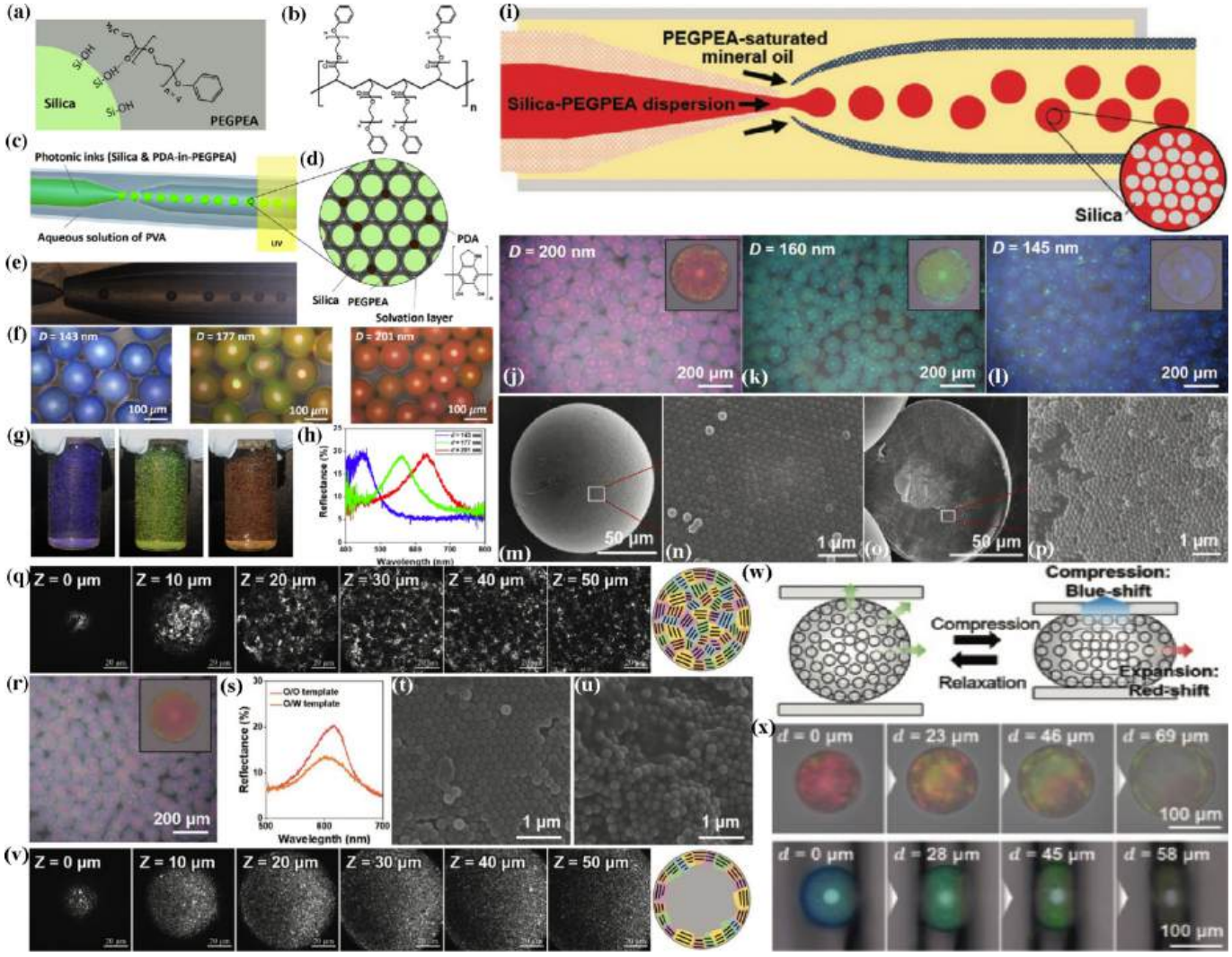


**Fig. 13.** (a) The illustration figure shows the hydrogen bond interaction between the acrylate group of the PEGPEA and the silanol group in the silica surface. (b) The illustration figure shows the chemical structure of the polymerized PEGPEA resin. (c) The illustration figure shows the microfluidics fabrication of elastic photonic microbeads. (d) The illustration figure shows the compositions of the droplet precursor. (e) OM image of the microfluidics fabrication process. (f) OM images of the elastic photonic microspheres with different colors from blue (left), orange (middle) to red(right). (g) Photographs of aqueous suspensions of the different colors of the photonic microspheres. (h) Reflection spectra of different colors of the photonic microspheres [175]. Reprinted from ref. 175 with permission from the American Chemistry Society, copyright 2020. (i) The illustration figure shows the fabrication of elastic photonic microbeads formed from O/O emulsion templates. (j)-(l) OM images of photonic microbeads with different colors. (m)-(p) SEM images of the surface and cross-section and their corresponding enlarged SEM images of the photonic microbeads formed from O/O emulsion templates. (q) *Z*-direction confocal microscope images of a cross section of microbeads formed from O/O emulsion droplet templates. (r). OM image of red photonic microbeads templated by O/W emulsion droplets. (s) Reflection spectra comparison of red photonic microbeads using O/O and O/W emulsion templates, respectively. (t)-(u) SEM images of the surface (t) and cross-section (u) of the O/W templated red microbead. (v) Z-direction confocal microscope images of a cross section of microbeads formed from O/W emulsion droplet templates. (w) The illustration figure shows a microsphere's mechanochromic property. (x) OM images of a microsphere's reversible color change property [176]. Reprinted from ref. 176 with permission from Wiley, copyright 2022. (For interpretation of the references to color in this figure legend, the reader is referred to the web version of this article.)

color saturation of the resulting microbeads templated from O/O emulsion droplets with better performances than that of the microbeads templated from the O/W emulsion system. The structural colors of the microbeads were tuned by using different diameters of $SiO_2$ CPs as the building blocks. For example, $SiO_2$ CPs with diameters of 200 nm, 160 nm, and 145 nm were used as the building blocks for producing microbeads with red, green, and blue colors, respectively (as shown in Fig. 13j-l). It is worth mentioning that OM images showing the entire individual microbead were full of tiny crystallites due to the homogeneous crystallization within the microbeads. SEM and confocal microscopy images unveiled that both the interior and interface parts of microbeads produced from O/O emulsion droplets are full of crystallites (as shown in Fig. 13m-q). While the ordered crystallites only exist at the interface of the microbeads that were produced from the O/W emulsion droplets (as shown in Fig. 13r-v). Consequently, the microbeads from O/O emulsion templates display a more intense reflection spectrum than that of the microbeads from the adversary case (as shown in Fig. 13s). SEM images further verified that interior parts of the two different microbeads showed different orderliness, where microbeads from the O/O emulsion droplets had better orderliness (as shown in Fig. 13o-p) than that of the microbeads from the O/W emulsion droplets (as shown in Fig. 13u). Due to the deformable property of the polymerized PEGPEA matrix, the microbeads were subsequently endowed with reversible mechanoresponsive property when compressed between two glass slides (as illustrated in Fig. 13w). As a result, the vertical and horizontal directions of the microsphere were respectively subjected to a blue-shift and red-shift when compressed. (as shown in Fig. 13x). These phenomena were due to the decreased and increased lattice spacing in the

vertical and horizontal directions caused by the compression process. This property can be further utilized for the construction of mechanoresponsive pattern structures. The same strategy was also used to fabricate photonic microcapsules using ETPTA suspension as the photonic core and PEGDA hydrogel as the shell. The photonic microcapsules feature =enhanced color saturation when compared with that of the photonic microspheres possessing the same photonic suspension but without the hydrogel shell [177].

## 3. Photonic microspheres with anisotropic photonic properties

### 3.1. Photonic microspheres with janus or multicompartment structures

Despite the above-mentioned reports having successfully achieved the manufacturing of colloidal-based photonic microobjects, they still lacked multifunctionality. To endow the microobjects with multifunctionalities, one strategy is to integrate different components into individual microobjects, such as the generation of colloidal photonic microobjects with Janus or multicompartment structures. Gu and Zhao et al. reported the construction of photonic microobjects with Janus structure via microfluidics in a facile manner (as shown in Fig. 14) [178]. The microfluidics strategy in the study was, in its simplest form, to use single emulsions as the templates, where the continuous phase and dispersed phase were silicone oil and an aqueous suspension of a mixture containing $SiO_2$ CPs and ultrafine magnetic $Fe_3O_4$ NPs (12 nm), respectively (as shown in Fig. 14a). The droplet templates were collected in a container and subjected to a magnetic field stimulus from the bottom-up direction. The synergistic effect of droplet evaporation and magnetic field induced the aggregation of magnetic NPs at the bottom part of the resulting supraparticles, yielding photonic supraparticles with a Janus configuration (as shown in Fig. 14b). The resulting Janus supraparticles displayed different structural colors and reflection spectra (as shown in Fig. 14c-f). Meanwhile, due to the aggregation of magnetic NPs at one pole, the resulting Janus supraparticles displayed magnetic field-controlled rotation (as shown in Fig. 14 g). As a consequence, the suspension of the photonic supraparticles displayed different macroscopic phenomena (as shown in Fig. 14 h-j). This concept was also applied to construct Janus photonic supraparticles by using two different shapes of CPs, such as $SiO_2$ spheres and $Fe_3O_4$@$SiO_2$ (core/shell) ellipsoids, as building blocks through droplet microfluidics. Le et al. adopted such a kind of strategy and prepared droplets of an aqueous suspension of a mixture of spherical CPs and nanoellipsoids [179]. The droplets were evaporated under a magnetic field at room temperature. The magnetic field induced the phase separation of the two different shapes of colloids and consequently resulted in the formation of Janus photonic supraparticles after evaporation of water (as illustrated in Fig. 14k). As a result, the two sides of the resulting supraparticles displayed two different colors (as shown in Fig. 14l). SEM images further verified the phase-separated two parts, and a clear boundary formed at the interface (as shown in Fig. 14m-o). The ratio of the two parts of the individual microsphere can be regulated by varying the initial volume fraction of $Fe_3O_4$@$SiO_2$ and $SiO_2$ CPs (as shown in Fig. 14p-r). Additionally, the motion behaviors of the photonic microspheres can be tuned by an external magnetic field (as illustrated and shown in Fig. 14s-v).

Besides the external magnetic field-guided formation of photonic Janus supraparticles from the droplets containing homogeneously distributed CPs, Shui and Eijkel et al. introduced another approach to generate photonic microballs with a flower-like cap made of nanowires, which enabled individual photonic microballs with a smooth part and a relatively rough part (as shown in Fig. 15) [180]. To produce such microobjects, microfluidics was firstly used to generate uniform-sized droplets of aqueous suspension of $SiO_2$ CPs. The droplets were subsequently evaporated to form close-packed and solidified $SiO_2$ CP-based photonic crystal supraparticles, which were further coated with an Au film on the top part of the supraparticles through a deposition process. Followed by a high-temperature annealing process, which could trigger Si-based nanowire (NW) growth on the surface of the supraparticles, therefore, transforming the supraparticles with different surface morphologies (as shown in Fig. 15a). Specifically, photonic crystal microobjects with a 'flower-like' NWs cap and $SiO_2$ CPs lattice bottom part (as shown in Fig. 15b). The resulting photonic microobjects formed from different diameters of $SiO_2$ CPs then displayed different photonic properties, such as blue shift of the Bragg diffraction peaks after the annealing process. This was due to the synergistic effect of the narrow nanogaps of adjacent $SiO_2$ CPs and the refractive index change of the variation of Si and air (as shown in Fig. 15c). Furthermore, after being subjected to treatment with hydrophobic silanes, such as perfluorodecyltrichlorosilane, the flower-like NWs-capped microobjects displayed a remarkable superwettability to oil compared to that of the non-annealing treated photonic microobjects (as shown in Fig. 15d-e).

Simply by redesigning the microfluidic device and introducting two parallel streams into the microfluidic channels, photonic microballs with anisotropic photonic properties can be obtained (as shown in Fig. 16a-c) [109]. However, these microballs lack stimulus-responsive properties due to the fact that both the $SiO_2$ building blocks and the resin are non-stimulus-responsive materials, limiting their application scopes. In this regard, Yang et al. introduced smaller carbon black (CB) NPs (~ 23 nm) into the ETPTA suspension of $SiO_2$ CPs and manufactured Janus photonic microballs through a multi-bore capillary-based microfluidic device. Therefore, the Janus microballs can be consequently rendered with electroresponsive properties due to the incorporation of the electroconductive CB NPs (as shown in Fig. 16d-e) [172]. The matrix composition of the two faces' of the Janus structure is both ETPTA resin, which makes the CB NPs cover the majority of the Janus ball's surface due to viscosity mismatch, where the CB NPs' higher diffusivity than that of the $SiO_2$ NPs (as shown in Fig. 16f). The Janus microballs were further used as building blocks for secondary assembly within a PDMS matrix to generate a *Gyricon* display, which enabled the microballs to show electrical actuation (as shown in Fig. 16g-h) [172]. To integrate multiple photonic properties on an individual photonic microball, Gu et al. utilized a quad-channel microfluidic device to produce microballs with compartmental structural colors, including Janus, three-compartment, and even quad-compartment particles (as shown in Fig. 16i-j) [181]. These multicompartmental colors were achieved through injecting different colors of ETPTA suspension of $SiO_2$ CPs into the quad-channel microfluidic device and subsequently generating the multicompartmental microobjects upon UV light irradiation (as shown in Fig. 16k-p). The similar concept was also applied in Kim and Yang's report in a separate study to generate patterning structures [182]. To endow the microobjects with magnetic responsiveness, an ETPTA suspension of α-$Fe_2O_3$ magnetic NPs (< 50 nm) was used as one compartment composition for the microfluidic experiments. Due to the matrix materials of these Janus or multicompartmental structures, photonic microballs are all the same, which is the ETPTA resin; the resulting Janus or multicompartmental structures can be simply controlled by the flow rates of each photonic stream. However, both examples require the synthesis and purification of $SiO_2$ CPs with different diameters or the preparation of different concentrations of $SiO_2$ CPs to produce photonic suspensions with different structural colors, complicating the microobjects' fabrication process. Moreover, instead of using different photonic suspensions to construct Janus or multicompartmental photonic microobjects, Hu et al. brought out an approach to construct Janus photonic microobjects formed from single photonic suspension [183]. To fabricate the Janus photonic microobject, spherical photonic microspheres composed of photonic suspension of single-sized $SiO_2$ CPs were fabricated from microfluidics. The microspheres were embedded into a PS film by a solvent evaporation method, through which one part of each microsphere was embedded in the PS film while the other part was exposed to the air. The uncovered part of the microsphere can be subsequently etched by HF solution with a controlled period (illustrated in Fig. 16q). Therefore, each photonic microsphere integrating both the

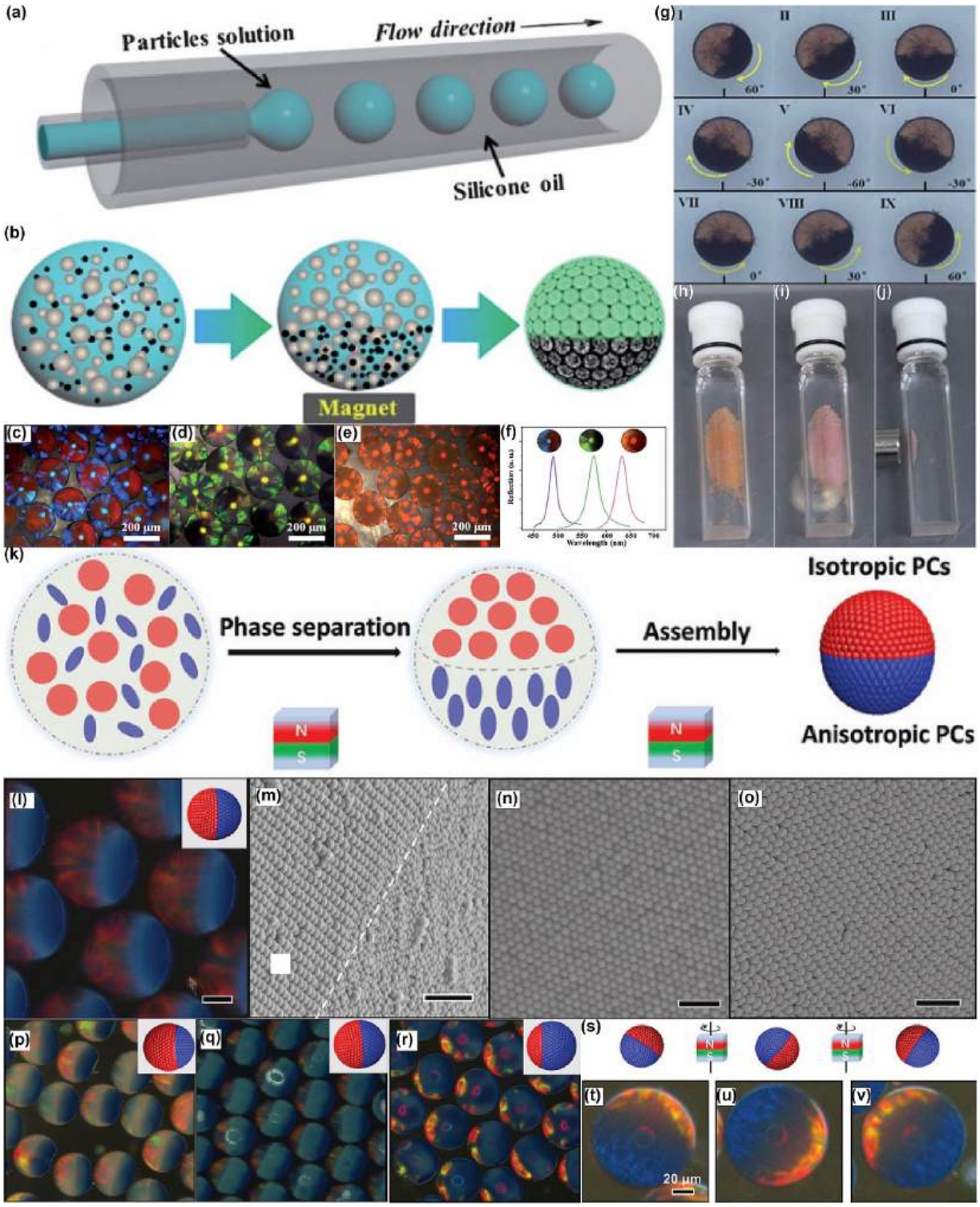


**Fig. 14.** (a) The illustration figure shows the fabrication of single emulsion droplets using a co-flow microfluidic device. (b) The illustration figure shows how the droplets of aqueous suspension of two different CPs with homogeneous distributions evolve into a Janus structure. (c)-(f) OM images of Janus microparticles with different structural colors (c-e) and their corresponding reflection spectra (f). (g). Magnetic field-controlled rotation of the Janus microparticles. (h)-(j) Photographs of the Janus microobjects under different directions of magnetic field stimulus [178]. Reprinted from ref. 178 with permission from the Royal Society of Chemistry, copyright 2013. (k) The illustration figure shows microfluidics-assisted fabrication of Janus photonic supraparticles based on two different shapes of CPs. (l) OM image of the resulting Janus supraparticles with their two sides showing blue and red colors. (m)-(o) SEM images of different regions of the photonic supraparticles in (l). (p)-(r) OM images show the different ratios of the two sides of the supraparticles. (s)-(v) Illustration figure(s) shows the magnetoresponsive behaviors of the supraparticles and their corresponding OM images under the effect of magnetic field(t-v) [179]. Reprinted from ref. 179 with permission from the Royal Society of Chemistry, copyright 2021.

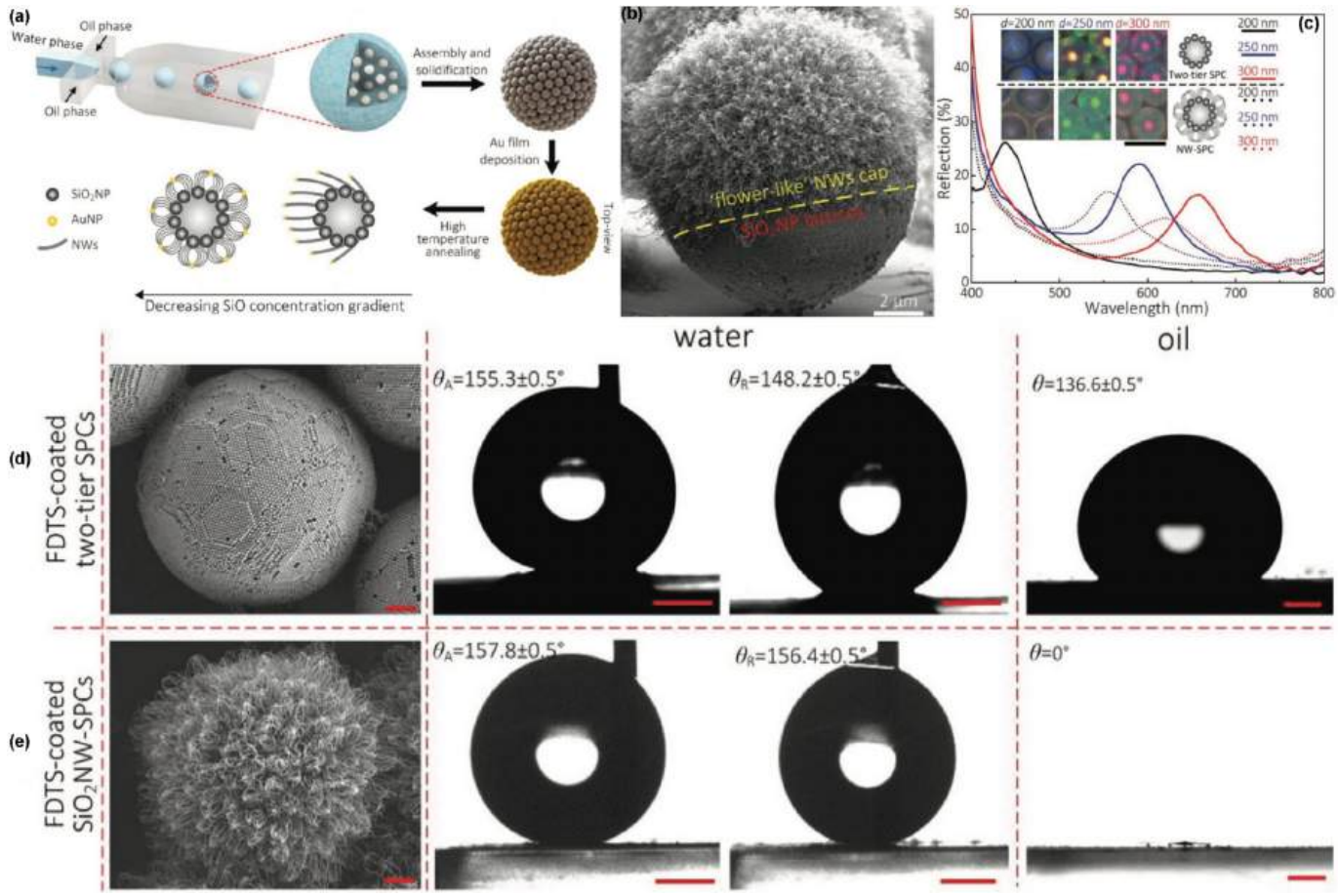


**Fig. 15.** (a) The illustration figure shows the fabrication of close-packed $SiO_2$ NPs-based photonic supraparticles and the subsequent generation of photonic microobjects with different surface morphologies. (b) SEM image of a photonic microobject with a 'flower-like' Nanowires (NWs) cap and a $SiO_2$ CPs lattice bottom part. (c) Reflection spectra of the microobjects formed from different diameters of $SiO_2$ CPs and with different surface morphologies. (d)-(e) Comparison of the super-wettability of two different kinds of photonic microparticles on a fused Si substrate: microparticles of self-assembled $SiO_2$ CPs and the microparticles that were further coated with Si-NWs. Clearly, the microparticles coated with Si-NWs displayed remarkable oil wettability [180]. Reprinted from ref. 180 with permission from Wiley, copyright 2020.

inverse opal and opal structures can be generated. The initial isotropic microsphere was subsequently transformed into a microsphere with anisotropic properties; for example, the microsphere with an initial single reflection peak was turned into a microsphere possessing two reflection spectra peaks (Fig. 16r-u). Similarly, this strategy was also used to prepare bullet-like photonic microobjects with dual stopbands and tunable structural configurations [184]. This approach refrained from the synthesis of CPs with different diameters or different compositions as compared with that of other methods.

The above-mentioned compositions inside the different photonic microparticles were relatively facile to control given that the matrix materials of the photonic streams are almost identical (both matrix materials were ETPTA resin) regardless of the dispersed CPs. While in some more complicated cases, the nature of photonic compositions may be completely distinct; for example, one phase of the photonic composition is hydrophilic and the other phase is hydrophobic. When the two distinct photonic compositions were emulsified by another immiscible phase (such as silicone oil with surfactant), it involved more complicated parameters for the generation of microobjects with isotropic properties. In this regard, Chen et al. utilized a PDMS-based triphasic co-flow microfluidic device to manufacture Janus photonic microobjects. The two sides of the microobjects were a hydrophobic photocurable resin and a hydrophilic aqueous suspension of PS CPs (208–256 nm), respectively, while silicone oil was used as the continuous phase (as illustrated and shown in Fig. 17a-e) [110]. Unlike other previous reports, where the configurations of the Janus microobjects were controlled by flow rates, the configurations of the photonic microobjects in this study were manipulated by the spreading parameter $S$ among the three phases. That being said, the configurations were controlled by the interfacial tensions between any given two different phases involved in the experiments (as illustrated in Fig. 17a). Except for the configuration control, the microobjects were also functionalized with magnetic properties by premixing magnetic $Fe_2O_3$ NPs (< 50 nm) with the photocurable resin phase in the suspension preparation step. The resulting colloidal photonic crystal (CPC) supraparticles with Janus structure were further used as building blocks for the construction of magnetic field-manipulatable pattering structures (Fig. 17f-h). The structures varied from crescent, meniscus, and ellipsoid to spherical through precise control of the interfacial tensions. Except for the configuration control, the similar microobjects using poly (tert-butyl acrylate) (P(t-BA) colloids as the building blocks were also functionalized with magnetic properties by premixing $Fe_3O_4$@C CPs (199 nm) with the photocurable resin phase. The resulting Janus colloidal photonic crystal (CPC) supraparticles were further used as building blocks for the construction of magnetic field-manipulatable pattering structures and energy-saving displays (as illustrated in Fig. 17i) [185,186]. Despite this, the resulting CPCs lacked dual structural colors on an individual CPC microball. To further leverage this strategy, individual CPC supraparticles integrating two distinct structural colors were constructed (as shown in Fig. 17j). In this case, monodispersed PS CPs (240 nm) and

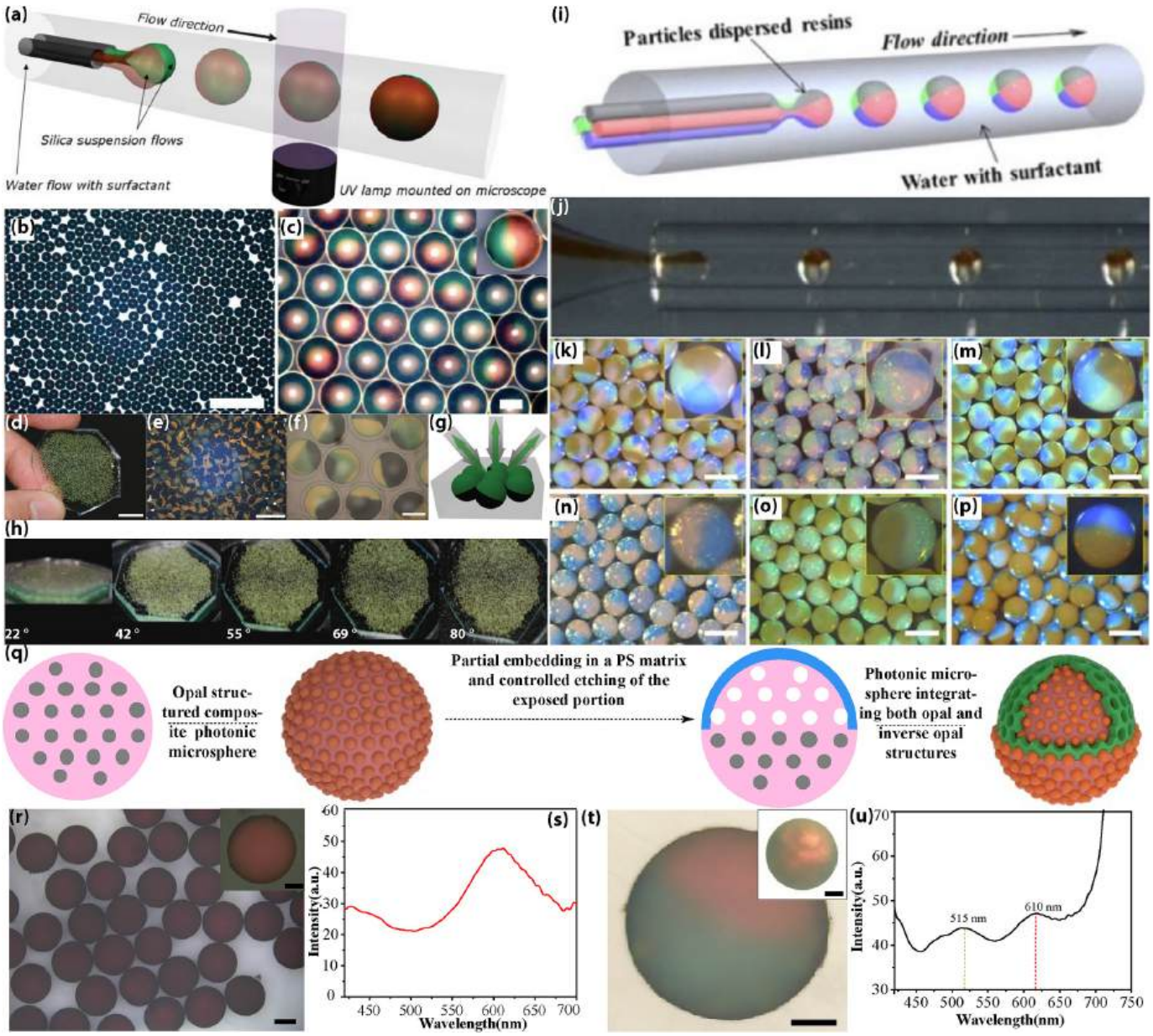


**Fig. 16.** (a) The illustration figure shows the fabrication of Janus photonic microballs using a microfluidic device with parallel channels. Different concentrations of ETPTA dispersions of silica CPs were used as the parallel streams of the photonic compositions. (b)-(c) OM images of Janus photonic microspheres with low (b) and high (c) magnifications [109]. Reprinted from ref. 109 with permission from Wiley, copyright 2008. (d)-(f). OM images of the resulting electroresponsive Janus photonic crystal microballs in a PDMS matrix (d) and their corresponding microscopy images at low (e) and relatively high (f) magnifications (e)-(f). (g) The illustration figure shows the angle-independent structural colors of the Janus photonic microballs. (h) The microballs are embedded in a PDMS matrix and viewed at different angles of observation [172]. Reprinted from ref. 172 with permission from Wiley, copyright 2008. (i)-(j) The illustration figure and OM image show the fabrication of multicompartmental photonic microballs through a glass capillary-based microfluidics device with quad-channels. (k)-(p) OM images of the multi-compartmental photonic microballs with different combinations of resin suspensions [181]. Reprinted from ref. 181 with permission from the American Chemistry Society, copyright 2013. (q) The illustration figure shows the generation of a Janus photonic microsphere using a partial etching method. (r-s) OM image of red photonic microspheres and the corresponding reflection spectrum. (t-u) OM image of a Janus microsphere integrating both opal and inverse opal structures using the partial etching method and the corresponding reflection spectrum [183]. Reprinted from ref. 183 with permission from Elsevier, copyright 2024. (For interpretation of the references to color in this figure legend, the reader is referred to the web version of this article.)

$Fe_3O_4$ CPs (150 nm) were used as the building blocks of the two hemispherical parts, respectively. A magnetic field was also introduced to tune the alignment of the $Fe_3O_4$ NPs in the resin phase. The arrangement of the $Fe_3O_4$ CPs can be either parallel to the J-1 type Janus microball or vertical to the J-2 type microball (as shown in Fig. 17k-l). The two parts displayed distinct surface morphologies, given one part was covered with resin and the other part was full of bare PS CPs (as shown in Fig. 17m-n). Furthermore, the photonic properties of the J-1 type supraballs can also be regulated by adjusting the intensity of the visible light. For example, a supraball is initially composed of a dim green hemisphere and a bright red hemisphere. The dim green part gradually turned to bright green, while the bright red part transitioned to white due to overexposure when the intensity of the incident light was increased (as shown in Fig. 17o). However, in terms of the reflective intensities, the intensity of the red (94 %) part is almost four times that of the green (23 %) part (as shown in Fig. 17p). This distint intensity difference was especially important for designing day/night dual-viewed bead-based panel displays. Due to the incorporation of

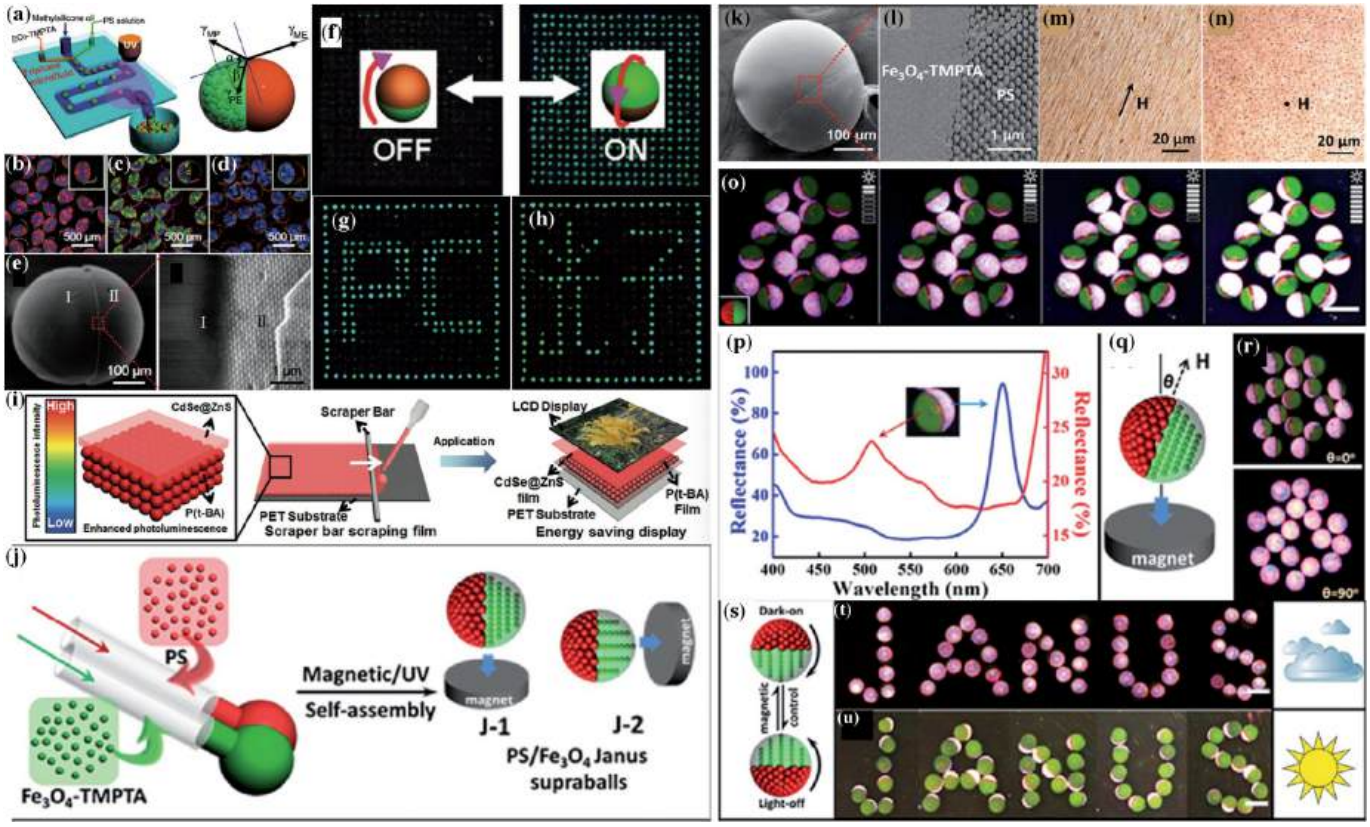


**Fig. 17.** (a) The illustration figure shows the fabrication of Janus photonic microobjects using photonic suspensions of two different properties: one suspension is hydrophilic and the other is hydrophobic; (b-d) Janus photonic microobjects using different diameters of PS CPs as building blocks; (e) SEM image of a colloid-based Janus supraparticle (left) and an enlarged figure of the equator region of the supraparticle. (f) The illustration figure shows the face-switch of the Janus photonic microobject. (g)-(h) Two different patterns formed from the assembling of the Janus photonic microobjects [110]. Reprinted from ref. 110 with permission from Wiley, copyright 2012. (i) The schematic figure show the Janus photonic microobjects were used as building blocks for secondary assembly to generate energy-saving displays [185]. Reprinted from ref. 185 with permission from Wiley, copyright 2019. (j) The illustration figure shows the fabrication of Janus photonic supraparticles using a parallel two-channel microfluidic device, where the parallel two streams were TMPTA resin suspension of magnetic $Fe_3O_4$ CPs and aqueous suspension of PS CPs, respectively. (k)-(l) SEM image of a Janus supraparticles (k) and magnified SEM image of the equator region (l). (m)-(n) OM images of the magnetic CPs with different alignments. (o) OM images of the Janus supraparticles show different structural colors under different intensities of illumination light. (p) Reflection spectra of the Janus supraparticles. (q) The illustration figure shows the magnetic field induces the rotation of the Janus supraparticles. (r) Microscopy images show the Janus supraparticles under the impact of a magnetic field. (s) OM images of the pattern 'Janus' formed by the assembly of Janus supraparticles, and the pattern was adjusted by an external magnetic field [187]. Reprinted from ref. 187 with permission from the Royal Society of Chemistry, copyright 2014.

magnetic CPs into the microball, the orientations of the microballs can be regulated by adjusting the $\theta$ values, which represent the angle between the magnetic direction and the initial CNC chain angles as indicated in Fig. 17q. Furthermore, by leveraging the combination effect of magnetic-field manipulation capability (as illustrated in Fig. 17s) and the incident light regulation property, the microballs canserve as pixel units in a bead display whose properties can be tuned by magnetic field and visible light intensity (as shown in Fig. 17t-u).

Although the above-mentioned Janus photonic microobjects can be functionalized with magnetic properties, the superparamagnetism from the magnetic CPs normally shows a slow response, which results in the lack of simultaneous control over distinct photonic properties of the Janus balls. This was due to a weak magnetic moment generated by an external field. To overcome the shortcomings, Kim et al. reported the fabrication of Janus photonic microballs with a controlled magnetic moment and density asymmetry through a microfluidics-assisted approach [188]. To produce the Janus balls, a theta configuration capillary-based microfluidic device was employed in the study. ETPTA suspension of silica CPs and silicone precursor suspension of CB (~ 24 nm) and barium ferrite (~ 100 nm) NPs were injected into the theta capillary, simultaneously; the two streams were emulsified by an external aqueous phase to generate two-compartment Janus droplets, which were subsequently transformed into Janus microspheres upon UV light irradiation (as illustrated in Fig. 18a). The droplets were further subjected to a series of procedures, including self-alignment of the two paired compartments due to the density difference, alignment of the barium ferrite NPs under an external field, and photopolymerization of the droplets (as illustrated in Fig. 18b). Simply by changing the concentrations of silica CPs in the ETPTA suspensions, the structural colors of the ETPTA part of Janus balls can be varied from red to green to blue, while the silicone resin part remains black (as shown in Fig. 18c). The orientations of the Janus photonic balls can be regulated by changing the directions of the magnetic fields: upwards, parallel to the substrate, and downward (as illustrated in Fig. 18d). As a result, different-colored Janus balls showed different color patterns upon the effect of the external magnetic field, demonstrating a permanent magnetic moment (as shown in Fig. 18e-g).

In addition to designing and producing Janus microobjects purely with photonic properties, photonic microobjects with some other properties, such as plasmonic properties, were also conceived and manufactured [189]. Plasmonic structural colors as emerging characteristics have been studied [190,191]. Kim et al. reported the fabrication of Janus microobjects integrated with photonic property and plasmonic property simultaneously via a Pickering emulsion-templated microsphere combined with CPs' etching and metallic coating process [192]. The fabrication process involved three steps: Firstly, fabrication of

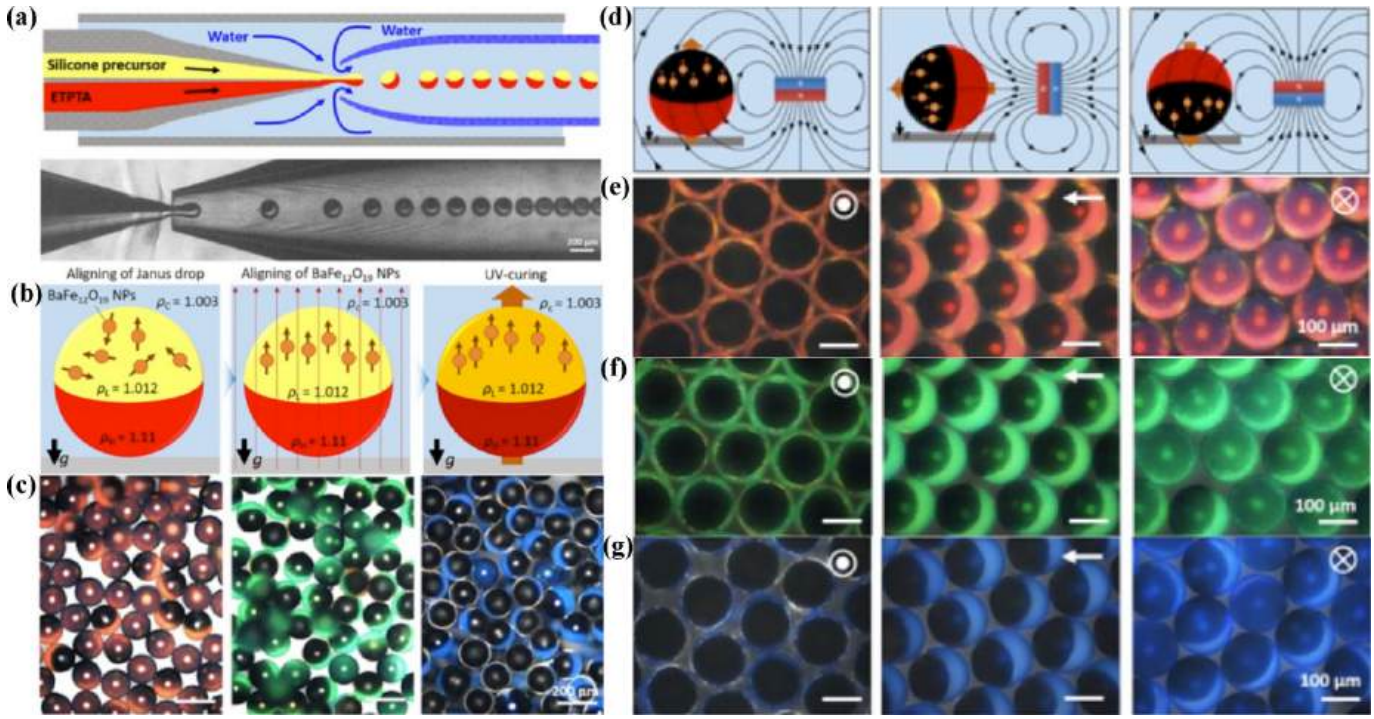


**Fig. 18.** (a) Top: The illustration figure shows the microfluidics fabrication of Janus photonic microspheres with superparamagnetic properties using a microfluidic device with a theta channel; Bottom: The OM image shows the microfluidics process. Silicone precursor and ETPTA resin were used as the two components for the Janus droplets. (b) Illustration figures showself-alignment of the Janus droplets under the effect of gravity (left), alignment of magnetic NPs under a magnetic field (middle) and photopolymerization of the Janus droplets (right). (c) OM images of Janus balls with the ETPTA resin part having different structural colors: red (left), green (middle) and blue (right). (d) Illustration figures show the different orientations of the Janus balls under different directions of the external magnetic fields. (e)-(g) OM images of different-colored Janus balls show different orientations under different directions of the magnetic fields [188]. Reprinted from ref. 188 with permission from the American Chemistry Society, copyright 2020. (For interpretation of the references to color in this figure legend, the reader is referred to the web version of this article.)

Pickering emulsion droplet templates using ETPTA resin suspension of $SiO_2$ CPs (volume fraction was ~33 %) as the compositions for droplets. When incubated in an aqueous collecting solution for a certain period, a layer of $SiO_2$ CPs gradually migrated towards the surface and anchored on the surface of the microspheres [66,109]. Secondly, $SiO_2$ CPs were removed by the HF etching, resulting in the formation of porous resin microspheres. Periodic cavities were left behind after the HF etching of the surface layer of $SiO_2$ CPs. Finally, the upper hemisphere of the microspheres was subsequently sputtered with noble metals, such as Au, leading to the formation of periodic metal nanostructures that could generate plasmonic colors [190]. These procedures are illustrated in Fig. 19a. The microobjects at different stages (from stage ① to ③) displayed different colors: for example, the $SiO_2$ CPs-filled microspheres with an initial red hue (Fig. 19b left panel) were transformed into a green hue (Fig. 19b middle panel) after the $SiO_2$ CPs were etched by the HF and eventually exhibited a red hue (Fig. 19b right panel) after deposition with a layer of 50 nm-thick gold. Correspondingly, the reflection spectrum peak values of the microsphere at stages ① and ② were approximately 597 nm and 536 nm, respectively (as shown in the left panel of Fig. 19c). This blue shift was due to the porous microsphere possessing a smaller refractive index (effective refractive index of PETPTA resin and air) than that of the microsphere (effective refractive index of PETPTA resin and $SiO_2$ CPs) prior to the etching process. Moreover, due to the deposition of the 50 nm thick gold layer (at stage ③), the reflection spectrum from the photonic structure was completely suppressed, as there was no trace of reflection spectrum peak signal from the photonic structure. The entire surface of the microsphere was covered with a hexagonal array of dimples due to wet etching (as shown in Fig. 19d). The top hemisphere of the microspheres was then covered with a thin layer of gold under the influence of sputter coating. Therefore, the microspheres either displayed plasmonic color from the gold coating or photonic color depending on the orientation of the microspheres (as shown in Fig. 19e). Furthermore, due to the coated Au layer being conductive, the microsphere arrays exhibited electric tunable properties and were further used as building blocks for electric manipulable displays (as shown in Fig. 19f).

## 4. Colloid-based structurally anisotropic photonic microobjects

The fabrication of colloidal photonic microobjects through microfluidics normally requires the generation of droplet templates from the microfluidic device. The prepared droplet templates were all spherical in shape under normal conditions due to the minimization of interfacial energy [193]. Therefore, the resultant microobjects inherited the spherical shape when no external intervention was involved in the fabrication process. However, colloidal photonic microobjects with nonspherical shapes may possess advantages over spherical counterparts [194,195]. In this regard, researchers have conceived various approaches to prepare colloidal photonic microparticles with nonspherical shapes. Borrowed from an idea of evaporation of droplets of CPs' suspension at an interface, which could induce the evolving of the droplets into nonspherical photonic superparticles [54], Xu et al. brought an approach to generate colloidal photonic microparticles with dimpled structures by using microfluidics-fabricated gas-containing droplets as templates (as shown in Fig. 20a) [195,196]. This strategy utilized gas-containing droplets of aqueous suspension of PS CPs as templates, together with a solvent extraction method, which consequently enabled the droplets to evolve into colloidal photonic structures with different irregular shapes. By controlling the gas portion of the individual gas-containing droplet templates, the shapes of the resultant photonic microobjects ranged from plate-like and bowl-like to tomato-like, all of which featured a dimpled structure (as shown in Fig. 20b). More

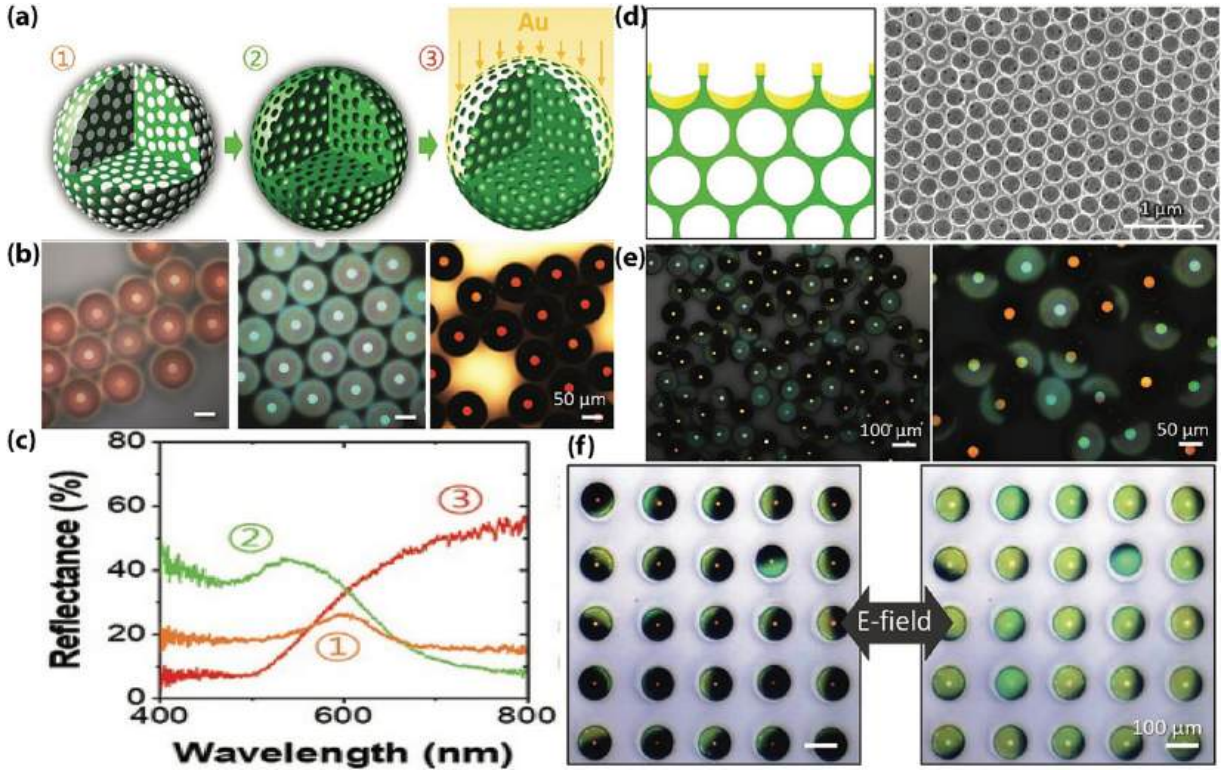


**Fig. 19.** (a) Illustration figure showing the fabrication of photonic microobjects with plasmonic properties under a series of different statuses: ① composite microsphere; ② porous microsphere; ③ Janus microobjects via direct deposition of Au coatings. (b) From left to right, the OM images of the microobjects corresponding to the procedures in (a). (c) Reflection spectra of a single microobject measured at different steps in (a). (d) The illustration figure shows the surface and cross section of the gold-deposited microsphere (left panel) and a scanning electron microscope (SEM) image of the hexagonal arrays of dimples on the surface (right panel). (e) OM images of the randomly oriented Janus microspheres at low (left) and higher (right) magnifications. (f) OM images show the collective behavior of the orientation of the Janus microsphere array under an alternative electric field [192]. Reprinted from ref. 192 with permission from Wiley, copyright 2022. (For interpretation of the references to color in this figure legend, the reader is referred to the web version of this article.)

importantly, the resulting colloidal photonic microparticles with nonspherical shapes exhibited stronger reflection intensities than that of the spherical colloidal photonic microparticles (as shown in Fig. 20c-d). Despite these achievements, the resulting microobjectse still lacked stable mechanical properties, limiting their further applications. Gu et al. utilized the on-chip confining effect of microfluidic channels to generate rod-like and disk-like photonic microobjects [197,198]. This was achieved by producing spherical droplets in a relatively larger microchannel and then delivering them to a microchannel with a relatively smaller size, either in a horizontal or vertical direction to the flow direction of the droplets. The confining effect induced the droplet templates to deform, which were immediately cured using UV irradiation to fix the deformed shapes. This conception utilized single emulsions or multiple core double emulsions as templates. The photonic composition of the droplet templates was an aqueous suspension of $SiO_2$ CPs and poly (ethylene glycol) diacrylate (PEG-DA) (as shown in Fig. 20e). Depending on the type of confining capillary that was used, the droplets were deformed into rod-like, cuboid-like, or disk-like structures, which were immediately solidified upon UV irradiation due to the polymerization of PEG-DA. Therefore, colloidal photonic microobjects with different geometries were produced (as shown in Fig. 20f-k). Furthermore, this strategy was also utilized to produce more complex structures by integrating multiple photonic components into individual microobjects [197]. To achieve the multicomponent integration, a multichannel microfluidic device was utilized to inject different-colored photonic suspensions of silica CPs. The single stream of multiple photonic suspensions was subsequently sheared and emulsified by a photocurable PEGDA hydrogel precursor solution. The sheared multiple core droplets were further emulsified by an external oil phase, such as a hexadecane solution of Abil EM90 (as illustrated in Fig. 20l). The multi-core droplets were subjected to the following confining effect, and rod-like multi-core droplets can be formed inside the confining glass capillary. The rod-like multi-core photonic microobjects can be subsequently formed upon the UV exposure. Due to the incorporation of multiple cores with different colors, the microobjects can be used for encoding (as shown in Fig. 20m).

The aforementioned studies regarding the colloidal photonic structures mostly utilized the colloid's conventional short interactions, such as electrostatic interaction, etc. Among traditional colloids, some other short interactions, for instance, the preprogrammed short interaction between DNA molecules, were also introduced to study and understand the crystallization dynamics of these colloids. Despite diverse crystal structures from DNA-coated PS colloids having been reported, the poor understanding and control of the crystallization dynamics has limited their further applications [199–201]. In light of this, Rogers et al. leveraged the short interactions among DNA-coated colloids and quantitatively studied the crystallization dynamic behaviors of DNA-coated colloids within uniform droplets from droplet microfluidics [57,202]. To adjust the interactions, monodispersed colloids were respectively coated with two different DNA strands; the strength of the short-range attraction between the colloids can be tuned by the temperature (Fig. 21a-b). By controlling the temperature at just below the melting point, the binary colloids can assemble into an alloy closely resembling the isostructure of Cu—Au (Fig. 21c-d). The colloids experienced a series of different statuses inside each individual droplet from nucleation towards crystal growth. As a result, the colloids gradually grow to a single crystal structure, and the droplets gradually become brighter (Fig. 21e). Eventually, colloid-based single-crystal superstructures formed within

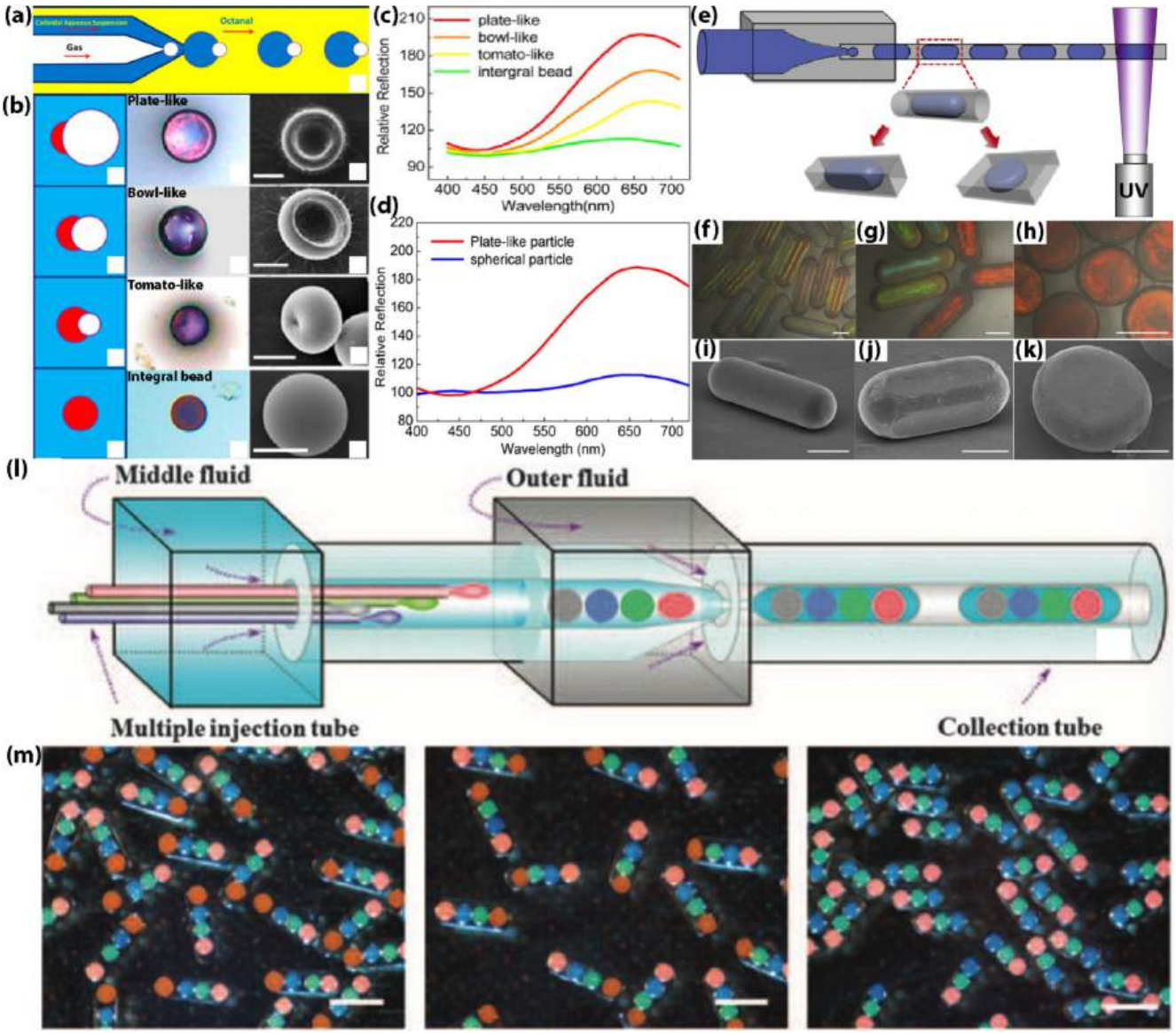


**Fig. 20.** (a) The illustration figure shows the microfluidics fabrication of gas-filling droplets, which were composed of aqueous suspension of monodispersed CPs. (b) Different configurations (left row) of gas-filling droplets and their resulting OM images (middle row) after the solvent-extraction process and corresponding SEM images (right row). (c) Reflection spectra comparison of the colloidal crystal microobjects in (b). (d) Reflection spectra comparison of particles with plate-like shape and spherical shape [195]. Reprinted from ref. 195 with permission from the American Chemistry Society, copyright 2014. (e) The illustration figure shows the microfluidic fabrication of photonic microobjects with different geometries using the microchannel's confining effect. (f)-(h) OM images of the photonic microobjects with different geometries. (i)-(k) SEM images of the photonic microobjects in (f)-(h) [198]. Reprinted from ref. 198 with permission from Elsevier, copyright 2014. (l) The illustration figure shows the microfluidic fabrication of a multi-core photonic microrod using the microchannel's confining effect. (m) OM images of the microrods with different colorful core combinations. Multifunctional photonic crystal barcodes from microfluidics [197]. Reprinted from ref. [197] with permission from Springer Nature, copyright 2012.

individual droplets (Fig. 21f).

In addition to Xu's report about the construction of anisotropic photonic microobjects by a droplet's evaporation route, this similar approach was also adapted by Zhao et al., who carried out droplet's slow evaporation experiments and obtained photonic microobjects with a Janus structure [203]. Instead of using a single type of CP as the building blocks, they utilized a mixture of monodispersed silica CPs and graphene oxide (GO) sheets as the building blocks for a Janus structural color particle (SCP). Initially, the microfluidics-fabricated droplets that contained homogeneously distributed graphene oxide (GO) sheets and silica CPs were subjected to a slow solvent evaporation, which subsequently induced the redistribution of the two kinds of components. Specifically, silica CPs and GO sheets aggregated at the bottom and top parts of the droplet, respectively, under the impact of an evaporation-induced phase separation, which was plausible due to the synergistic effect of charge and density of the two kinds of components. Complete evaporation of solvent results in the formation of the anisotropic Janus SCP (as illustrated in Fig. 22a, and the real droplet evolution process was shown in Fig. 22b). Eventually, the obtained nonspherical Janus microobjects contain a GO sheets-based dark part and a silica CPs-based photonic part. The photonic part of the microobjects displayed different structural colors by changing the diameters of silica CPs (as shown in Fig. 22c-e). Further SEM characterizations revealed that the photonic and the dark parts had different kinds of microstructures: the photonic part was constructed by orderly assembled silica CPs (as shown in Fig. 22f-g), and the dark part was constructed by the mixture of silica CPs and GO sheets (Fig. 21h). More importantly, the spherical SCPs and the anisotropic Janus SCPs demonstrated different motion behaviors under the impact

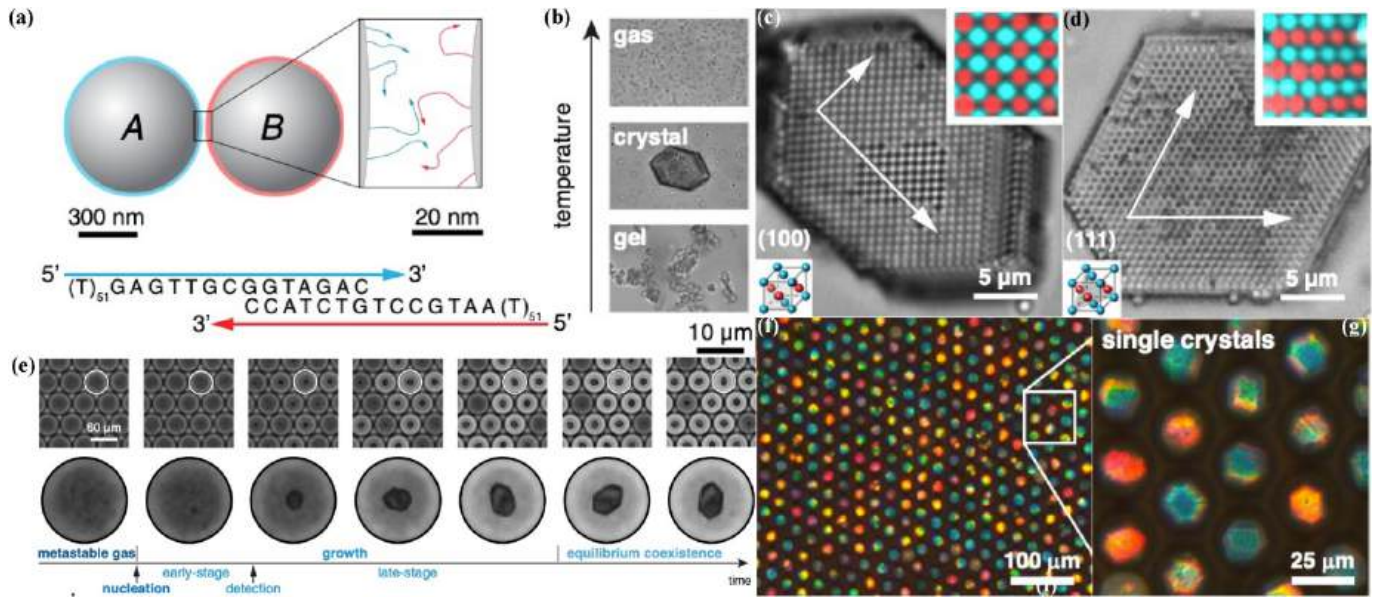


**Fig. 21.** (a)-(b) The illustration figure shows the short interactions among DNA-coated colloids. (b) Relationship between the status of the DNA-coated colloid supraparticles and the temperature. (c)-(d) OM images of different crystal plane structures. (e) OM images show the evolution of DNA-coated colloids inside a population of droplets, where the colloids assembled into different superstructures as a function of time. (f)-(g) OM images of the formed single crystal structures inside individual droplets [57]. Reprinted from ref. 57 with permission from the National Academy of Sciences of the USA, copyright 2022.

of the same flow stimulus: the spherical SCPs rolled more easily than the Janus SCPs when subjected to similar fluid shock. The majority of the spherical SCPs rolled from the left side of the microchannel (as shown in Fig. 22j-l), while the majority of the Janus SCPs almost stayed still on the left side of the microchannel (as shown in Fig. 22m-o). This construction strategy was further utilized to fabricate micromotors for label-free multiplex assays [204]. Apart from the abovementioned methods, such as the evaporation-assisted shape regulation or confining effect from microchannels, to tune the shapes of colloidal photonic microobjects, an alternative approach was brought up to shape the structures of colloidal photonic microcapsules via an osmotic pressure effect-induced shape transformation [205]. For example, Lee et al. reported the fabrication of photonic microcapsules with buckled shapes by an osmotic pressure regulating process [206]. Specifically, photonic microcapsules respectively using an aqueous suspension of PS CPs as the core part and curable silicone rubber as the shell part were fabricated via a glass capillary-based microfluidic device. The microcapsules were placed in an aqueous solution of salt with low concentrations, such as 50 mM, to regulate the shapes of the entire microcapsules. The osmotic pressure from the incubation solution triggered outflow of the water from the microcapsule, which can enrich the CPs in the core part and induce the formation of a dimpled and eventually buckled structure of the microcapsules. This formation of dimpled structure was due to the osmotic pressure exerted on the weakest point of the microcapsules and eventually triggered the buckling effect [207]. The osmotic pressure not only reshaped the elastic shell but also transformed the suspension core into a quasi-hemisphere structure (as illustrated in Fig. 22p). Simultaneously, the curing process gradually fixed the deformed structure. As a result, the resulting microcapsules exhibited a buckled structure with multiple concentric rings from a top-down view (as shown in Fig. 22q). The structural colors of the inner core part of the microcapsules can also be regulated by using different diameters of PS CPs in the core part (as shown in Fig. 22r-t), where the core parts display vivid blue, green, and red colors, respectively.

Except for the abovementioned utilization of the osmotic pressure effect, other external fields, such as an external magnetic field, were also introduced to regulate the resulting shapes of the photonic microobjects that evolved from the aqueous suspension of CPs, specifically nonspherical CPs. In this aspect, He et al. synthesized $Fe_3O_4$@$SiO_2$ ellipsoids (as shown in Fig. 23a) and prepared spherical droplets (as shown in Fig. 23b) of aqueous suspension of the nanoellipsoids via a PDMS-based microfluidic device. The droplets can spontaneously evolve into photonic microobjects after complete evaporation of water [208]. Interestingly, the resulting microobjects displayed different shapes under the condition of whether a magnetic field was applied to the droplets during the solvent evaporation process. For example, the resultant microobjects displayed a spherical shape under magnetic field-free conditions during the evaporation process, while the microobjects were all in a spindle shape when the magnetic field was applied during the evaporation process (as illustrated in Fig. 23c). Further study indicated that the initial droplets' size and the intensity of the external magnetic field can significantly affect the final shapes of the microobjects. On the one hand, droplets with smaller initial sizes tended to form spherical supraparticles, while droplets with larger initial sizes were prone to result in elongated supraparticles with relatively large aspect ratios; on the other hand, a stronger external magnetic field resulted in the final supraparticles with larger aspect ratios (as shown in Fig. 23d).

Fluorescence property could provide photonic microobjects with more characteristics. To impart colloid-based photonic microobjects with fluorescence properties and obtain photonic structures with multiple functionalities, attempts have also been made to construct photonic microobjects by using colloids with fluorescence properties as the building blocks. Typically, semiconductor quantum dots (QDs), such as CdS QDs, have been used as the fluorescence composition. By leveraging the fluorescence property of CPs together with microfluidics and external field-assisted shaping routes, photonic microobjects with multiple nonspherical configurations can be realized. For example, Chen et al. synthesized core-shell (poly(styrene-*co*-2-hydroxyethyl acrylate) (PS-PHEA) as core and poly(N-vinylimidazole-*co*-2-hydroxyethyl acrylate) (PVI-PHEA) as shell) CPs, which were further loaded with CdS semiconductor dots in the shell part of the CPs, yielding hybrid latexes with fluorescence properties (as shown in Fig. 24a). The hybrid latex suspension (termed phase A) and resin suspension of magnetic $Fe_3O_4$ NPs (termed phase B) were parallelly injected into a PDMS microfluidic device and sheared by a silicone oil phase to obtain magnetic particle-functionalized droplets, where phase A of the droplets can be immobilized by a subsequent UV-curing process (as shown in Fig. 24b). The

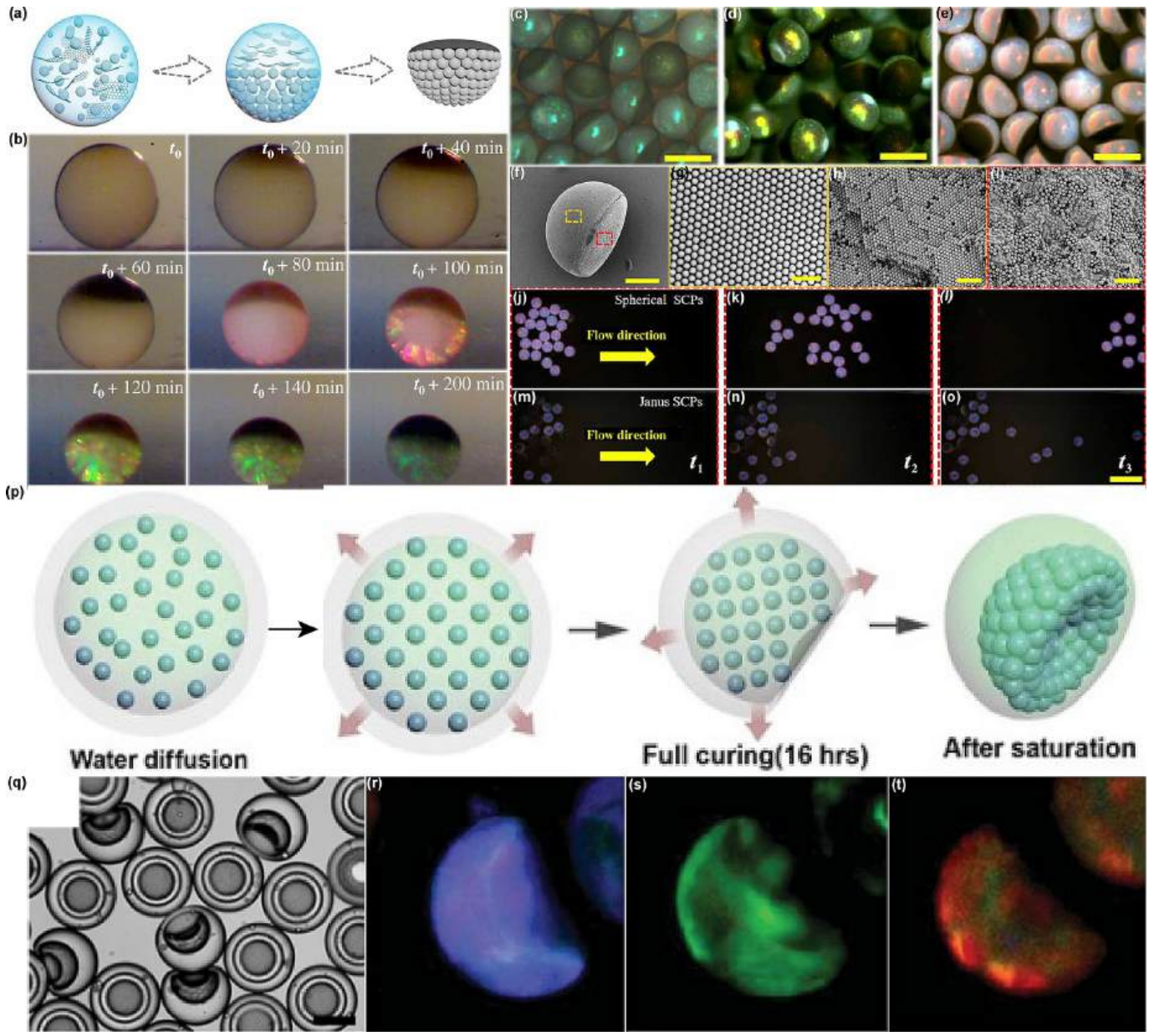


**Fig. 22.** (a) The illustration figure shows the evolution of droplets containing graphene oxide (GO) and silica CPs evolving from spherical into anisotropic Janus structural color particles (SCPs). (b) OM images showing the time-lapse evolution of a spherical droplet containing homogeneously distributed graphene oxide (GO) and silica CPs gradually evolved into Janus SCPs under the effect of slow solvent evaporation. (c)-(e) Janus SCPs with different structural colors formed from the assembly of silica CPs with different diameters. (f) SEM image of an anisotropic Janus SCP. (g)-(h) SEM images of the surface (g) and inner microstructure (h) of the photonic section framed by the yellow dashed line in (f). (i) SEM image of dark section framed by red dash line in (f). (j)-(*l*) OM images of spherical SCPs in a microchannel under the impact of the flow direction indicated by the yellow arrow in (j). (m)-(o) OM images of Janus SCPs in a similar microchannel as that of (j) and under the impact of the same flow conditions as that of (j)-(l) [203]. Reprinted from ref. 203 with permission from the American Association for the Advancement of Science (AAAS), copyright 2020. (p) The illustration figure shows the generation of buckled photonic microcapsules using an osmotic pressure-mediated approach. (q) OM image of a population of photonic microcapsules with buckled geometry; (r)-(t) OM images of buckled microcapsules with different structural colors from blue (r), green (s) to red (t), respectively [206]. Reprinted from ref. 206 with permission from the Royal Society of Chemistry, copyright 2015. (For interpretation of the references to color in this figure legend, the reader is referred to the web version of this article.)

droplets were initially with an utterly double-faced geometry (termed as AB1) and can be further manipulated to form multiple different geometries (theoretically ranging from AB1 to ABn) by interplaying the magnetic field-induced droplet merging and interfacial tensions among the resin phase, CPs' suspension phase, and the external continuous phase (as illustrated in Fig. 24c). As a proof-of-concept demonstration, the resulting photonic microobjects with configurations from AB1 to AB5 were prepared (as shown in Fig. 24d and the corresponding illustration figure shown in Fig. 24e) [111]. While an extensive amount of research attention has been paid to the construction of photonic microobjects with fluorescence properties via integrating colloidal building blocks with semiconductor QDs, such as CdSe/ZnS and CdTe/ZnS QDs, the toxicity of those QDs is a non-negligible factor. In light of this, environment-friendly carbon dots have been incorporated onto the surface of core-shell CPs (i.e., CDs/PS@P(MMA-AA) CPs), which have been used as the building blocks for photonic microobjects (the synthesis route of the CPs is illustrated in Fig. 24f) [209–211]. A similar microfluidic approach was utilized to generate magnetic-functionalized

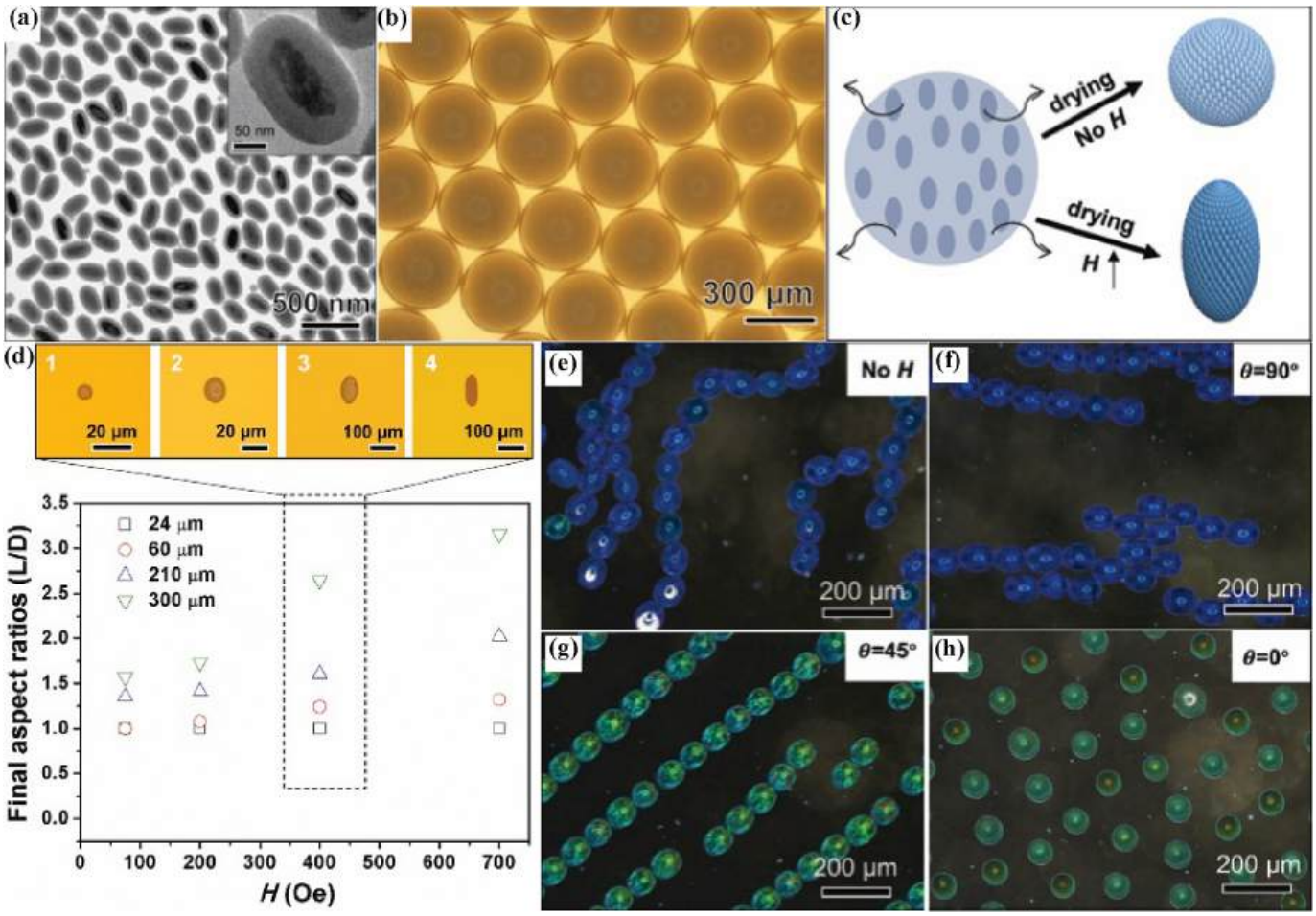


**Fig. 23.** (a) TEM image of $Fe_3O_4$@$SiO_2$ ellipsoids. (b) Droplets of an aqueous suspension of $Fe_3O_4$@$SiO_2$ ellipsoids. (c) The illustration figure shows the evolution of initially spherical droplets of the aqueous suspension of $Fe_3O_4$@$SiO_2$ ellipsoids under a magnetic field and magnetic field-free conditions. (d) Top row: OM images of the supraparticles with different shapes; bottom row: plot shows the relationships among final aspect ratios of the supraparticles. (e) OM images show the different structural colors and orientations of the spindle-like supraparticles under different conditions: without and with a magnetic field of different angles exerted on the supraparticles [208]. Reprinted from ref. 208 with permission from the Royal Society of Chemistry, copyright 2019.

photonic microobjects with different nonspherical configurations (as shown in Fig. 24g-h). The resulting photonic microobjects can be subsequently used to construct QR code patterns or displays, which display magnetic field-controlled information storage and reading, or even for energy-saving applications [71,210].

Besides the colloidal photonic microobjects with abovementioned nonspherical structures via different approaches, photonic microobjects with different geometries or shapes have also been achieved through the confining effect of microfluidic channels. Specifically, a PDMS-based microfluidic device was utilized to generate cylinder colloidal photonic microobjects reported by Kim's group [212,213]. The device featured a main cylinder channel and different numbers of inlets (as illustrated in Fig. 25a-b). A photomask was placed in a predesigned region over the objective lens. When different numbers of streams of colloidal photonic suspensions (photocurable ETPTA resin of $SiO_2$ CPs) pass through the main channel and are subsequently irradiated with UV light, cylinder photonic microobjects with single composition or multi-compartment structures can be obtained (as shown in Fig. 25c). By changing different diameters of the $SiO_2$ CPs from 140 nm, to 160 nm to 200 nm, the structural colors and the corresponding spectra can be modulated from blue, green, and red (as shown in Fig. 25d). Furthermore, the compartment numbers of the resulting cylinder photonic microobjects can be varied from one to four when the inlet numbers of the microfluidic device increase from 1 to 4. For example, photonic microcylinders with dual colors (Fig. 25e-f), triple colors (Fig. 25g), and triple colors together with a magnetic composition (Fig. 25h) were respectively prepared in the study.

## 5. Photonic microcapsules

### 5.1. Photonic microcapsules with photonic property only in the core part

Instead of using the colloidal embedding or calcination method to generate photonic microobjects with stable properties, an alternative approach to produce stable photonic microobjects was through the confining of CPs into miniaturized chambers, which were produced from microfluidics and can protect the entrapped CPs from undergoing interruption from external media. Yang et al. firstly reported the fabrication of photonic microcapsules through a co-flow optofluidic approach (as shown in Fig. 26a). Three phases were used in the experiments. An aqueous phase containing 1 wt% surfactant ethylene oxide-propylene oxide-ethylene oxide (PEO-PPO-PEO) triblock copolymers was used the outer phase. Photocurable ETPTA resin containing 2 wt% surfactant sorbitan monooleate (Span 80) and a suspension of highly charged PS CPs with an average diameter of ~328 nm was used as the middle and inner phases, respectively [165]. Through proper adjustment of the flow rates of the three phases, water-in-oil-water (W/O/W) core-shell droplets produced from the microfluidic device were immediately transformed into core-shell microcapsules by UV curing of the resin shell (as shown in Fig. 26b). The addition of the surfactants in the

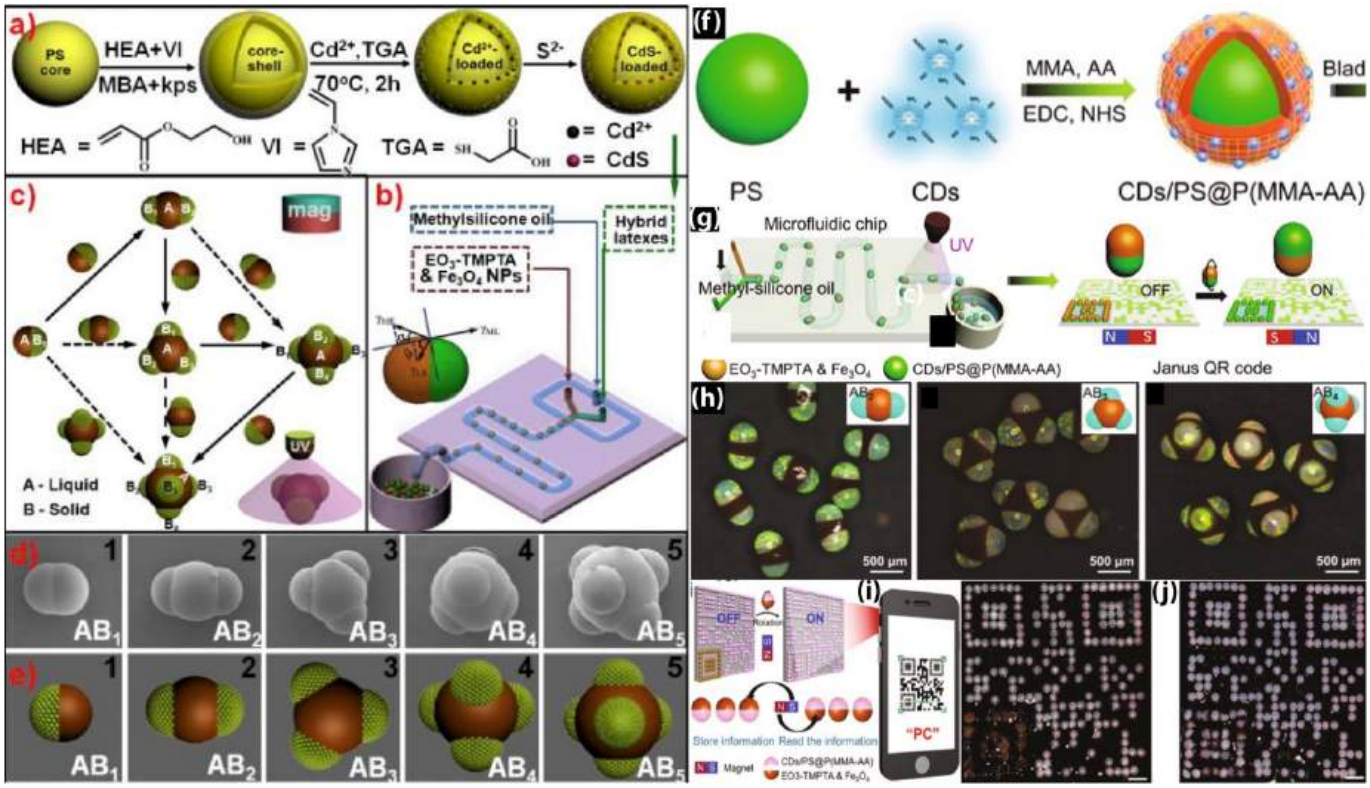


**Fig. 24.** (a) The illustration figure shows the synthesis of CdS quantum dots-loaded PS-PHEA/PVI-PHEA core-shell CPs. (b) The illustration figure shows the microfluidics fabrication of rod-like Janus photonic microobjects assisted by microfluidics. (c) Cartoon figures show the tuning of different geometries of photonic microobjects via magnetic assembly of microfluidics-fabricated primary Janus droplet templates. (d) SEM images of the photonic microobjects with different geometries via magnetic field-induced assembly, the configurations of resulting microobjects termed as AB1 through AB5. (e) Cartoon figures show the corresponding photonic microobjects in (d) [111]. Reprinted from ref. 111 with permission from the American Chemistry Society, copyright 2016. (f) The illustration figure shows the CBs-functionalized PS@(PMMA-AAc) CPs. (g) The illustration figure shows the microfluidics fabrication of Janus rod-like photonic microobjects assisted by microfluidics and the subsequent construction of the Janus QR code. (h) OM images of the photonic microobjects with different configurations from left to right: AB2, AB3, and AB4, respectively. (i) Left panel: The illustration figure shows the PC QR code prepared by Janus PC supraballs. Middle and right panels show the photographs of the code patterns under on (middle) and off (right) modes, respectively [210]. Reprinted from ref. 210 with permission from Elsevier, copyright 2021.

middle and outer phases was used to tune the interfacial tensions among the three phases, and then the spreading parameter $S = \gamma_{I-M} - (\gamma_{O-M} + \gamma_{O-I})$, where $\gamma_{I-M}$, $\gamma_{O-M}$, and $\gamma_{O-I}$ are the interfacial tensions between the inner phase and middle phase, outer phase and middle phase, and outer phase and inner phase, respectively. The $S < 0$ could ensure the core and shell parts to be the PS suspension and UV-curable ETPTA resin, respectively [214]. The volume fraction of the prepared PS CPs suspension was ~10 %, above which there was a high possibility of clogging the microfluidic device, leading to the failure of the experiments [165]. The highly charged properties of the PS colloids allow them to be assembled into colloidal crystal arrays through the repulsive force. Due to the protection from the transparent ETPTA resin, this array can be refrained from the disturbance of ions and other impurities or in an electric field, which can induce the array to lose stability. However, the photonic property of these microcapsules mainly originated from the secondary diffraction of the self-assembled PS CPs, given that the diameters of the PS colloids are far larger than conventionally used colloids with diameters in the range between 100and 300 nm, given their non-close packing configurations (as shown in Fig. 26c-d). Nevertheless, the microcapsules displayed the characteristics that photonic stopbands were independent of the position on the spherical surface due to their spherical symmetry (as shown in Fig. 26e). This phenomenon was contrary to that of Vogel's study, where the photonic supraparticles constructed by polyhedral CPs showed angle-dependent phenomena [20]. Borrowed from the same encapsulating strategy, Zhu and Yang et al. utilized the similar microfluidic device to encapsulate aqueous suspension of core-shell colloids (PS as core and pNIPAAm as shell, PS@pNIPAAm) with smaller diameters (from ~120 nm to ~180 nm) into ETPTA shell microcapsules [215]. Unlike the case in Kim's study, the concentrations of the core-shell colloids were all much higher and at more than 20 wt% given their small diameters. The photonic properties in this case originated from the first-order diffraction. Despite the colloidal building blocks containing a pNIPAAm shell, the photonic property of the photonic microcapsules was thermoresistant when subjected to temperature stimulus from 5 to 50 °C. This thermoresistant photonic feature was different from the bulk photonic film using the PS@pNIPAAm colloids with a larger total diameter (335 ± 8 nm) and a much thicker shell (~ 70 nm) as the building blocks, where the photonic film showed highly thermoresponsive properties with its reflection peak value shifted from 640 nm to 450 nm when being heated from 20 °C to 40 °C [216]. The discrepancy was likely because the pNIPAAm shell in Zhu's case was too thin (the thickness of the pNIPAAm shell is below 10 nm, less than 10 % of the entire diameter of the CPs) to display any obvious temperature-induced size change of the CPs and thus the photonic property change (as shown in Fig. 26f-i). It was also worth mentioning that large colloidal crystal domains were visible from the OM images, suggesting heterogeneous nucleation likely took place within the microcapsules. As a result, the photonic properties can be inhomogeneous across the individual photonic microcapsule and can be a disadvantage when high-resolution photonic properties are required for some practical applications.

Although colloidal crystal-based photonic microobjects could be obtained by confining organized close-packing or non-close-packing colloidal crystal arrays within microobjects through the above-

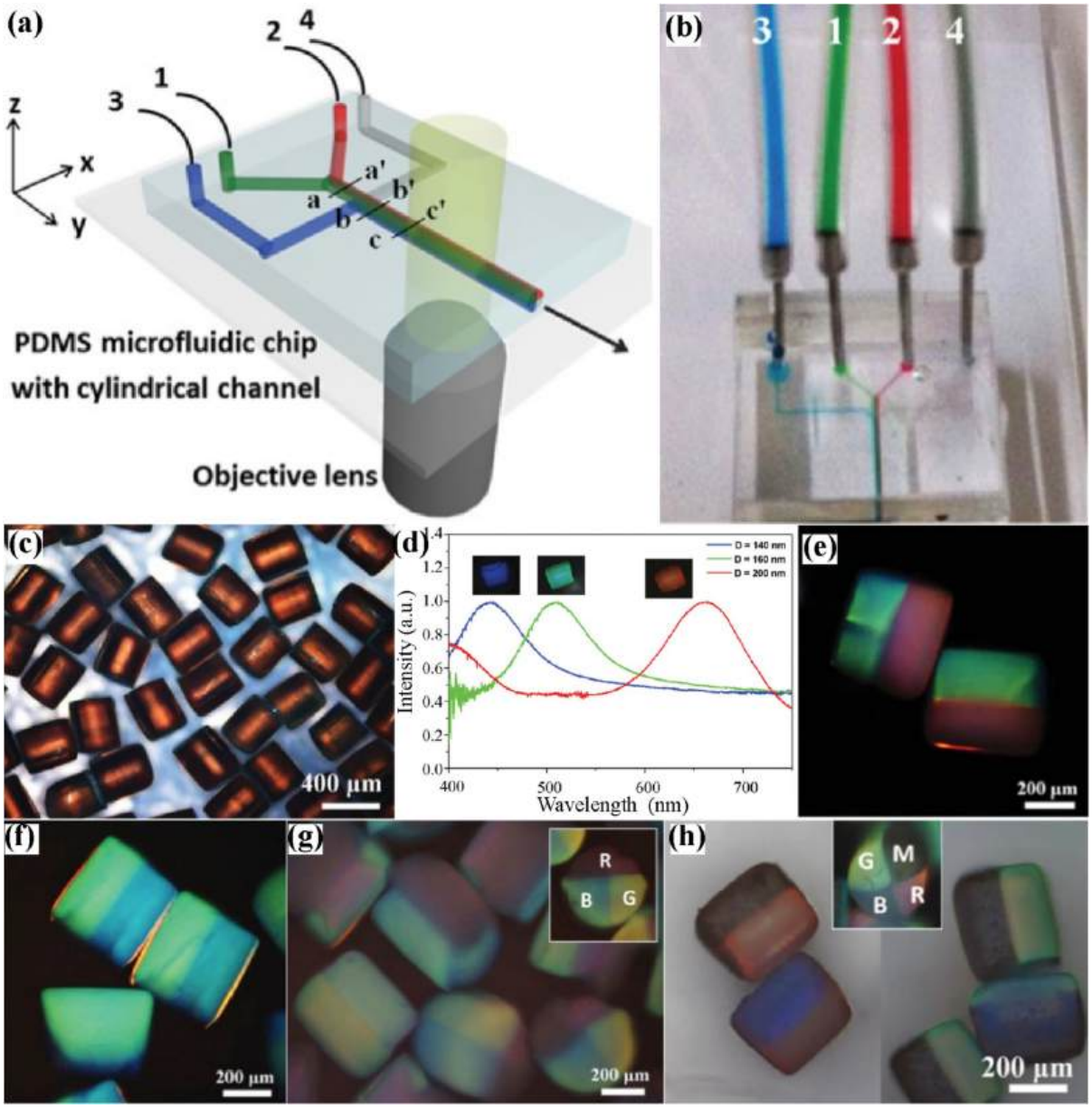


**Fig. 25.** (a) The schematic figure shows the structures of a PDMS-based microfluidic device and the structure of the objective lens of an optical microscope. (b) OM image of the microfluidic device and the four different inlets. (c) OM image of red-colored photonic microcylinders. (d) OM image of microcylinders with red, green, and blue colors and their corresponding reflection spectra. (e)-(f) OM images of two-compartment microcylinders with half red and half green (e) and half green and half blue (f). (g) OM image of three-compartment microcylinders. The microcylinders are composed of a red hemisphere, a quarter green, and a quarter blue. (h) OM image of four-compartment microcylinders. The microcylinders are composed of a quarter green, a quarter blue, a quarter red, and a quarter magnetic composition [212]. Reprinted from ref. 212 with permission from Elsevier, copyright 2021. (For interpretation of the references to color in this figure legend, the reader is referred to the web version of this article.)

mentioned approaches, photonic properties of the resulting microobjects strongly relied on the properties of the colloidal suspensions. It is desired to encapsulate colloidal building blocks with stimulus-responsive characteristics into microcapsules via microfluidics to impart the resulting microcapsules with stimulus-responsive properties. In this regard, Gu et al. encapsulated $Fe_3O_4$/PS-pMAAc (poly(styrene-*co*-methyl acrylic acid) composite magnetic colloids with an average diameter of ~138 nm into microfluidics-fabricated droplet capsules also using photocurable ETPTA resin as the shell part. The resultant uniform microcapsules had diameters ranging from 210 to 425 μm. Upon the subsequent UV light irradiation, all liquid capsules were transformed into capsules with a solid shell. Although the diameter of the colloidal building blocks was at least 30 nm smaller than generally used colloids (with a diameter of 170–210 nm) to build the non-close packing photonic structures, the microcapsules can be endowed with photonic properties by applying an external magnetic field. Through the introduction of the magnetic field, the synergistic effect of the magnetic attractive force and repulsive force can modulate the lattice spacing, therefore regulating the photonic characteristics. These microcapsules can be further used as building blocks for displays, which feature magnetochromism [217]. For example, the display assembled by using the photonic microcapsules can show a magnetic field-induced pattern appearing and disappearing (as shown in Fig. 26m-o).

In addition to the construction of magnetic-responsive photonic microcapsules using the microfluidic encapsulating techniques, Zhu et al. reported the preparation of thermoresponsive microcapsules by

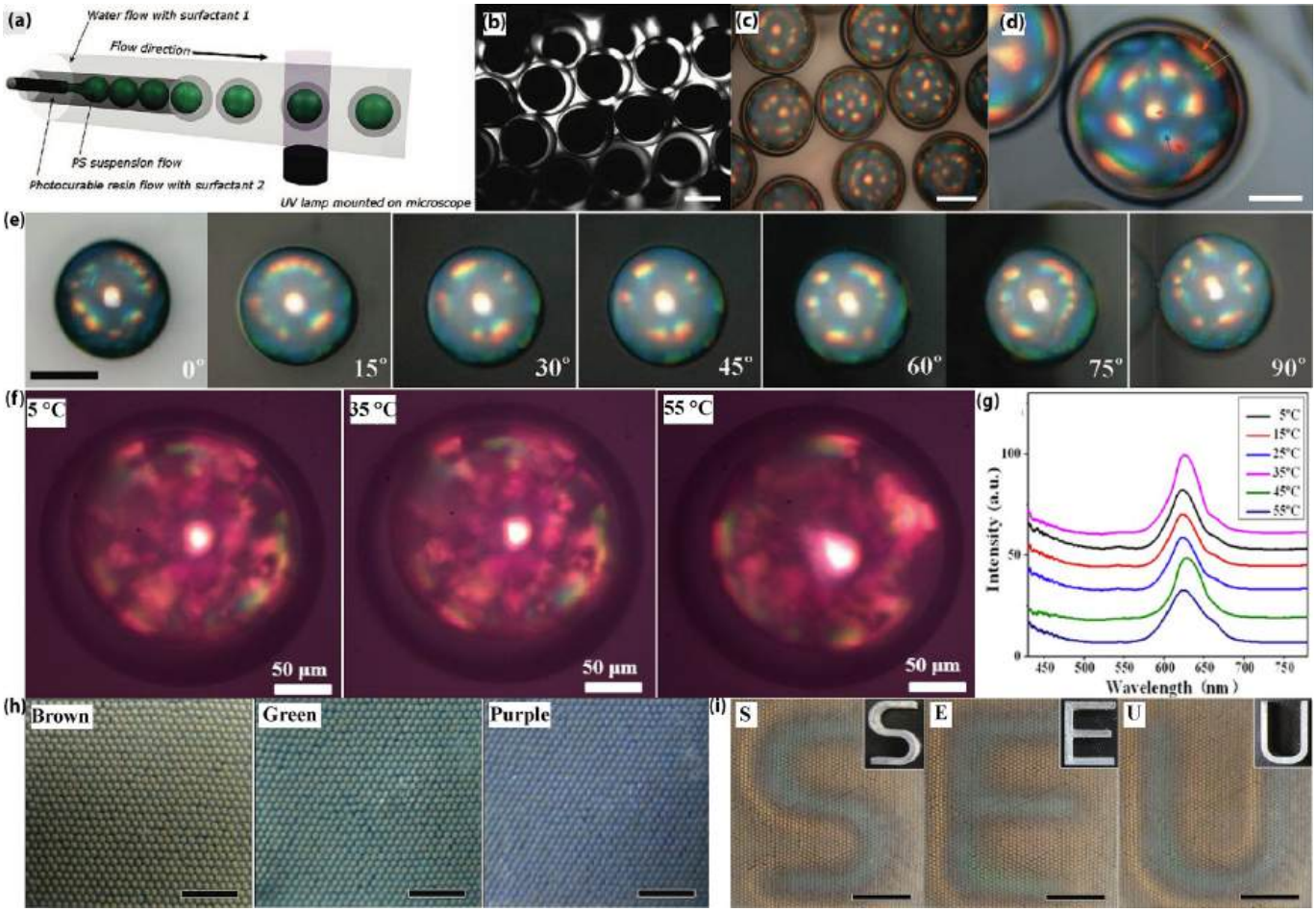


**Fig. 26.** (a) The illustration figure shows the co-flow microfluidics fabrication of photonic microcapsules using photocurable ETPTA resin and aqueous suspension of PS CPs as the shell and core parts, respectively. (b)-(c) OM images of the photonic microcapsules under b. transmission mode and c. reflection mode; (d) an enlarged OM image of a photonic microcapsule under reflection mode. The arrows denote the diffraction colors from the self-assembled colloidal crystal arrays (SCCAs). (e) OM images of a photonic microcapsule taken at various angles between observation direction and substrate normal [165]. Reprinted from ref. 165 with permission from American Chemistry Society, copyright 2008. (f) OM images of a photonic microcapsule under different temperatures at °C, 35°C, and 55°C, respectively. The microcapsule uses ETPTA as the shell part and an aqueous suspension of PS-pNIPAAm core-shell NPs with photonic properties as the core part. (g) Reflection spectra of the photonic microcapsule at different temperatures from 5°C to 55°C [215]. Reprinted from ref. 215 with permission from the American Chemistry Society, copyright 2014. (h) OM images of microfluidics-fabricated photonic microcapsules using photocurable ETPTA resin and aqueous suspension of magnetic CPs as the shell materials and core part, respectively. (i). Photographs of the letter patterns displayed by the magnetochromatic microcapsule array [217]. Reprinted from ref. 217 with permission from Wiley, copyright 2011.

encapsulating pre-assembled photonic suspension of pNIPAAm-co-AAc gel particles into ETPTA microcapsules that were fabricated from a droplet microfluidic device (as shown in Fig. 27a-d). Due to the thermoresponsive nature of the gel particle building blocks, the microcapsules displayed thermoreversible hue change upon a heating and cooling cycle due to the individual CPs' volume change as a function of temperature while interparticle separation remained unchanged [218], leading to no color change or no spectrum wavelength shift of the microcapsules (as shown in Fig. 27e-f). When subjected to a certain period of centrifugation, the gel particles inside the microcapsules gradually stacked to one pole of the microcapsule, yielding a Janus-like core part (as shown in Fig. 27g), which displayed a color gradient under reflection mode of OM (as shown in the inset figure of Fig. 27g). This was likely because of the centrifugation-induced stacking of gel particles in the microcapsules in a gradient fashion. The color gradient was further verified by the different wavelength peak values of reflection spectra (as shown in Fig. 27h). Therefore, the microcapsules were featured with the capability of sensing centrifugation force [219].

Except for the case of using stimulus-responsive colloidal building blocks, there were very limited measures to adjust the photonic properties of the photonic microobjects once the initial size or initial volume fraction of the colloids was fixed [220]. Colloidal photonic microcapsules with flexible shells and photonic microcapsules starting from a colloidal suspension with low concentrations have been adopted to avert this issue. To achieve this goal, researchers can either use intrinsically soft, flexible materials as the shell materials or prepare microcapsules with a thin shell, which consequently renders the shell part with abnormal properties when compared with that of bulk conditions (for example, a polymerized ETPTA shell with a thickness below a certain value (i.e., 25 μm) can display deformable properties, while beyond this value, it would be much more resistant to deformation) [205,221]. Alternatively, due to high concentrations of $SiO_2$ CPs that could potentially clog the microchannels of microfluidic devices, researchers can prepare photonic microcapsules starting from low concentrations of CPs (below which value the colloidal suspensions can't exhibit photonic properties) and place the droplet microcapsules into hypertonic solutions to induce enrichment of the colloidal suspension core part. Consequently, the enrichment effect turned the microcapsules with no photonic property into ones with tunable photonic property [222–224].

In terms of using soft and flexible materials as the shell materials of photonic microcapsules, Martinez et al. encapsulated an aqueous suspension of diluted $SiO_2$ CPs into a two-composition curable PDMS

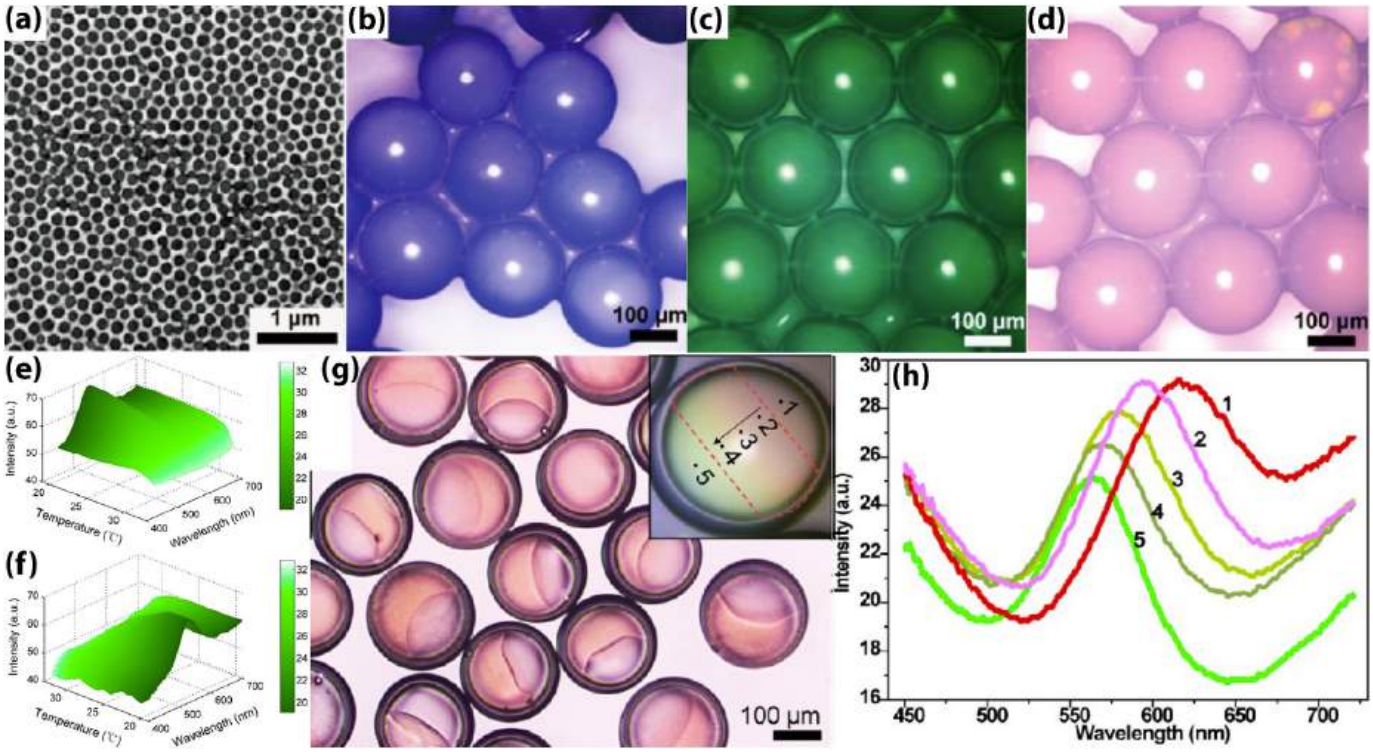


**Fig. 27.** (a) TEM image of pNIPAAm-co-AAc gel particles that were used as the building blocks of photonic suspension. (b)-(d) OM images of photonic microcapsules with different colors from blue (b), green (c) to red (d). (e)-(f) Reversible thermoresponsive property of microcapsule with green color [133]. Reprinted from ref. 133 with permission from the American Chemistry Society, copyright 2013. (g) OM image of a photonic microcapsule after centrifugation effect, where the microcapsules with homogeneously distributed gel particles inside gradually transitioned to uneven distribution of gel particles in the two halves of an individual microcapsule. (h) Reflection spectra of different regions inside the microcapsules in g [219]. Reprinted from ref. 219 with permission from the American Chemistry Society, copyright 2013. (For interpretation of the references to color in this figure legend, the reader is referred to the web version of this article.)

rubber precursor solution by a glass-capillary-based microfluidic device, leading to the formation of core-shell droplets, which don't have photonic properties at the very beginning due to the low volume fraction of the $SiO_2$ CPs (as illustrated in Fig. 28a). Then, the droplets were collected in an aqueous solution with higher osmolarities than that of the aqueous suspension of diluted $SiO_2$ CPs. Through this operation, the core-shell droplets started to show a decrease in size due to the semi-permeable nature of the shell part and therefore led to the outflow of the water molecules from the core part under the osmotic pressure effect, which induced the enrichment of $SiO_2$ CPs and eventually formed colloidal crystal structures within the core part (as illustrated in Fig. 28b) [222]. The shell part can be gradually cured under an ambident environment and eventually form a stable shell. The microcapsule featured a colloidal crystal core (as illustrated in Fig. 28c). Through this design, one can obtain photonic microcapsules without the need of a predetermined photonic composition, such as a specific colloidal volume fraction, etc. However, it took a long period to obtain a fully solidified shell, given that the curing period of the rubber precursor was half a dozen hours and full cross-linking of the shell part took more than one day to complete in the solution. This long curing period of the shell part can be problematic for researchers to obtain desired microcapsules in a timely fashion.

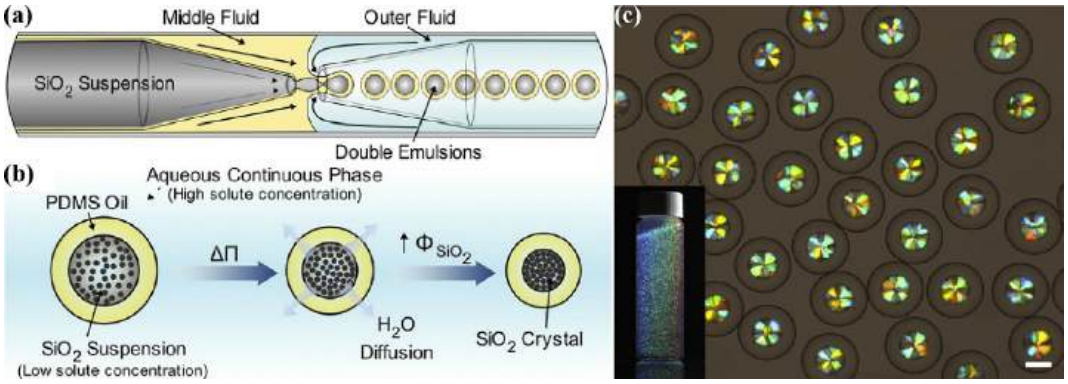


**Fig. 28.** (a) The illustration figure shows the fabrication of core-shell droplet capsules using an aqueous suspension of $SiO_2$ CPs as the core part and thermocurable PDMS resin as the shell part. (b) The illustration figure shows the evolution of droplet microcapsules in a solution under hypertonic condition, which induced the core part to decrease in size due to the outflow of the water molecules from the core part. As a result, the $SiO_2$ CPs gradually form a crystal structure. (c) OM image of the microcapsules after the formation of crystalline in the core part. The inset figure shows the photograph of the suspension of microcapsules with a crystalline core [222]. Reprinted from ref. 222 with permission from the American Chemistry Society, copyright 2013.

Given that the photonic microcapsules produced from a standard double-emulsion microfluidic device normally have a relatively thick shell, such as over a few micrometers or beyond. This thick shell can have some undesired consequences for the resulting microcapsules. In this regard, Weitz, Manoharan, and Kim et al. leveraged the similar idea to fabricate core-shell photonic structures but replaced the $SiO_2$ colloidal building blocks and air-curable PDMS oil shell with charged PS CPs and photocurable resin shell, respectively [223–225]. The core-shell structures were fabricated using a specially designed microfluidic device, which was first invented by Kim et al. and was capable of generating core-shell structures in a thin-shell fashion (as shown in Fig. 29a-b). The shell thickness of the core-shell structure was approximately 1 μm or below, according to previous reports [226,227]. Microcapsules with shell thickness at this level not only facilitated the transport of water molecules across the shell but also transformed the normally rigid ETPTA shell (when the thickness was above tens of micrometers) to a

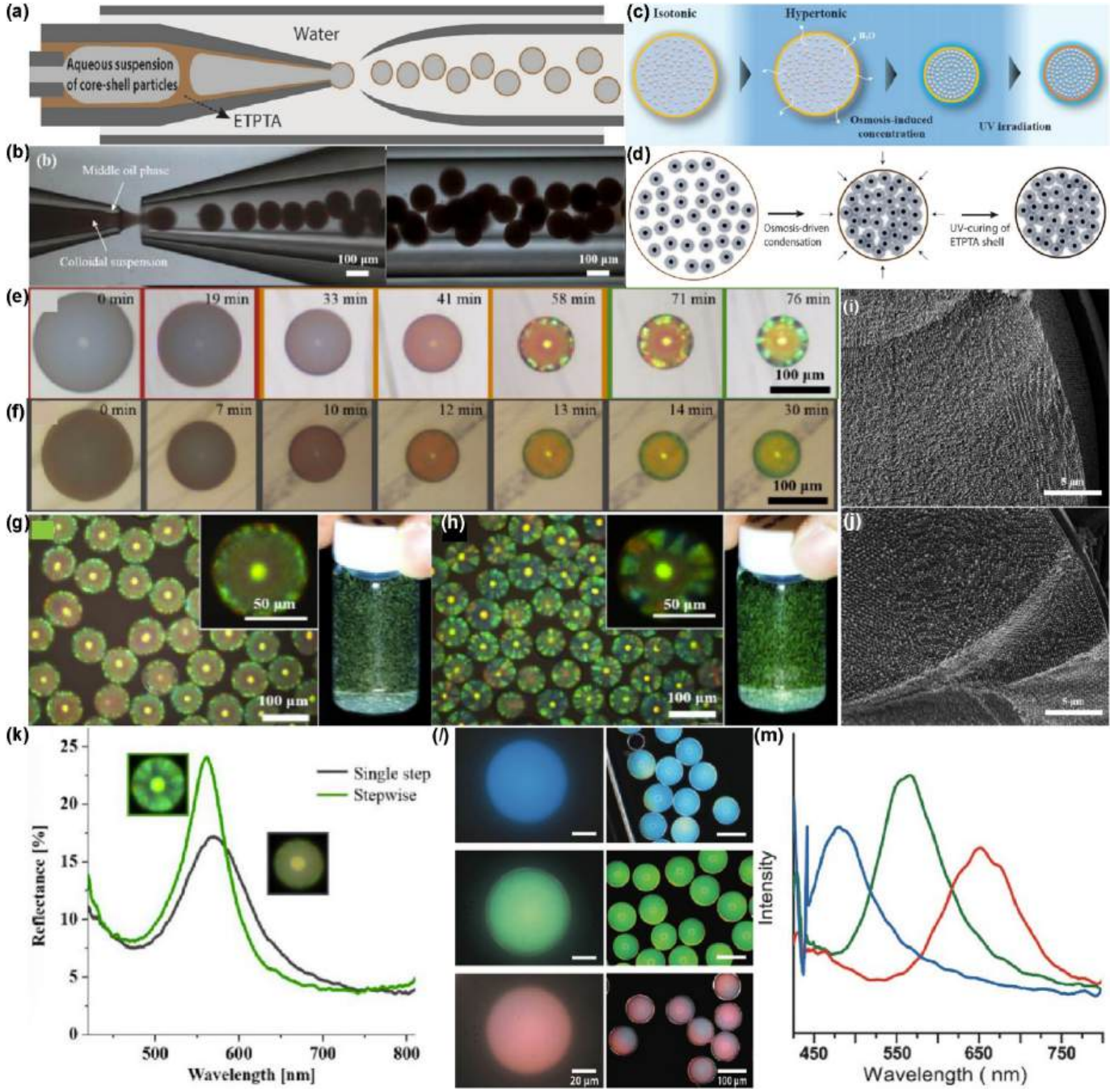


**Fig. 29.** (a)-(b) The illustration figure and OM image show the fabrication of droplet microcapsules with a thin shell, where ETPTA resin and an aqueous suspension of PS CPs were used as the shell and core parts, respectively. (c)-(d) Illustration figures show the evolution of ultrathin shell droplets under the impact of a relatively small osmosis difference (c) and a large osmosis difference (d). (e)-(f) OM images of the evolution of the microcapsule upon relatively small osmosis difference (e) and large osmosis difference (f). (g)-(h) OM images of photonic microcapsules formed using a single-step incubation and a two-step incubation route, respectively. (i)-(j) cryo-SEM images of the microcapsules formed from the single-step incubation (i) and the two-step incubation (j). (k) Reflection spectra comparison between microcapsules formed from the single-step incubation route and the two-step incubation routes [225]. Reprinted from ref. 225 with permission from the American Chemistry Society, copyright 2015. (l)-(m) OM images of photonic pigments (l) using aqueous suspension of different diameters of PS@poly(NIPAAm-AAc) core–shell CPs as the core part and their corresponding reflection spectra (m) [224]. Reprinted from ref. 224 with permission from Wiley, copyright 2014.

flexible state when subjected to an unbalanced osmotic pressure [205,221,226]. The photonic structures in the core part also started with a diluted suspension of PS CPs, the concentration of which was below the suspension's threshold that shows photonic properties. Upon a hypertonic condition, the core part of the droplets gradually shrank due to the outflow of water molecules across the shell part, leading to the increase in colloidal suspension's concentration in the core part and the formation of glass or crystal structures at different stages of evolution. In addition, the evolution of the droplet microcapsules displayed different photonic patterns in the core part when placed in external solutions with different concentrations of salt molecules (as shown in Fig. 29c-d). Moreover, the buckling phenomenon may emerge when the incubation solution contains relatively higher concentrations of salt molecules (as shown in Fig. 29d-e). The core-shell droplet microcapsules were subsequently transformed into photonic microcapsules upon UV light irradiation, which induced the formation of a relatively solid pETPTA shell and a flexible rubber shell when ETPTA and photocurable PDMS precursor were used as the shell components, respectively. The photocured microcapsules displayed different properties due to the different nature of the shell materials under the stimulus of hypotonic osmotic pressure. Instead of using single-step incubation, a two-step incubation route was also introduced to tune to the photonic patterns inside individual droplet capsules [225]. It was found that a single-step incubation led to the formation of photonic microcapsules with uniform color patterns (as shown in Fig. 29f and h) in the core part, while a two-step incubation approach resulted in the formation of microcapsules with sparkling color patterns in the core part (as shown in Fig. 29 g and i). This was due to the single-step incubation inducing the formation of a large portion of amorphous structures (that extend from the center of the capsules to 5 μm from the inner wall, Fig. 29j) in the core part of the microcapsule, while that of the microcapsules formed from the two-step incubation resulted in the formation of ordered structures throughout their entire core part (as shown in Fig. 29k). Correspondingly, the microcapsules formed from the single-step incubation displayed a weaker and wider reflection spectrum when compared with that of the microcapsule formed from the two-step incubation route (as shown in Fig. 29l). To further take advantage of the microcapsules with colloid-based amorphous core, Kim et al. encapsulated PS@poly(NIPAAm-AAc) core-shell CPs into the ultrathin ETPTA shell droplets using a similar microfluidic device [224]. Through the osmotic pressure-driven enrichment effect plus post-UV curing of the ETPTA shell, photonic microcapsule pigments with different structural colors can be obtained by tuning the initial hydrodynamic diameters of the core-shell CPs (as shown in Fig. 29m-n). The utilization of PS@poly(NIPAAm-AAc) core-shell CPs and controlled microcapsules' diameter at approximately 100 μm could effectively suppress the multiple light scattering.

Almost all of the above-mentioned photonic microcapsules' photonic properties originated from CPs with non-deformability (i.e., $SiO_2$, PS et al.) or limited deformability (such as PS@pNIPAAm core-shell CPs with responsive properties from the pNIPAAm shell part). Colloidal particles, such as hydrogel CPs, with full deformability possess the merit of tuning their sizes/volumes simply by changing external parameters, for instance, temperature, pH values, ionic strength, etc. These properties enabled researchers to change volume fractions of CPs in suspensions by feasibly varying the parameters without the need to of adjust CP's concentrations when the deformable gel particles were used as building blocks for photonic structures [85,91,228–231]. As a result, these advantages allowed researchers to tune the photonic properties of the colloidal photonic structures using these fully deformable CPs as building blocks in a straightforward manner. While a large amount of research reports have focused on the construction of 'hard' colloid-based photonic microobjects via microfluidic approaches, very few studies have shed light on the construction of photonic microobjects via microfluidics using the fully deformable CPs as the building blocks. Actually, in our natural world, many living species, such as, chameleons, could change not only in structural colors but also part of the physical body when encountered with predators [21]. So it was highly demanded to develop photonic microstructures that could couple their physical structure changes with structural color variations [232,233]. Despite the large amount of research efforts that have been devoted to designing and constructing photonic microobjects with tunable photonic properties, microobjects with tunable photonic properties accompanied by isotropic physical shape changes have also been realized. Very few studies have focused on the construction of photonic microobjects featuring photonic property changes simultaneously coupled with anisotropic shape changes. In this regard, Zhu and Yang et al. leveraged an osmotic pressure-driven buckling of microcapsules and prepared photonic microcapsules that can display photonic properties and geometry changes simultaneously [205,234]. They utilized a standard glass capillary microfluidic device for double emulsion generation and encapsulated an aqueous suspension of fully deformable pNIPAAm-co-AAc gel particles with photonic properties into a thin ETPTA resin shell (as illustrated in Fig. 30a). Followed by UV curing of the shell part, photonic microcapsules covering full visible spectra wavelengths can be subsequently obtained (as shown in Fig. 30b-c). The different structural colors of the microcapsules originated from the different concentrations of gel particles inside the microcapsules. The shell thickness of the microcapsules was controlled in a matter of hundreds of nanometers (~700 nm), which endowed the shell part with flexibility. Taking a microcapsule with an initial pink hue, for example, the flexibility of the shell part enabled the microcapsules' shell part to experience a dimple emerging towards a buckling process after being placed in a hypertonic aqueous solution, i.e., 2 M of NaCl solution. Simultaneously, the inner core suspension of gel particles gradually enriched and displayed a gradual color shift from pink to green and eventually blue (as shown in Fig. 30d). As a result of the outflow, the water molecules from the core part move toward the ambient medium [223]. It took up to one hour for completion of the evolution, and the blueshift of the reflection spectra peak value was up to 150 nm (as shown in Fig. 30e-f). This phenomenon was not only due to the flexibility of the thin shell but also ascribed to the deformable property of pNIPAAm-co-AAc gel particles in the core part. Owing to the synergistic effect both from the shell and core parts, the microcapsules exhibited synchronized shape deformation and optical property change upon the hypertonic osmotic pressure impact (as illustrated in Fig. 30g).

While the above-mentioned CPs encapsulation and volume fraction of the CPs in the core part of the microcapsules can be regulated by external media, which led to the formation of microcapsules with different photonic properties, and the inside assembled structures of colloids can be regulated by the osmotic pressure difference between the inside and outside the microcapsules so as to form colloid-based photonic crystal or glass structures. However, systematically controlling the microdomains of colloidal-based superstructures and then the photonic properties inside the tiny spaces has rarely been reported, despite efforts to tune the colloid-based microstructures through different interactions, such as charge screening effects, curvature effects, and depletion attraction effect, which have been realized in bulk conditions or inside droplets [216,235–240]. In light of this, Kim et al. moved one step further in designing photonic microcapsules with new properties. Instead of simply encapsulating CPs into core/shell droplets, an aqueous suspension containing PS@pNIPAAm-co-AAc core/shell CPs, salt molecules, and linear polymers pNIPAAm-*co*-AAc was encapsulated into core/shell droplets [241]. The salt molecules and linear polymers served as electrostatic screening reagents and macromolecular depletion reagents, respectively [216]. Due to the curvature effect from the microcapsule templates and the depletion-driven phase separation effect, the CPs assembled into multiple microdomains inside the microcapsules when incubated in a hypertonic solution and subjected to a hypertonic osmotic pressure effect (as shown in Fig. 31a-c). Confocal microscopy images indicated that the microdomains were actually single crystals formed from the assembly of the core-shell CPs (as shown in Fig. 31d-e). Unlike the work from Zhu's report, where the photonic microcapsules using PS@pNIPAAm-co-AAc core-shell CPs as the building blocks

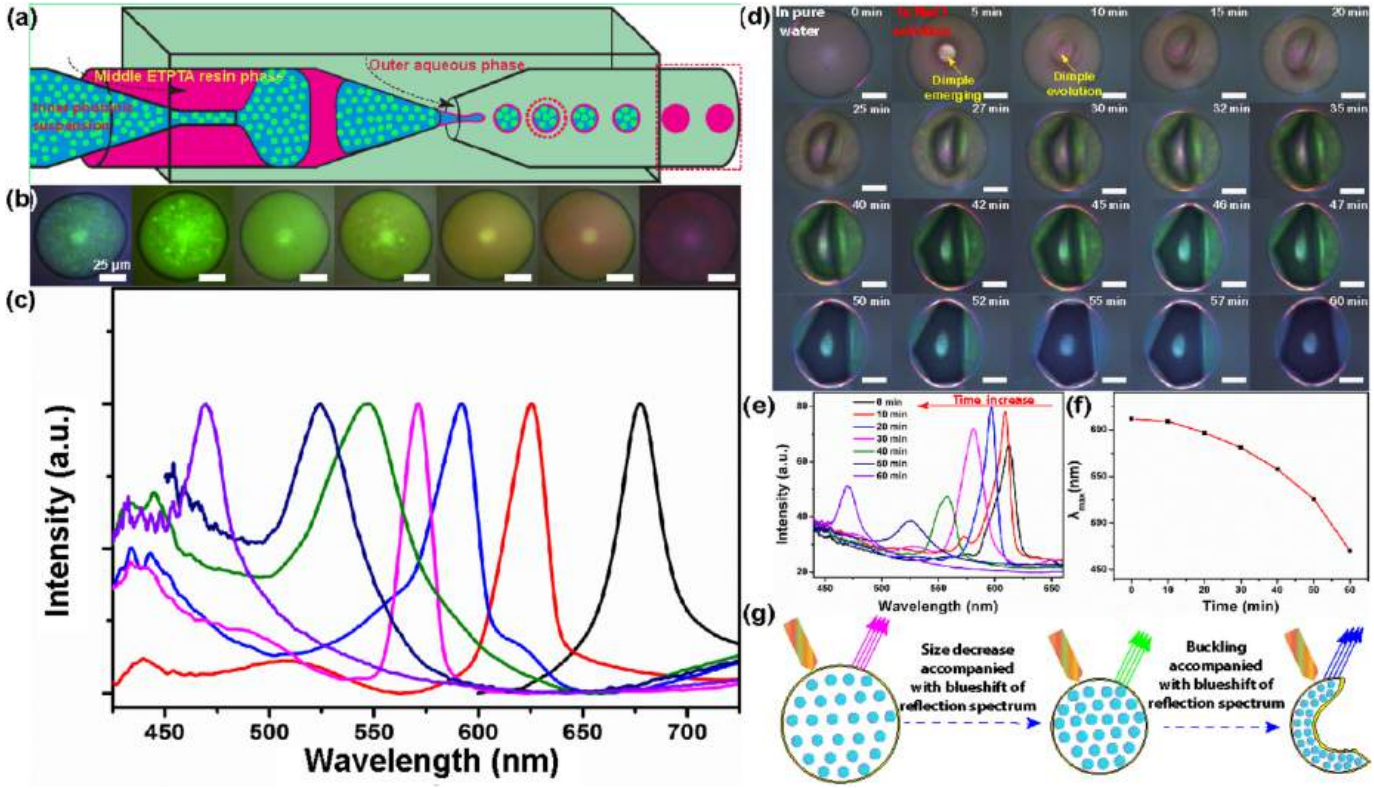


**Fig. 30.** (a) The illustration figure shows the fabrication of photonic microcapsules with a thin shell. An aqueous suspension of pNIPAAm-co-AAc gel particles and ETPTA resin were used as the core and shell parts, respectively. (b) OM images of the thin-shell microcapsules with different colors, which were tuned by the initial gel particle concentrations inside the microcapsule. (c) Reflection spectra of the thin-shell microcapsules with different colors from blue to red, covering the entire visible light spectrum. (d) OM images show how a microcapsule with an initial pink hue evolved after being transferred from pure water to an aqueous solution of NaCl (2 M). (e) Reflection spectra change of the pink microcapsule in d after being transferred into the aqueous solution of 2 M NaCl. (f) The maximum wavelength values of reflection spectra change as a function of time. (g) The illustration figure shows how the microcapsule evolves under the impact of the hypertonic osmotic pressure effect [234]. Reprinted from ref. 234 with permission from Elsevier, copyright 2020. (For interpretation of the references to color in this figure legend, the reader is referred to the web version of this article.)

displayed no thermoresponsive properties [215], the microcapsules in this case displayed a rapid temperature-induced color change phenomenon due to the thermoresponsive shell (pNIPAAm-co-AAc) of the PS@pNIPAAm-co-AAc core-shell CPs, the corresponding wavelength of the refractive spectrum shifted as much as 80 nm (as shown in Fig. 31g-h). More importantly, the response time was only 6.4 s, which was a significant improvement when compared with that of the bulk hydrogel materials that normally required several minutes (as shown in Fig. 31i-j) [231].

In addition to the thermoresponsive property regulation and micropattern adjustment through this depletion-driven phase separation, it was further applied to construct a series of photonic microcapsules with different shell materials. Other factors, such as deformed microcapsules and osmotic pressure differences between the outer medium and inner core suspension, were also taken into account to adjust the assembly behaviors of the CPs inside the microcapsules. Kim et al. continued their exploration in tuning the assembly behaviors of the charged PS CPs within microcapsules with a flexible shell, such as a PDMS shell. The microcapsules were also generated using a standard co-flow microfluidic device. The PS CPs inside the droplet microcapsules were enriched by incubation under hypertonic conditions (aqueous solution of NaCl) and at 4 °C. The PDMS prepolymer shell of the incubated droplet microcapsules can be further cured at 25 °C (as shown in Fig. 32a). Different extents of osmotic pressure could result in the formation of different sizes of crystallites. Specifically, the incubation solution with a lower concentration of salt (NaCl) resulted in the formation of a few large crystallites; vice versa, the incubation solution with a higher concentration of salt (NaCl) led to the fast crystallization and formation of multiple small crystallites along the inner surface of the microcapsules. This was due to the curvature effect from the microcapsules (as shown in Fig. 32b-d and illustrated in Fig. 32f-g) [235,242]. Correspondingly, the microcapsules containing fewer and relatively larger crystallites displayed narrower but more intense reflection spectra than that of the microcapsules containing more and smaller crystallites (as shown in Fig. 32h). Additionally, the soft nature of the shell part can also be leveraged to tune the properties of the photonic microcapsules. Typically, when the microcapsules were confined between two glass slides, the deformation effect could induce the rearrangement and dense packing of the crystallites due to the area fraction decrease of the crystallites. This rearrangement boosted the photonic property and correspondingly enhanced the intensity of the reflection spectrum peak but without shifting the peak values. This phenomenon indicated that there was no crystalline lattice change during the deformation process (as shown in Fig. 32i-k), featuring the resulting microcapsules with different properties, such as mechanochromism and optical anisotropy repulsive [243]. Since the polycrystalline grains normally grew from the inner surface of the microcapsules due to the curvature effect, this resulted in the low reflectivity of the microcapsules. It was difficult to control the crystal orientations despite single-crystalline microspheres being able to be produced [244,245]. To address the shortcoming, Kim et al. introduced a method to obtain microcapsules with density anisotropy assisted by a gentle centrifugation effect, which initiated colloidal nucleation and growth of single-crystalline grains through depletion attraction. The multiple microdomains on the heavy side of the individual microcapsule eventually merged into a single large grain through the ripening effect. As a result, single-crystalline grains

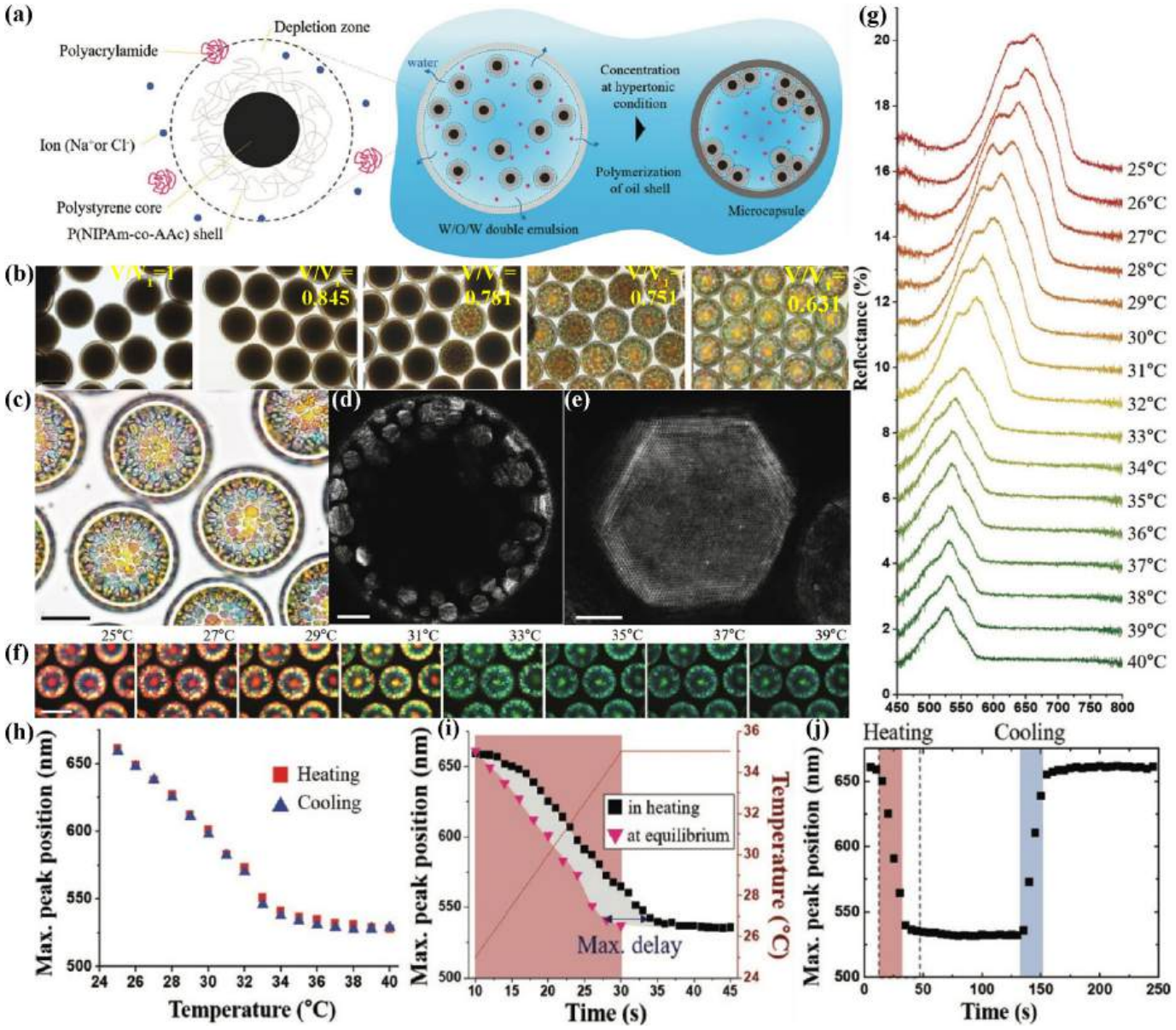


**Fig. 31.** (a) The illustration figure shows the osmotic pressure-driven formation of multidomain inside droplet microcapsules assisted by a combination of the depletion effect from linear polymers and the osmotic pressure-driven enrichment effect. (b) OM images of the evolution of the droplet microcapsules under the drive of osmotic pressure. (c) The OM image shows each individual photonic microcapsule containing multiple microdomains. (d) Confocal microscopy image of the multidomain inside an individual microcapsule. (e) Enlarged confocal microscopy image of a microdomain. The hexagonal structure clearly revealed the single crystal structure assembled from CPs. (f) Thermo-induced color pattern changes of the microcapsules. (g) The reflection spectrum of the microcapsule changes as a function of temperature. (h) The maximum reflection spectrum peak value of the microcapsule changes as a function of temperature. (i) Temperature (right y-axis) and peak position (left y-axis) of the microcapsules change as a function of time. (j) Reflection spectra peak position of an initial red-core microcapsules changes as a function of time [241]. Reprinted from ref. 241 with permission from Wiley, copyright 2018. (For interpretation of the references to color in this figure legend, the reader is referred to the web version of this article.)

distributed along the heavy side of the microcapsules can be produced (as illustrated and shown in Fig. 32l) [246]. Fig. 32m shows large single green grains inside individual microcapsules, and most of the grains are composed of stacking of hexagonal arrayed CPs from the bottom part (as illustrated in Fig. 32n). To accommodate the single crystallite grain on the curved surface of the microcapsule, the hexagonal array should develop along the inward direction, as shown in Fig. 32o. Correspondingly, the reflection spectra from the large single crystallite exhibited a narrow and intense spectra signal (as shown in Fig. 32p). As a result, the microcapsule displayed different intensities of reflection spectra values when measured from different orientations (as shown in Fig. 32q). In other words, this kind of microcapsule possesses orientation-dependent photonic properties.

Moreover, the pure interparticle potential among CPs was also utilized to tune the microstructures formed from the assembly of charged CPs within a confining space, such as microcapsules. By tuning the repulsive interaction among the charged CPs, Kim et al. reported controllable formation of PS CPs-based microdomain patterns inside the microcapsules (as shown in Fig. 33a-b) [244]. The formation of microdomain patterns was achieved through the combination of osmotic-pressure-mediated crystallization of an aqueous suspension of charged PS CPs and the tuning of the repulsive potentials among PS CPs. The repulsive potentials were regulated by adding different amounts of NaCl to the suspension of PS CPs. The PS CPs within microcapsules with

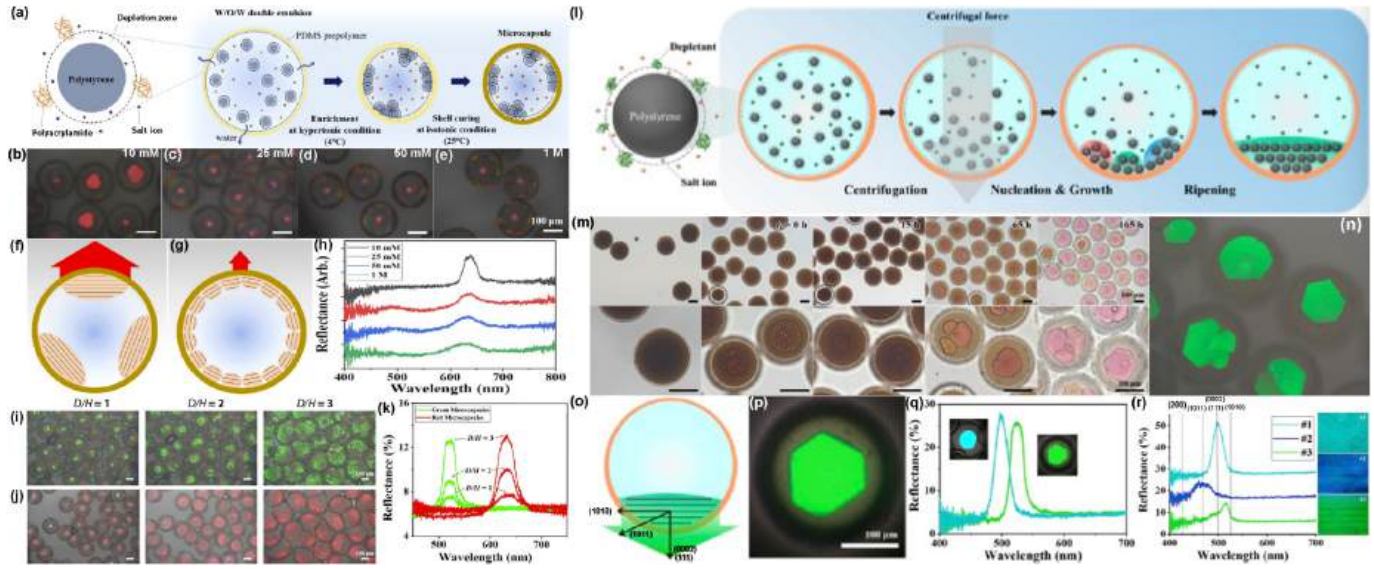


**Fig. 32.** (a) The illustration figure shows the composition of the inner core part of double emulsion droplets, osmotic pressure-induced enrichment and assembly of the colloids inside the droplets, and the subsequent shell solidification for producing elastic photonic microcapsules containing crystallites along the shell. (b)-(e) OM (reflection-mode) images of the elastic photonic microcapsules containing red-hue crystallites. (f)-(g) Cartoon figures show the resonant reflection on microcapsules containing large (f) and small crystallites (g) when microcapsules were being illuminated from vertically incident light. (h) Reflection spectra of the microcapsules incubated in different concentrations of NaCl solutions. (i)-(j) OM images of the green (i) and red (j) microcapsules with D/H values from 1 to 3. (k). Reflection spectra of the green and red microcapsules with different geometries in (i)-(j) [243]. Reprinted from ref. 243 with permission from the American Chemistry Society, copyright 2021. (l) The illustration figure shows the formation of a single-crystal microcapsule assisted by the centrifugation effect. (m) OM images (transmission mode) of microcapsules before and after centrifugation for 80 min under 140 *g* and incubation for different periods from the very beginning to 165 h. (n) OM image of microcapsules containing green crystallites. (o) The schematic figure shows the stacking of horizontal crystal planes along the vertical direction from the bottom of the microcapsule. (p) The OM image shows a uniform green color from the projection of the crystal grain. (q) Reflection spectra and the corresponding OM images of two microcapsules containing different single crystallites. (r) Reflection spectra and the corresponding OM (reflection mode) images of one crystallite at different orientations [246]. Reprinted from ref. 246 with permission from the American Chemistry Society, copyright 2023. (For interpretation of the references to color in this figure legend, the reader is referred to the web version of this article.)

relatively strong repulsive potentials tended to assemble into onion-like structures (as shown in Fig. 33c); vice versa, PS CPs within microcapsules with relatively weak repulsive potentials tended to form single crystal structures (as shown in Fig. 33d). Moreover, the microcapsules formed under the strong repulsive potentials showing vivid onion-like color patterns under OM (as shown in Fig. 33e-f). The reflection spectra of these microcapsules show a wide and relatively weak reflection spectra peak. Comparatively, the microcapsules with the CPs in the core part formed under relatively weak repulsive potentials, showing a uniform color pattern and some stripe patterns (as shown in Fig. 33 h-i), where the latter case was due to stacking faults. Correspondingly, the reflection spectra show relatively narrow but more intense peak values (as shown in Fig. 33j). These phenomena indicated that it may be difficult to obtain microcapsules with the same structural colors in one batch unless a proper method is developed to separate the photonic microcapsules with different photonic properties.

The temperature field as another useful measure has been widely used to produce crystal and amorphous structures. This approach has been used not only in colloidal assembly but also for other kinds of materials processing [63,220,247]. Despite a variety of effects, including charge screening effect, depletion effect, and tunable external field, such as osmotic pressure effect, have been leveraged to regulate the assembly behaviors of CPs, particularly thermoresponsive colloids (PS@pNIPAAm-co-AAc) within a confined space, and temperature-dependent transitions between fluidic and crystalline phases of thermoresponsive colloids within a confined space have also been reported. How the temperature field, specifically the cooling rate, affects the assembly structures of CPs and the corresponding photonic properties within a confined space has yet to be explored. In light of this, Kim et al. encapsulated PS@pNIPAAm-co-AAc CPs inside ETPTA microcapsules by microfluidics to produce droplet microcapsules [245]. The volume fraction of the CPs inside the droplet microcapsules was adjusted to 0.619 by a hypertonic osmotic pressure effect, and subsequently UV light irradiation was introduced to transform the droplets into stable microcapsules (as illustrated in Fig. 34a). The microcapsules were then incubated at 25 °C, and the inner core part was developed into single crystalline arrays. The microcapsules exhibited no color at a wide range of orientations despite green or red color that may appear at certain orientations (as shown in Fig. 34b). The reflection spectra of the red and green hues showed two distinct peaks at 624 and 540 nm, which respectively corresponded to the Bragg's diffraction for the (111) and the (200) planes of a face-centered cubic (FCC) lattice (as shown in Fig. 34c). Afterwards, the microcapsules were heated to 60 °C and cooled down to 15 °C at different rates. When the microcapsules were cooled down at a rate of 30 °C/min, small crystal grains gradually formed along the inner surface of the microcapsules and eventually occupied the entire core part (as illustrated and shown in Fig. 34d). The resulting microcapsules showed consistent color appearance at any orientation (as shown in Fig. 34e). Correspondingly, the reflection spectra consistently had a maximum reflection peak value at 624 nm (as shown in Fig. 34f). Alternatively, the inner core part gradually developed into large crystallites along the inner surface of the microcapsules when the cooling rate was at a low value, such as 0.1 °C·min$^{-1}$. The large crystallites eventually stacked the entire core part of the microcapsule (as illustrated and shown in Fig. 34g). Therefore, the microcapsule displayed orientation-dependent color appearance (as shown in Fig. 34h). The resulting colors were predominantly green and red, and the corresponding reflection spectra peaks are well matched with the Bragg diffraction wavelengths for different crystal planes, such as (111) and (222) planes for FCC (as shown in Fig. 34i).

The common point of the abovementioned photonic microcapsules was that almost all the building blocks in the core part were a single type

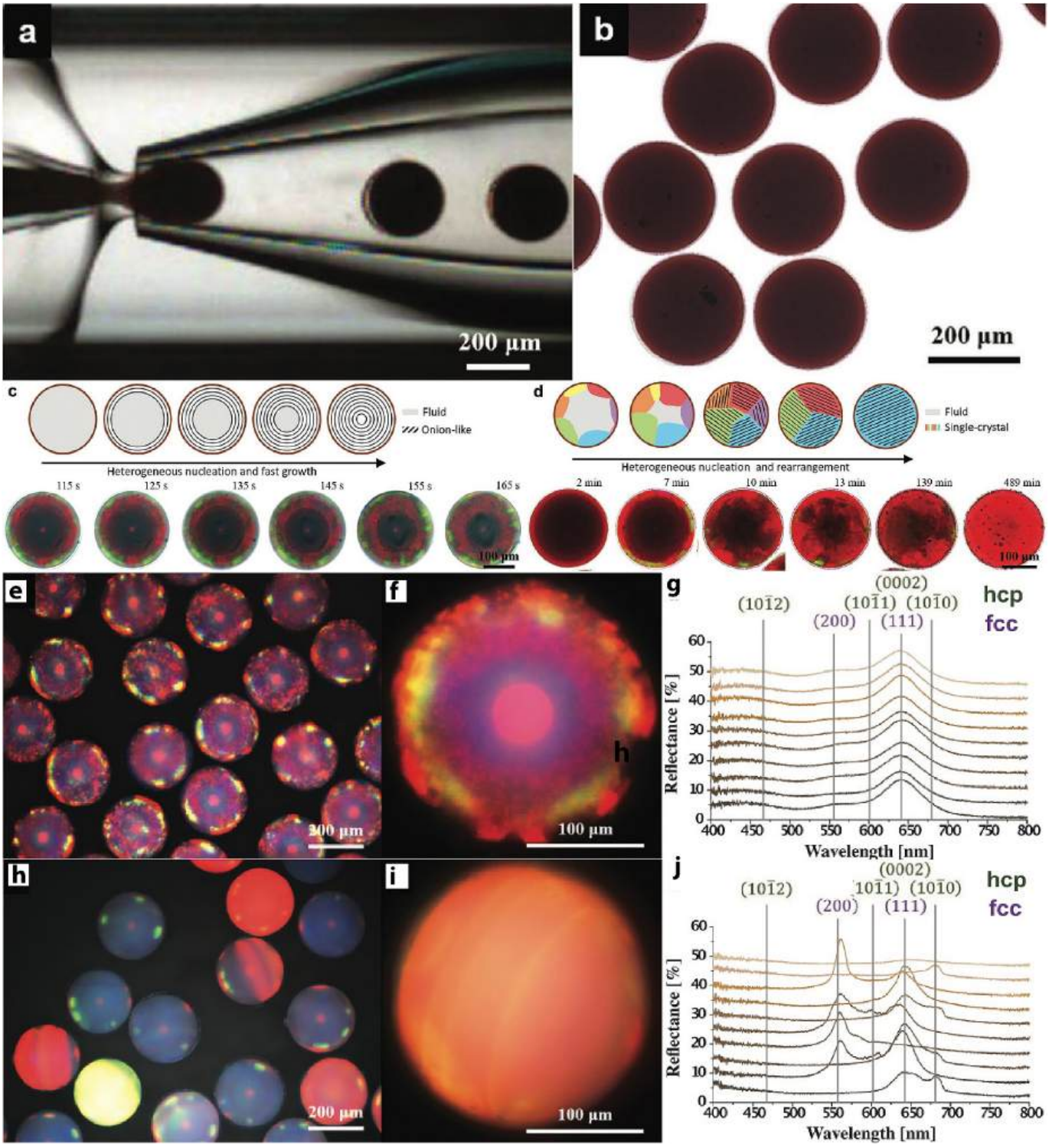


**Fig. 33.** (a)-(b) OM images of the microfluidic generation of core-shell photonic microcapsules (a) and the resulting core-shell photonic microcapsules (b). (c) Top row: The illustration figure shows how the droplet microcapsule gradually evolved from a fluid status to an onion-like structure; bottom row: OM images show the corresponding evolution process. (d) Top row: The illustration figure shows how the droplet microcapsule gradually evolved from fluid status to single-crystal structures; bottom row: OM images show the corresponding fluid-to-single-crystal evolution process. (e)-(f) OM image of several onion-like microcapsules (e) and enlarged OM image of the individual microcapsule (f). (g) Reflection spectra of the microcapsule in (f) and their corresponding crystal plane structure. (h)-(i) OM image of several single crystal microcapsules (h) and enlarged OM image of an individual microcapsule (i) with single crystal structure. (j) Reflection spectra of the microcapsule in (i) and their corresponding crystal plane information interpretation [244]. Reprinted from ref. 244 with permission from Wiley, copyright 2019.

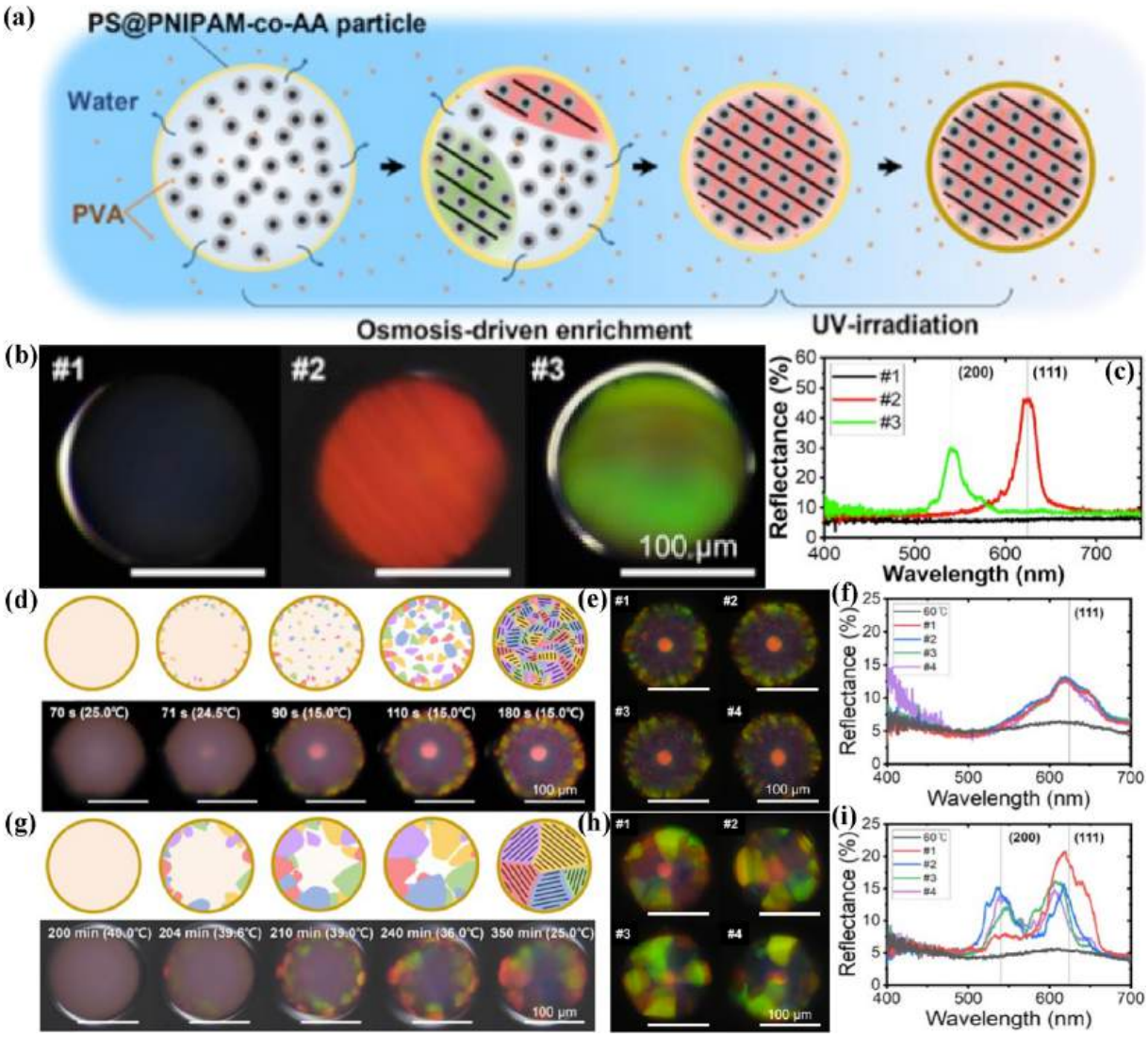


**Fig. 34.** (a) The illustration figure shows the regulating of photonic properties of the microcapsules by the combination of osmosis-driven enrichment and a subsequent UV curing process. (b) The individual microcapsule shows different optical phenomena at different orientations. (c) Reflection spectra of the photonic microcapsule at different orientations in (b). (d) Illustration figure (top row) and OM images (bottom row) showing the evolution of a microcapsule containing PS@pNIPAAm-co-AAc core-shell CPs under the influence of a fast cooling rate. (e)-(f) OM images (reflection mode) of a microcapsule with fully stacked small crystallites at different orientations (e) and the corresponding reflection spectra (f). (g) Illustration figure (top row) and OM images (bottom row) showing the evolution of a microcapsule under a slow cooling rate. (h)-(i) OM images (reflection mode) of a microcapsule with fully stacked large crystallites at different orientations (e) and the corresponding reflection spectra (i) [245]. Reprinted from ref. 245 with permission from the American Chemistry Society, copyright 2022.

of CP with monodispersed size distribution. How binary CPs assemble inside microcapsules under the impact of osmotic pressure regulations and what kind of photonic features the resulting microcapsules process having been rarely explored and understood, despite crystal structures formed from the assembly of binary CPs under 2D bulk condition have been well studied and some 1D confining conditions having been reported [248–257]. In this regard, Deravi et al. investigated the assembly of binary CPs inside microcapsules through an osmotic pressure annealing process (as illustrated in Fig. 35a) [258]. Xanthommatin-tethered PS CPs with diameters of100 nm (termed PS100-XA) and pure PS CPs with varying diameters (200–300 nm) were used as the building blocks for the photonic composition. After collecting in a 1 M NaCl solution, the inner core part of the microcapsules displayed a significant decrease in size due to the osmotic pressure-induced outflow of water from the inner core part (as shown in Fig. 35b-c). By varying the combinations of the CPs, i.e., the inner core part of the microcapsules containing aqueous suspension of pure PS CPs or a mixture of PS CPs and PS100-XA, photonic properties of the microcapsules can be modulated accordingly (as shown in Fig. 35d-f). Apparently, the photonic microcapsules using binary CPs as the inner core part possess limited controllability over the photonic properties of the resulting microcapsules. In order to control the assembly behaviors and then photonic properties of the binary CPs in the inner core part in a controllable manner, Kim et al. utilized the depletion-induced attraction approach to regulate the assembly of binary CPs inside confined microcapsules [259]. The microcapsules produced from a conventional double emulsion microfluidic device were composed of a thermocurabale PDMS shell and an aqueous suspension of mixed components in the core part, such as binary PS CPs, linear polymers pNIPAAm-*co*-AAc, and a certain amount of NaCl. The osmotic-pressure-driven colloidal enrichment and subsequent depletion-attraction effect were leveraged to tune the assembled microstructures from CPs and the corresponding photonic properties (as illustrated in Fig. 35g). The synergistic effects of depletion attraction, electrostatic repulsion, and van der Waals attraction result in the formation of different crystalline arrays based on the CPs. Unlike previously reported crystalline arrays that were formed from the

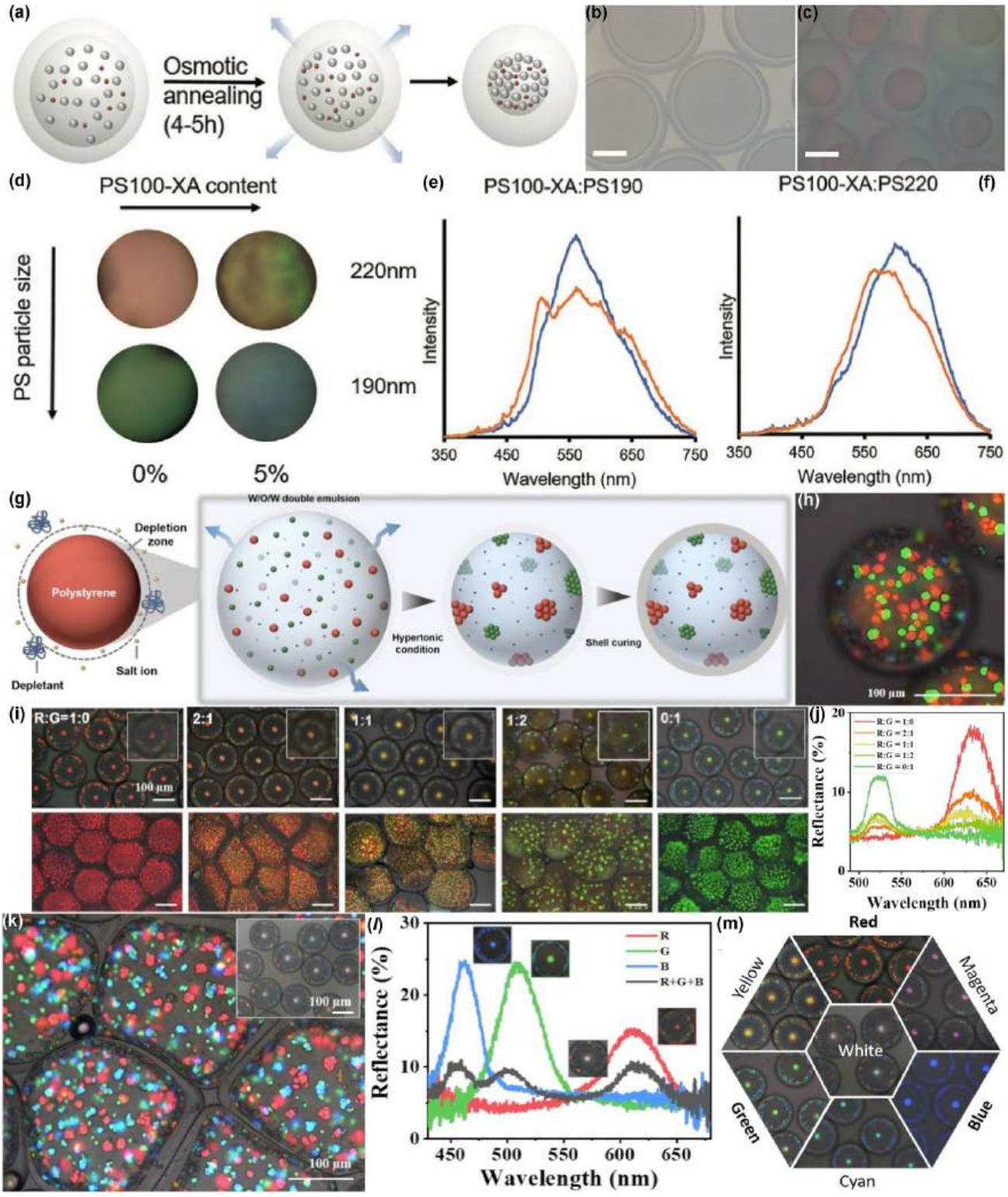


**Fig. 35.** (a) The illustration figure shows the formation of photonic microcapsules using binary CPs as the inner core part through osmotic pressure annealing. (b)-(c) OM images of microcapsules before (b) and after (c) osmotic pressure annealing. (d) OM images of the microcapsules using different combinations of CPs with different diameters as the inner core part. (e)-(f) Reflection spectra of the different microcapsules in d [258]. Reprinted from ref. 258 with permission from Wiley, copyright 2021. (g) Illustration figures show the formation of multiple grains based on binary CPs inside microcapsules. (h) The OM image shows photonic microcapsules containing multiple grains with green and red structural colors that were formed from the assembly of binary colloids. (i) OM images of photonic microcapsules containing different ratios of green and red grains. (j) Reflection spectra of the photonic microcapsules containing different ratios of red and green grains. (k) OM image shows the microdomain patterns inside microcapsules, where the microdomains formed from the assembly of three different diameters of PS CPs. (l) Reflection spectra of four different kinds of photonic microcapsules using three different monodispersed PS CPs and a mixture of the three different-sized PS CPs as the inner core part, respectively. (m) Gallery of photonic microcapsules with single colors and mixed colors [259]. Reprinted from ref. 259 with permission from Wiley, copyright 2023. (For interpretation of the references to color in this figure legend, the reader is referred to the web version of this article.)

assembly of single-sized CPs featured with a single stopband, the crystalline arrays formed from different-sized CPs in this study showed different grains, stopbands, and corresponding different structural colors. Fig. 35h shows an individual microcapsule containing different grains that feature green and red colors. Furthermore, the final patterns inside individual microcapsules can be controlled by adjusting the weight ratio of the green and red compositions (as shown in Fig. 35i). Therefore, the intensities of the red and green parts can be accordingly regulated (as shown in Fig. 35j). To move one step further, individual photonic microcapsules containing three microdomains, such as green, blue, and red can be achieved when three kinds of PS CPs are simultaneously encapsulated into the initial individual microcapsule (as shown in Fig. 35j). As a result, the individual microcapsule featured three distinct reflection spectra peaks, whose maximum reflection spectra positions were consistent with the position of the reflection spectrum from the microcapsules using the corresponding single-sized PS CPs as the core part (as shown in Fig. 35l). Eventually, single-colored photonic microcapsules and various mixed-colored photonic microcapsules can be obtained by combining different colloidal compositions, as shown in the galleries in Fig. 35m.

### 5.2. Photonic microcapsules with the photonic property in the shell part

Despite the above-mentioned reports were all related to photonic microcapsules with their photonic compositions in the core part, photonic microcapsules with photonic compositions lie in the shell part were also constructed. Kanai and Weitz et al. utilized a glass-capillary based microfluidic device to fabricate photonic microcapsules, which the shell part was composed of a photocurable aqueous suspension of the mixture of charged PS CPs and NIPAAm-based monomers, the core part was a PDMS oil phase (as shown in Fig. 36a-c and g). Simply by varying the concentrations of the PS CPs in the shell part, the resulting microcapsules displayed different structural colors and correspondingly different characteristic reflection spectra peaks (as shown in Fig. 36d-f and h) [260]. Alternatively, Zhu et al. fabricated photonic microcapsules using ETPTA suspension of $SiO_2$ CPs as the shell composition (as shown in Fig. 36i-l). The photonic properties were tuned by the $SiO_2$ CPs concentrations in the resin suspensions (as shown in Fig. 36m) [261]. In addition, photocurable PEGPEA suspension of $SiO_2$ CPs was used as the shell material and the corresponding photonic microcapsules were fabricated using a similar microfluidic device (Fig. 36o) [262]. Different colors of photonic microcapsules were subsequently fabricated by changing the initial concentrations of $SiO_2$ CPs in the PEGPEA suspensions (Fig. 36p). Due to the elastic nature of the polymerized PEGPEA, the microcapsule displayed fully reversible compression-relax behaviors (Fig. 36q-r). The elastic property of the shell part also enabled the microcapsules with osmosis-dependent photonic properties along different directions of individual microcapsules. Specifically, in the pole and equator regions of an individual microcapsule respectively displayed red-shift and blue-shift due to the increased and decreased spacing among CPs in the corresponding regions (Fig. 36s-t).

### 5.3. Photonic microcapsules with photonic properties both in core and shell parts

Given that the droplet templates from different microfluidic devices

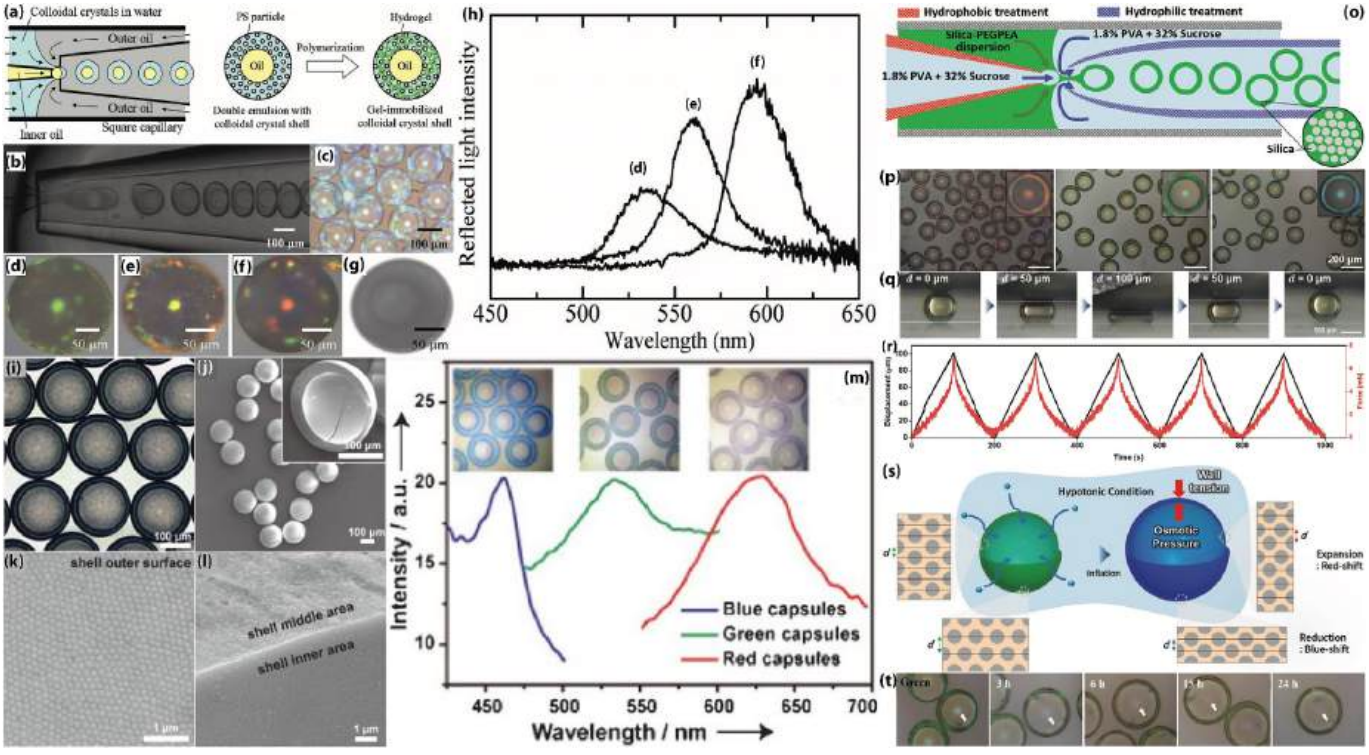


**Fig. 36.** (a) The illustration figure shows microfluidics fabrication of pNIPAAm hydrogel-based photonic microcapsules. (b)-(c). The microfluidics process (b) and the resulting photonic hydrogel microcapsules (c). (d)-(f) Microcapsules with different structural colors. (g) OM image (transmission mode) of the microcapsule. (h) The corresponding reflection spectra of the microcapsules (d)-(f) [260]. Reprinted from ref. 260 with permission from Wiley, copyright 2010. (i) OM image of photonic microcapsules using ETPTA suspension of $SiO_2$ CPs as the shell part. (j)-(l) SEM images of a bunch of photonic microcapsules (j), outer surface (k), and cross section (l) of the microcapsule. (m) Reflection spectra of the microcapsules with different colors and their corresponding OM images [261]. Reprinted from ref. 261 with permission from Royal Society Chemistry, copyright 2012. (o) The illustration figure shows the fabrication of PEGPEA resin-based photonic microcapsules. (p). Photonic microcapsules with red, green, and blue colors. (q) Compression-relax cycle of a green-colored photonic microcapsule. (r) Time-dependent changes of the displacement and the corresponding force change as a function of different cycles. (s) The illustration figure shows the evolution of photonic microcapsules evolving under hypotonic solution. (t). Time lapses OM images of green photonic microcapsules evolved in hypotonic solution [262]. Reprinted from ref. 262 with permission from Wiley, copyright 2023. (For interpretation of the references to color in this figure legend, the reader is referred to the web version of this article.)

are spherical in shape under normal conditions due to the minimization of interfacial energy, the structural color of spherically shaped photonic microobjects is normally anisotropic, singular, and mono-colored regardless of the viewing angle. Approaches have been brought to attain photonic microobjects with multiple colors on an individual microobject, despite bulk photonic structures with dual stopbands and beyond having been achieved in several studies [263–271]. Such as the fabrication of Janus-structured photonic microobjects or core-shell photonic microobjects with both the shell and core parts possessing photonic properties, namely photonic structures with dual and multiple stopbands. Specifically, instead of using the co-flow microfluidic device to encapsulate an aqueous suspension of CPs with photonic properties, Chen et al. utilized a microfluidic device with two parallel channels and interplayed spreading parameters between different phases to generate photonic microcapsules with both the shell and core parts featuring photonic properties (as shown in Fig. 37) [187]. The two parallel phases were a photocurable ETPTA suspension of $SiO_2$ CPs and an aqueous suspension of PS CPs with photonic properties (as shown in Fig. 37a). Through finely tuning the interfacial tensions among the two dispersed phases and a methylsilicone oil-based continuous phase, the Janus droplets formed from the paralleled two streams spontaneously evolved into a core-shell structure, which subsequently solidified to form microcapsules. The spreading parameter $S = \gamma_{bc} - (\gamma_{ab} + \gamma_{ac})$ among the three phases was introduced to predict the formation of core-shell structure. $\gamma_{bc}$, $\gamma_{ab}$, and $\gamma_{ac}$ represent the interfacial tensions between the two dispersed phases, between the continuous phase (methylsilicone oil) and the dispersed phase b (either the photocurable ETPTA suspension of $SiO_2$ CPs or aqueous suspension of PS CPs), and between the continuous phase and the dispersed phase c. In the specific case, to obtain the core-shell microcapsules, it was required the $S < 0$ [272]. Consequently, the shell and core parts clearly exhibited distinct colors, which corresponded to two reflection spectrum peaks (as shown in Fig. 37b-c). In addition, the photonic microcapsules with protection from the polymerized resin shell were resistant to several ordinary organic solvents, such as toluene, DMF (dimethyl formamide), and acetone, leading to the photonic properties of the core-shell photonic microcapsules being more stable than those of the photonic microobjects simply assembled from PS CPs (as shown in Fig. 37d-f). However, the photonic microcapsules were inert to external stimuli and may limit their further applications for diverse fields. Therefore, this fabrication strategy was also used to construct dual-stopband photonic microcapsules by employing an aqueous suspension of soft gel particles as the core part of the photonic composition [273]. The microcapsules may have special applications in the field of responsive materials.

Moreover, core-shell or quasi-core-shell photonic microobjects with more than one structural color can be accessed through another route. In addition to physically merging two or multiple photonic phases together and generating microobjects with multiple structural colors via microfluidics, microobjects initially with one structural color but subsequently treated with a solvent can be transformed into microobjects with dual or multiple structural colors. Yoo et al. reported the fabrication of core-shell-like photonic microobjects with dual structural colors via microfluidics-generated double emulsion droplets plus a core hatching approach (as shown in Fig. 38) [274]. The microcapsules' fabrication step was similar to that of Martinez's work published in 2013 [222]. Core-shell droplets with ETPTA resin as the shell part and a diluted aqueous suspension of PS CPs as the core part were prepared using a co-flow microfluidic device (as shown in Fig. 38a). After being collected in a container with an aqueous solution of NaCl (50 mM), the droplets were subjected to a hypertonic osmotic pressure, and the PVP-coated PS CPs concentration gradually increased due to the osmotic pressure-induced outflow of water from the inner core to the ambient collecting solution. Eventually, the PVP-coated PS CPs in the core part stacked into a close-packed colloidal photonic crystal (CPC) microsphere. The ETPTA shell can be subsequently hatched, leaving close-packed PS CPs-based spherical opal structure with a thin ETPTA layer. The opal microspheres were subsequently washed with ethanol to remove the ETPTA residues and surfactants. The PVP chains on the surface of PS CPs thus experienced a swelling process, leading to the slight swelling of the entire CPC microsphere. The PS CPs located close to the surface region of the CPC spheres underwent a slight contraction when being placed in pure water again. This was due to the better swelling performance of PVP molecules in ethanol than in water. While there were almost no changes for PS CPs that were close to the center of the CPC spheres. This eventually led the PS CPs close to the center region of individual microspheres possessing a relatively loose stacking, but the PS CPs close to the surface area of the microsphere with a compact stacking, yielding core-shell-like photonic microobjects. This action led to the appearance of two distinct structural colors (as shown in Fig. 38b-e) on an individual microobject and two distinct reflection spectrum peaks (as shown in Fig. 38f-g).

Instead of fabricating photonic microcapsules or microcapsule-like structures using the above-mentioned colloidal suspension encapsulating strategy or controlled contraction of CP building blocks by solvent

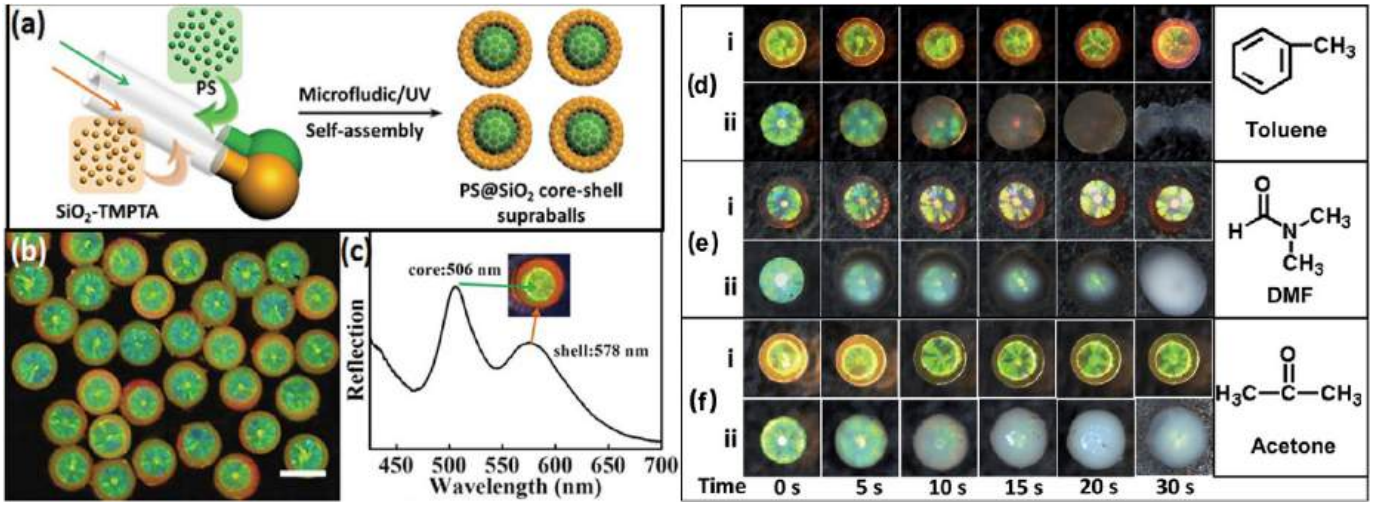


**Fig. 37.** (a) Schematic figure shows the fabrication of core–shell dual stopband photonic microcapsules using a two-parallel-channel microfluidic device. (b)-(c) OM image of an individual microcapsule with two distinct colors in the core and shell parts (b) and the corresponding reflective spectra in the core and shell parts. Scale bar in (b): 200 μm. (d)-(f) Evolution of (i) core-shell microcapsules and (ii) PS CPs-based supraballs immersed in different organic solvents: (d) toluene, (e) DMF, and (f) acetone [187]. Reprinted from ref. 187 with permission from the Royal Society of Chemistry, copyright 2014.

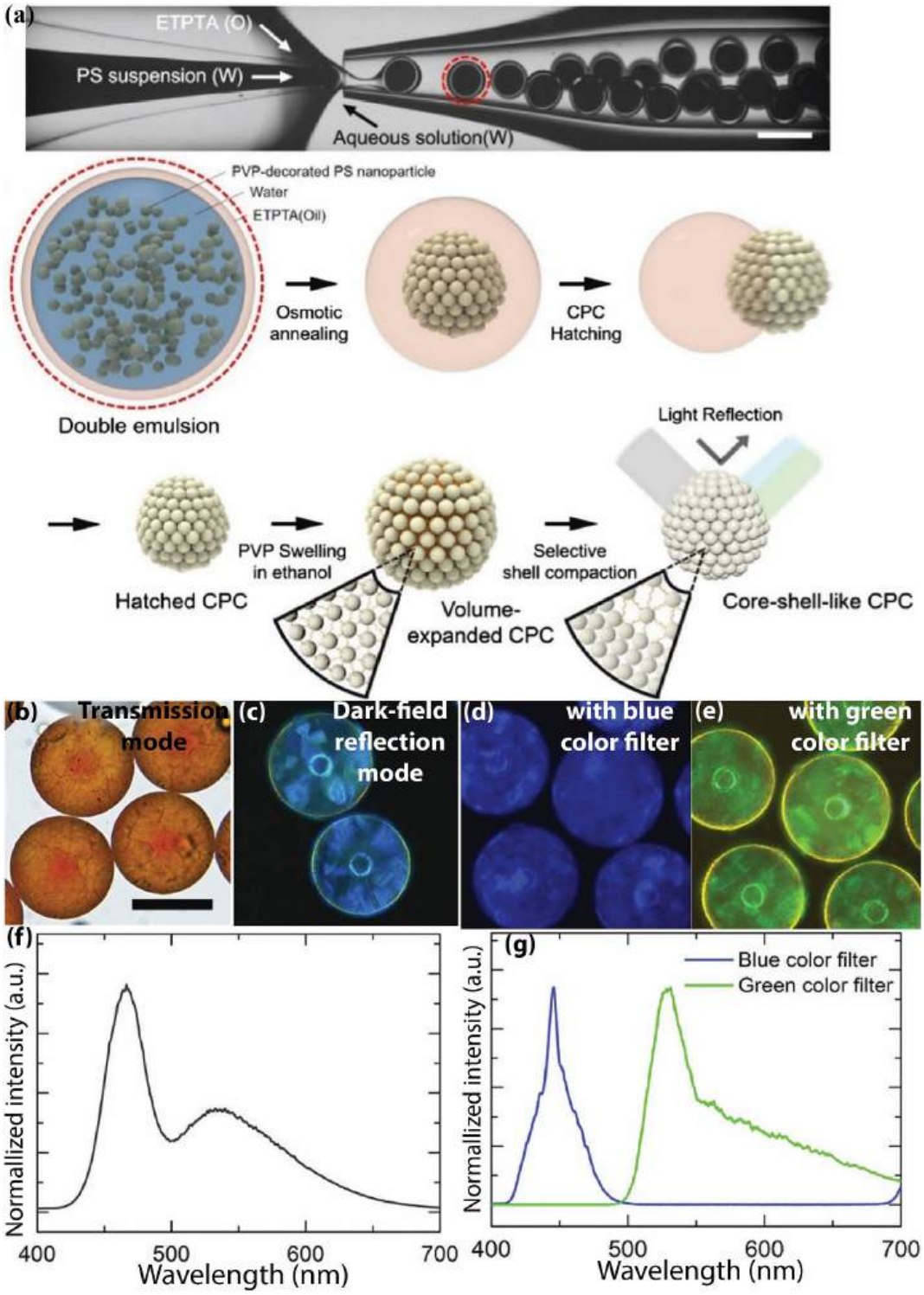


**Fig. 38.** (a) Top: OM image of the fabrication of core-shell-like photonic microcapsules using a co-flow glass capillary-based microfluidic device. Bottom: The illustration figure shows how the core-shell droplet microcapsules composed of PS CPs and ETPTA resin gradually evolved into PS CPs-based core-shell-like photonic microobjects (CPCs). (b)-(e) OM image (transmission mode) and dark-field reflection mode microscopy image (c), dark-field reflection mode microscopy image with a blue color filter (d), and (e) with a green color filter and of core-shell-like CPC microobjects. Normalized reflectance intensity spectra of core-shell-like CPC particles (f) without a color filter and (g) with color filters [274]. Reprinted from ref. 274 with permission from the Royal Society of Chemistry, copyright 2019. (For interpretation of the references to color in this figure legend, the reader is referred to the web version of this article.)

effect, a chemically operated system was conceived and implemented to generate photonic microcapsules with a core-shell structure, despite the core part being solid in such kinds of microcapsules. Gu et al. fabricated this kind of microcapsule using a two-step approach: Firstly, uniform-sized microballs with an opal structure using monodispersed $SiO_2$ CPs as building blocks through a microfluidic apparatus were fabricated [275]; subsequently, partial $SiO_2$ CPs (specifically the region close to the surface of the microballs) in each microball were etched in a controlled

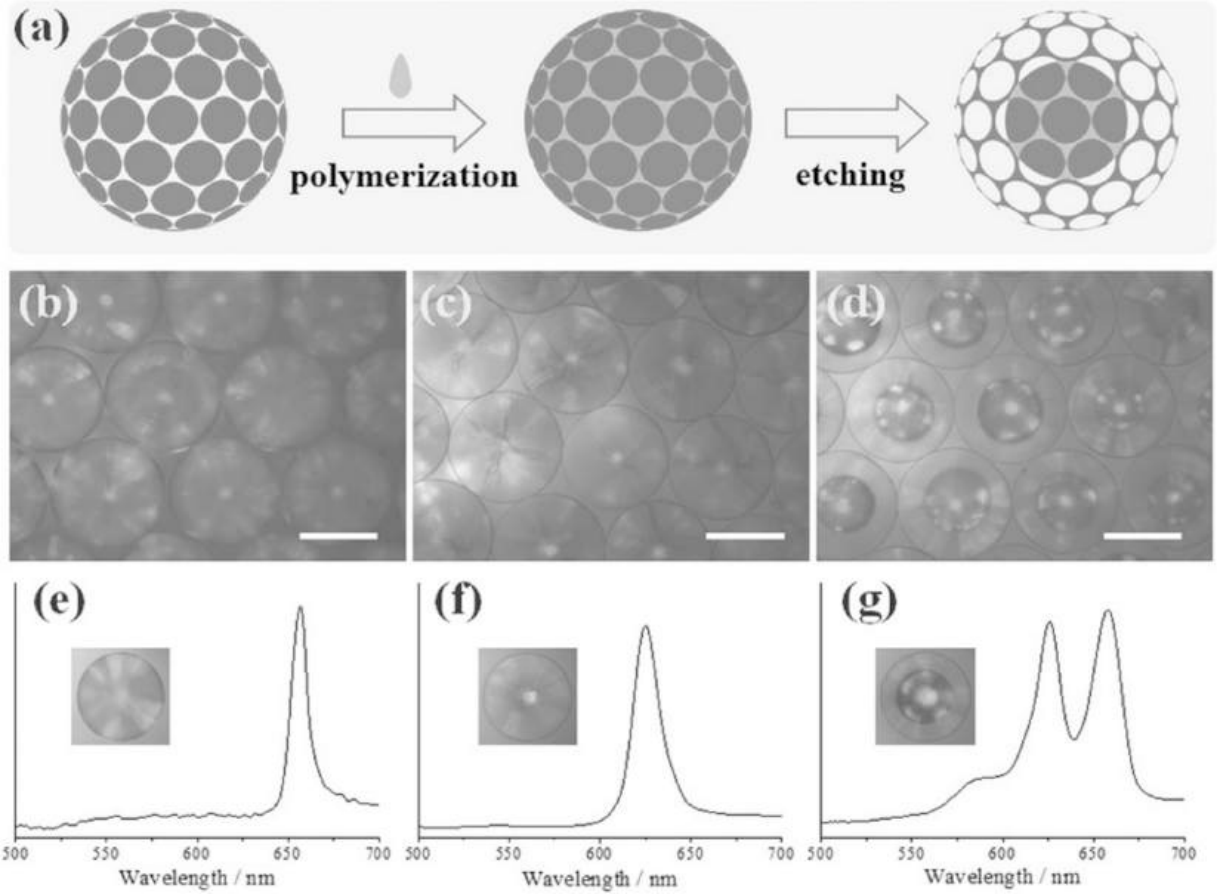


**Fig. 39.** (a) The illustration figure shows the preparation of photonic microcapsules using a controlled wet etching approach. $SiO_2$ CP-based supraparticles were firstly produced from a microfluidic approach and subsequently filled the voids among the CPs with monomers' solution. $SiO_2$ CPs-hydrogel composite microspheres can be obtained when the monomer solution-filled supraparticles are subjected to a polymerization process. The composite microsphere was subsequently transformed into a core-shell-like microcapsule when a controlled etching process was carried out. (b)-(d) OM images of colloidal crystal microbeads (b), hydrogel-$SiO_2$ CPs composite photonic crystal microspheres (c), and photonic microcapsules (d). (e)-(g). Reflection spectra of the microobjects corresponding to the microobjects in (b)-(d) [275]. Reprinted from ref. 275 with permission from Wiley, copyright 2014.

etching manner. Specifically, part of the $SiO_2$ CPs in the individual microball was etched while the remaining part was kept unreacted (as shown in Fig. 39a). Given the radial structure of the microball, the interface region that was far from the center of the microball was firstly etched while the center region was maintained unreacted. The etching reaction can be quenched by transferring the microballs into a large amount of water at any given moment, yielding each microball that was integrated with an opal core and an inverse-opal shell (Fig. 39b-d). Due to the different refractive indices between the core and shell parts, the resultant microcapsules were therefore endowed with dual photonic stopbands. The photonic microobjects can be further used for label-free multiplex detection, drug screening, and even the building blocks for anticounterfeiting materials [276,277].

## 6. Fully inverse opal photonic microobjects

Despite colloidal photonic microobjects with opal structures that could provide the microobjects with a variety of properties, photonic microobjects with inverse opal structures have also been prepared by microfluidics combined with different post-etching approaches. Kim and Yang et al. demonstrated the fabrication of inverse opal photonic microspheres using microfluidics combined with a post-etching process. ETPTA resin and silica CPs were used as the skeleton material and templates for the inverse opal structure, respectively. The inverse opal microspheres displayed a blue shift in reflection spectrum when compared with that of the unetched photonic opal balls (as shown in Fig. 40a-b) [109]. This was due to the enhanced refractive index mismatch after removal of the $SiO_2$ CPs; specifically, the removal of $SiO_2$ CPs decreased the effective refractive index of the photonic balls. Gu et al. reported the fabrication of silicone-based inverse opal photonic microbeads using a microfluidic-assisted fabrication process combined with a post-etching step [142]. To construct such kinds of microbeads, a suspension of monodispersed PS latex and ultrafine $SiO_2$ NPs (~ 5 nm) was used as the dispersed phase, while silicone oil was used as the continuous phase. Uniform-sized microballs composed of PS latex and $SiO_2$ NPs were produced from microfluidics combined with a post-solvent evaporation process under 70 °C. The microballs were subsequently treated at 500 °C to remove the PS latex; meanwhile, the remaining silica NPs formed the interconnected necks, leaving behind the porous silicone skeleton-based inverse opal structure. By using different diameters of PS latex as the template building blocks, microbeads with different pore sizes can be obtained, and the resulting structures featured different diffraction peak positions and the corresponding structural colors (as shown in Fig. 40c-f).

Despite considerable progress being made in the construction of inverse opal photonic microobjects, the skeletons of the above-mentioned inverse opal structures were all made of responsive-free materials, which limited their scope of applications, particularly the applications in the fields of sensing. To broaden the applications of photonic crystals with inverse opal structures, polymers with stimulus-responsive properties were used as skeleton materials for inverse-opal photonic structures [278–280]. Hydrogel-based materials have been used as skeleton

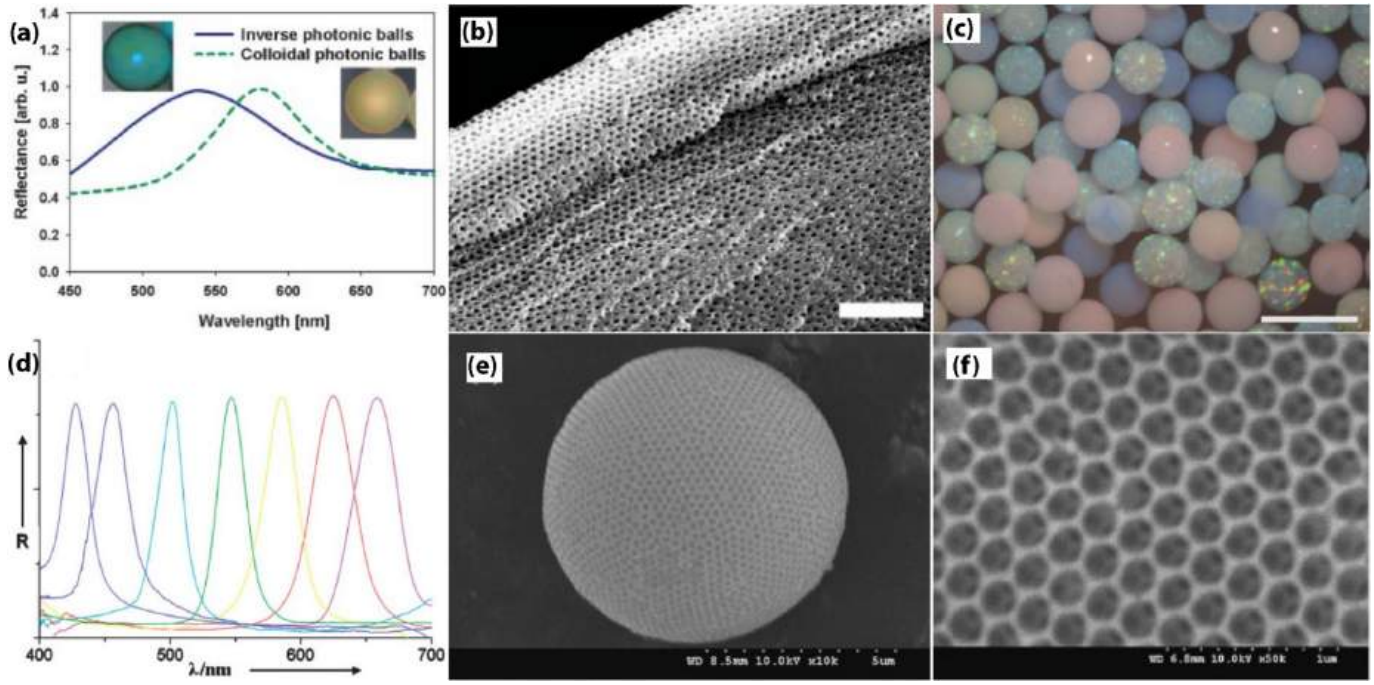


**Fig. 40.** (a) Reflection spectrum comparison of colloidal photonic ball and inverse photonic ball, where the colloidal photonic ball was constructed by using $SiO_2$ colloids as the building blocks and ETPTA resin as the matrix material, respectively. The inverse photonic ball was based on a pure ETPTA network. (b) SEM image of the inverse photonic ball [109]. Reprinted from ref. 109 with permission from Wiley, copyright 2008. (c) OM image of photonic beads with inverse opal structure prepared by using different sizes of PS CPs as sacrificial templates and $SiO_2$ as the matrix material. (d) Reflection spectra of seven inverse-opaline photonic beads; (e) SEM image of the inverse-opaline photonic bead; (f) High-magnification SEM image of the surface of a big bead, showing the hexagonal alignment of pores [142]. Reprinted from ref. 142 with permission from Wiley, copyright 2009.

materials for inverse opal structures [281], among which pNIPAAm and its analogues-based hydrogels have been the most frequently studied materials [282]. Zhu et al. reported the fabrication of multiresponsive inverse opal hydrogel microparticles [283]. To generate the hydrogel-based inverse opal structures, monodispersed droplets of an aqueous suspension of silica CPs were firstly produced from a glass capillary-based microfluidic device. Subsequent solvent evaporation from the droplets led to the formation of silica supraparticles, which were subsequently treated via calcination at a temperature above 500 °C to yield a stable opal structure. The calcinated supraparticles were immersed in an aqueous pregel solution of mixture (NIPAAm, methacrylic acid (MAAc), and crosslinker BIS) to introduce the pregel solution to fill the voids among silica CPs. The silica supraparticles together with the pregel solution were exposed to UV light exposure to generate stable hydrogel-silica composite photonic structures, where the silica CPs can be completely removed by a subsequent wet etching process. Eventually, pNIPAAm-based inverse opal microspheres were obtained. Due to the incorporation of multiple acrylic acid (AAc) groups, the inverse opal microspheres can be further functionalized with other reactive functional groups. In this specific study, photosensitive azobenzene groups were introduced to the skeleton of the polymer network, decorating the microparticles with photosensitive properties. Therefore, the inverse opal microspheres displayed responsiveness to multiple stimuli, such as temperature, pH value, and visible light. Remarkably, the microspheres exhibited significant color change and a large peak value shift (beyond 150 nm) in the reflection spectrum upon the stimulus of temperature and pH values (as shown in Fig. 41a-f). Meanwhile, the response time was less than one minute, which was also an advantage compared to that of bulk hydrogel photonic materials (normally the response time of bulk photonic hydrogel materials was a matter of several minutes) [231,284]. The microobjects also displayed reflection spectra shifting when irradiated with UV light (Fig. 41g). In addition to the responsive properties of such a kind of polymer skeleton-based inverse opal structure, the macroporous feature of the structure was employed as a drug delivery vehicle, which possessed self-reporting properties [39]. Gu et al. fabricated pNIPAAm-based inverse opal microspheres assisted by microfluidics [285]. The microspheres were used as loading vehicles for model molecules, such as fluorescein isothiocyanate (FITC)-dextran and sodium alginate molecules, at temperatures above the LCST of pNIPAAm-based polymer. The model molecules can be subsequently released from the inverse opal structures by the temperature cycle-induced extrusion effect (as shown in Fig. 41h). More importantly, the release behaviors can be monitored through the photonic property change of the microspheres due to their refractive index change. This subsequently induced the blue shift of the reflection spectra peak change as a function of the cycles of triggered release (Fig. 41i-j). Such kind of concept was also demonstrated in Wischerhoff's report, despite their work emphasizing the study of inverse opal hydrogel films [286]. Instead of directly using thermo stimulus, Ye et al. developed inverse opal photonic microspheres with near-infrared-induced thermoresponsive properties, which can also be used to control drug release behaviors [287]. This concept was achieved by incorporating the photonic microspheres with graphene oxide (GO) NPs, which were widely used as sensing components [288,289]. The notable property of the GO NPs is their photothermos effect. By leveraging this effect, the inverse opal microspheres underwent a deswelling process when irradiated with NIR light. Consequently, the composite photonic microspheres that were composed of NIPAAm, PEGDA, and GO showed a clear blue-shifting phenomenon (Fig. 41k).

Inverse-opal photonic microobjects with other sensing properties have also been developed. For example, instead of utilizing the thermo-induced squeezing effect, Zhao et al. introduced another type of hybrid hydrogel-based photonic microobjects with an inverse opal structure, where the polymer hydrogel skeletons were stimulus-responsive-free under normal conditions [290]. But with a combination of two different polymer hydrogels, they can impart the resulting photonic microobjects with certain responsive properties, such as responsiveness to alkaline phosphatase molecules. This characteristic can be used for

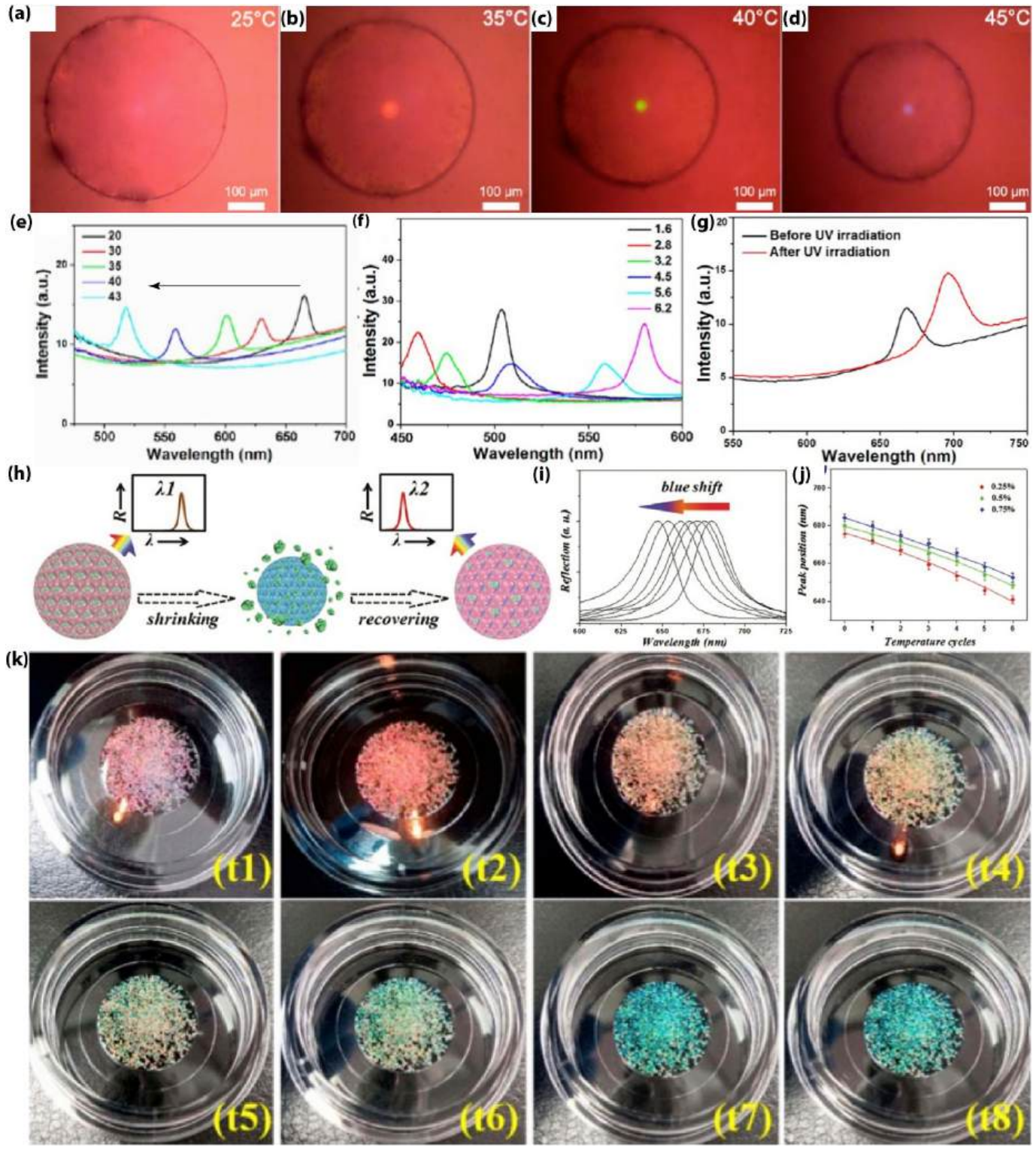


**Fig. 41.** (a)-(d) OM images of a pNIPAAm-co-MAA hydrogel-based inverse opal photonic microsphere under different ambient temperatures. (e) Reflection spectra change of the microsphere at different temperatures from 20°C to 43°C. (f) Reflection spectra change of the microsphere in solutions with different pH values. (g) Reflection spectra of the photoresponsive hydrogel photonic microsphere before (black dashed curve) and after (red dashed curve) the UV light irradiation [283]. Reprinted from ref. 283 with permission from the American Chemistry Society, copyright 2013. (h) The scheme figure shows the pNIPAM-based hydrogel inverse opal microspheres featured with self-reporting property during the release process. (i) Blue shift of the reflection spectra peaks of an inverse opal microsphere due to the triggered release at different cycles. The initial concentration of encapsulated calcium alginate hydrogel was 0.5 % (*w/v*). (j) The relationship between the reflection spectra peak change as a function of the cycles of the triggered release at different initial concentrations of calcium alginate hydrogel [285]. Reprinted from ref. 285 with permission from the Royal Society of Chemistry, copyright 2015. (k) Digital photographs of the color change of inverse opal hydrogel photonic microspheres when being irradiated with an NIR light [287]. Reprinted from ref. 287 with permission from the Dova Press, copyright 2020.

the detection of alkaline phosphatase molecules. The construction of the photonic microobjects through microfluidics was similar to that of the previous report, which employed $SiO_2$ CPs as building blocks and PEGDA hydrogel as the matrix materials for the construction of photonic microobjects, respectively [291–295]. After removing the $SiO_2$ CPs templates, the voids left behind were filled with carbon dots (CDs) and Cu-alginate hydrogel. The illustration process is shown in Fig. 42a. The obtained photonic microspheres displayed both structural color features and fluorescence properties. When exposed to a pyrophosphate ion (PPi) solution, the hydrogel photonic microspheres were subjected to a certain degree of gradual disintegration due to the stronger complexation effect between PPi and $Cu^{2+}$ than the interaction between $Cu^{2+}$ ions and alginate. Consequently, the hydrogel photonic microspheres displayed a blue shift in the reflection spectrum and a decrease in the fluorescence intensity (as illustrated in Fig. 42b). Fig. 42c-d show fluorescence images of the hydrogel-based photonic microspheres in response to different concentrations of PPi varying from 0, 1, 2, 4, 6, and 8 mM. It was clear that the fluorescence signal decreased with the increase in the concentration of PPi. Fig. 42e shows the reflection spectrum peak value change as a function of the concentration of PPi. The hydrogel-based photonic microsphere with an initial orange hue displayed an obvious blue shift when exposed to different concentrations of PPi solutions.

Inverse opal photonic microobjects have been widely used in sensing different analytes; however, when it involved sensing living organisms, particularly in eukaryotic cells, multiple enzymes played important roles simultaneously. Thus, it was necessary to develop microobject-based platforms for simultaneously sensing different target analytes [296]. Meanwhile, the microobjects had a controllable number, type, and spatial arrangement of enzymes, which controlled the cascade reaction and decreased the efficiency of the biological catalysts. In this regard, photonic microcarriers integrated with multiple inverse opal microobjects were constructed by a microfluidic electrospray approach (as shown in Fig. 43a-c) [297]. The inverse opal microparticles exhibited periodic porous structures (as shown in Fig. 43d-e). To generate photonic microobjects with multiple different functions, pAAm-based inverse opal microparticles were firstly developed. EDC-NHS was further utilized to mount the specific enzymes into the skeleton of the pAAm-based hydrogel microbeads. Subsequently, different numbers of inverse opal microbeads were entrapped into the alginate-based hydrogel microcapsules, which were produced from the microfluidic electrospray process. Fig. 43f-h show inverse opal microparticles with green, red, and blue hues. Fig. 43i shows the reflection spectra of five different inverse opal microparticles. Through appropriate control of the flow rates in microfluidic experiments, alginate hydrogel microcapsules containing one, two, and three inverse opal microparticles, respectively, were generated (as shown in Fig. 43j-l). These spatially arranged inverse opal microparticles within each microcapsule can be a good platform for the immobilization of different enzymes into individual microcapsules.

As an important class of compounds, ionic liquids (ILs) have shown a variety of unique properties due to their structures consisting of organic cations and anions. To leverage these unique properties, Li et al. developed inversed opal photonic structures by combing spherical colloidal photonic structures and polyionic liquid (PILs) together [298]. The construction of the polyionic liquid inverse opal microspheres (PIL-IOMS) followed the similar approach in the abovementioned literature but replaced conventional monomers with a category of imidazolium-based IL monomers. Through microfluidics manufacturing of the colloidal photonic microspheres, the resulting inverse opal microobjects displayed uniform size and periodic porous structures both on the surface and interior of the microobjects (as shown in Fig. 44a-c). Fig. 44d shows the microobjects having a reflection spectra peak value at ~490 nm. The microobjects were endowed with reactivity towards different kinds of solvents due to the presence of imidazolium moieties. Therefore, the microobjects displayed different extents of responsive properties when exposed to different counterions. For example, the microobjects exhibited different structural colors and reflection spectra peak values when exposed to a series of counterions from $ClO_4^-$, $NO_3^-$, $Tf_2N^-$, $PF_6^-$, $BF_4^-$ and $Br^-$ (as shown in Fig. 44e). This was due to the different sizes of the counterions that can be exchanged with the imidazolium moiety. This ion exchange therefore induced a volume change that eventually displayed on the entire microobject. The concept of using PILs as the matrix materials for inverse opal microobjects was further used to develop photonic microobjects that can be used for sensing a variety of chemicals, including saccharides and explosives [299,300].

Instead of construction of a fully inverse opal structure in a single-step etching, a controlled etching approach was also used to construct inverse opal microobjects with multicompartment structures in a concentric configuration. This was achieved through a so-called iterative etching−grafting approach, which could allow the resulting microobjects to integrate different functional groups at different regions in the individual microobject. For example, Li et al. developed two- and three-compartment inverse opal structures through the controlled stepwise etching process of microfluidics-fabricated opal microspheres (as illustrated in Fig. 45a) [301]. The resulting microobjects were subsequently functionalized with reagents of opposing properties, such as acid-base or electrophiles-nucleophiles, in different regions of an individual photonic microobject. Fig. 45b shows the OM images of a

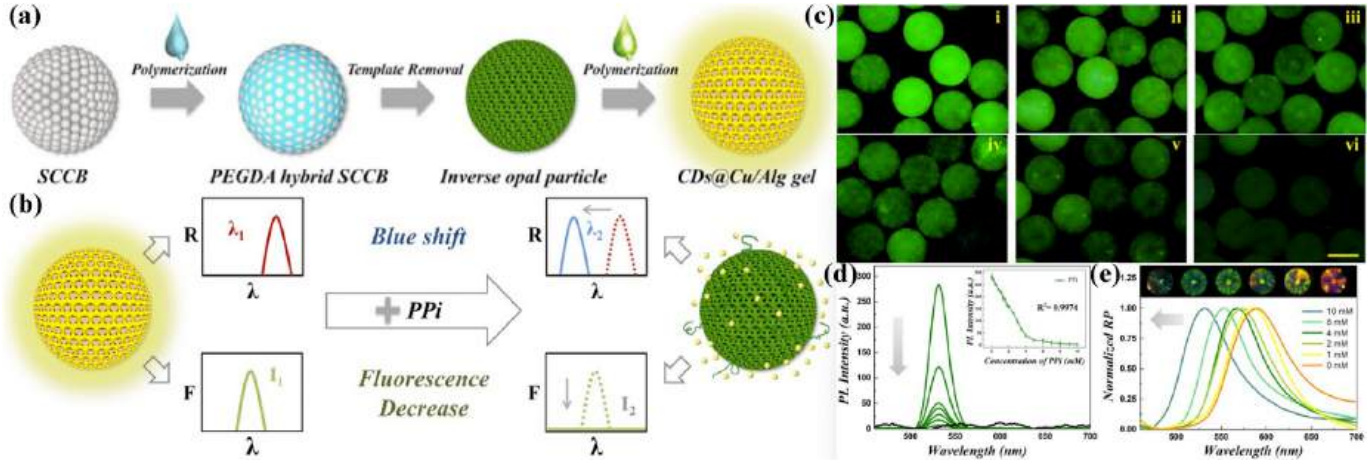


**Fig. 42.** (a) The illustration figure shows the construction of hybrid PEGDA-CDs@Cu/Alg photonic microspheres. (b) The illustration figure shows the dual-signal response behaviors of the hybrid PEGDA-CDs@Cu/Alg microspheres to PPi: the blueshift phenomenon in the reflection spectra and the decrease in fluorescence intensity are due to the disintegration of the CDs@Cu/Alg hydrogel [290]. Reprinted from ref. 290 with permission from Springer Nature, copyright 2022.

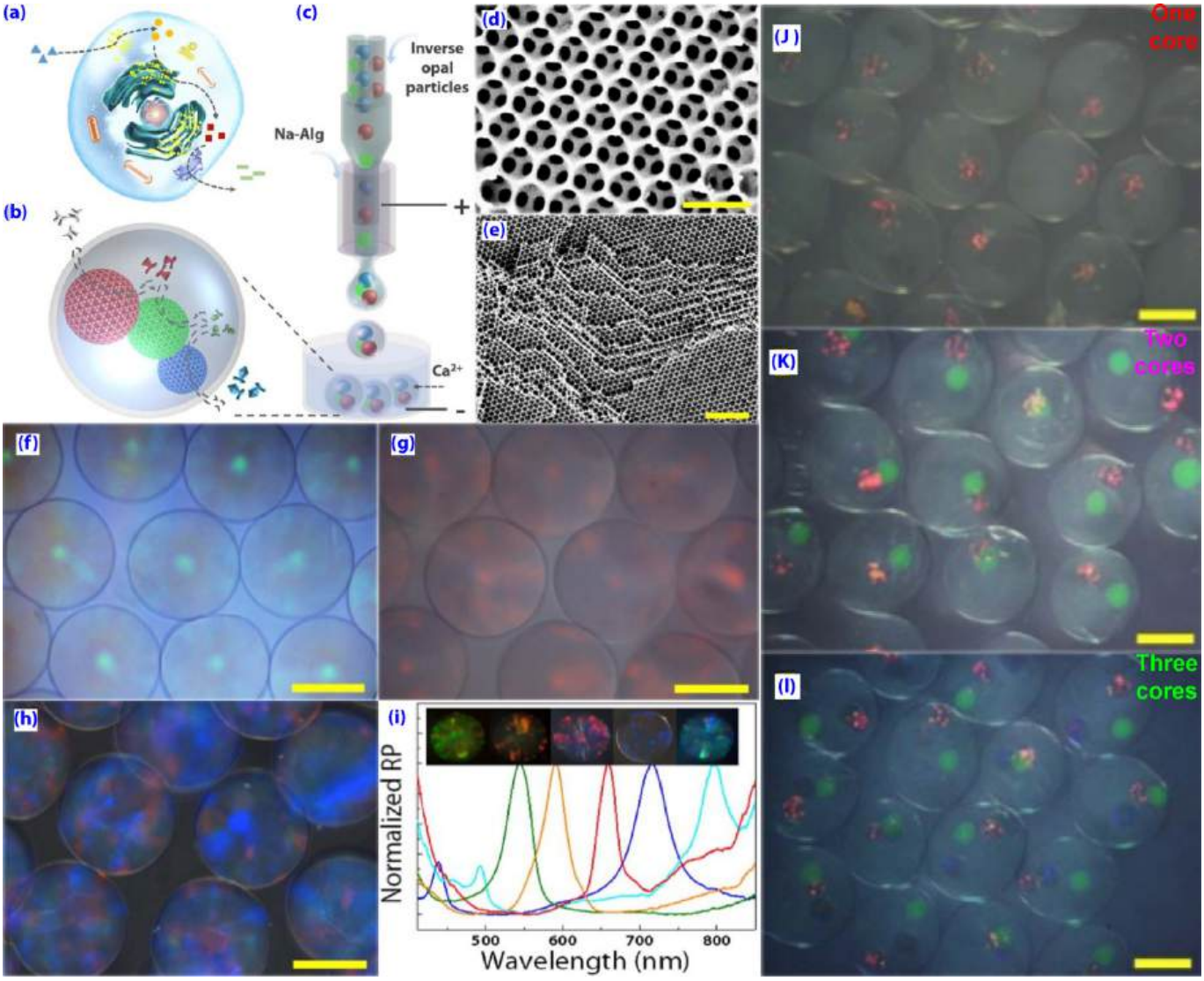


**Fig. 43.** (a)-(c) Schematics of the preparation of the bioinspired microcapsules. (d)-(e). SEM images of the outer surface and inner side of an inverse opal microparticle, scale bars: 500 nm (d) and 2 μm (e). (f)-(h). OM images (reflection mode) of inverse opal microparticles with green (f), red (g), and blue (h) colors, scale bars: 100 μm. (i) Reflection spectra of five different kinds of inverse opal microparticles. (j)-(l). OM images of alginate hydrogel microcapsules containing one (j), two (k), and three (l) different inverse opal microparticles. Scale bars: 400 μm [297]. Reprinted from ref. 297 with permission from the American Association for the Advancement of Science, copyright 2018.

photonic microsphere that was subjected to a two-round etching—-grafting process, which resulted in the distribution of different elements at different regions (as confirmed by the SEM images and element distribution mapping images in Fig. 45c). Similarly, when a colloidal crystal microsphere was subjected to a three-round etching-grafting process, the microsphere displayed a series of optical property changes (as shown in Fig. 45d). Further SEM image and element distribution mapping image also confirmed the integration of different functional groups into individual photonic microobject. The resulting multi-compartment photonic microobjects can be used for an artificial platform for different kinds of cascade reactions.

## 7. Conclusion and perspectives

Photonic microobjects shaped and tuned by a combination of droplet microfluidics processing, colloidal assembly, and the subsequent various treatment methods have achieved considerable progress. The resulting microobjects contain different compositions and consequently display various featured geometries, eventually affecting their diverse properties. Despite that great progress has been made, a number of scientific and technical difficulties remain, requiring further explorations. Firstly, in terms of the building blocks, a vast majority of research outcomes have focused on the utilization of nondeformable CPs, which normally possess a fixed volume fraction in a predetermined colloidal suspension. In order to adjust the volume fraction of CPs in the photonic suspensions in a straightforward manner, fully stimulus-responsive (deformable) CPs, such as stimulus-responsive nanogels, can be considered as good building blocks for the construction of colloidal photonic microobjects. Unlike photonic crystals based on 'hard' colloids, which require the concentration to change when it is demanded to regulate the volume fraction, it is not necessary to change their concentrations so as to tune their volume fraction when deformable micro/nanogels are used as building blocks [302,303]. Therefore, this property could allow us to readily regulate their photonic properties in a facile manner. In addition, crystallization can still occur in suspension of nanogels with polydispersity of up to 18.5 %, while this value is limited to 12 % for hard colloidal systems [303]. Despite some progress having been made in our previous studies, a lot more fundamental questions

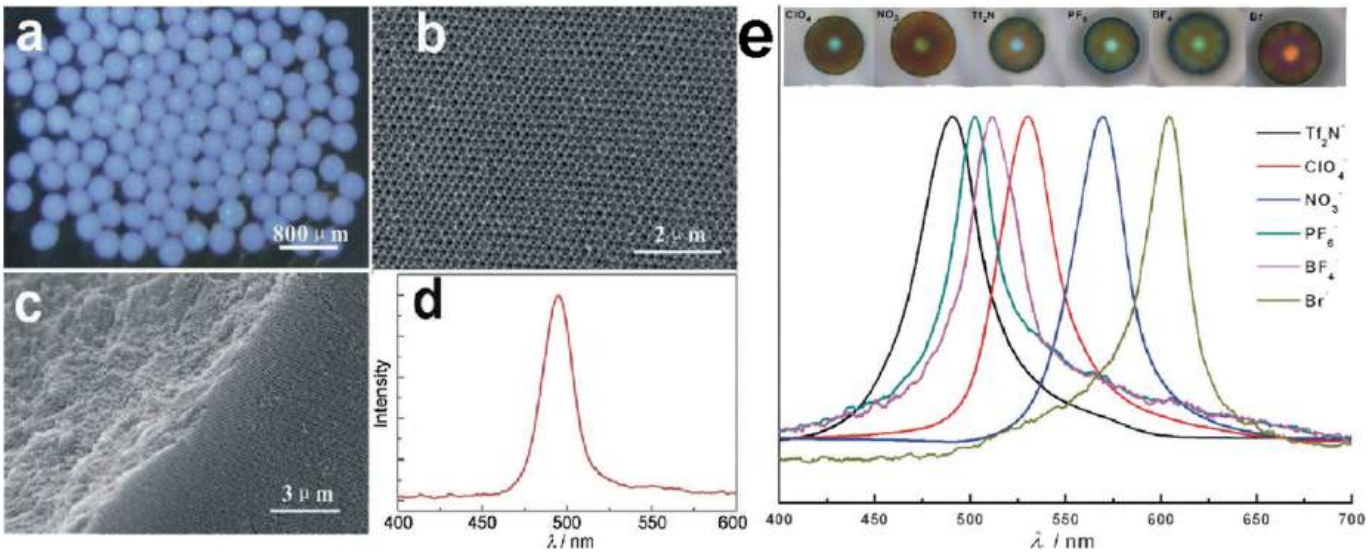


**Fig. 44.** (a) OM image of PIL-based inverse opal microspheres. (b)-(c) SEM images of the surface and cross-section of the PIL inverse opal microsphere. (d) Reflection spectrum of the inverse opal microsphere. (e) Reflection spectra of the PIL-IOMS after exposure to aqueous solutions of six different counterions and their corresponding OM images (inset figures) [298]. Reprinted from ref. 298 with permission from Wiley, copyright 2014.

remain to be explored. The stimulus-responsive properties of fully deformable gel particles can be a double-blade saw; that being said, the photonic property variations caused by ambient temperature fluctuations could be either an advantage or a drawback. For example, for pure thermosensing applications, this can be an advantage, while for some other applications, this thermoresponsive behavior can negatively impact the performance of the resulting photonic microobjects. In addition to many of the abovementioned traditional colloidal building blocks, it is also anticipated to expand the scope of CPs for the fabrication of photonic structures with new properties and functions. Fortunately, the emergence of DNA origami has provided new opportunities for creating novel photonic structures [304]. A recent study has shown that the use of DNA origami allowed scientists to create diamond lattices with a periodicity of 170 nm. The reflection spectrum of the photonic structure after coating with a high-dielectric material ($TiO_2$) exhibited a photonic band gap in the near ultraviolet [305]. Also, the assembly of DNA molecules into colloidal crystals has achieved unprecedented control and programmability [306]. Therefore, it is possible to combine the assembly of DNA colloids with a microfluidic platform to expand the design and shaping of visible-range photonic microobjects. Meanwhile, the rise of new methods for the synthesis of metallic colloids allows researchers to assemble metallic colloids in an easy-to-craft fashion [79, 307, 308]. The metallic colloidal crystals with close-packed structures enabled the unnaturally extreme light-matter interaction (metamaterials and metasurfaces), which was nearly impossible to achieve with the crystals of dielectric colloids. However, the high densities of those CPs cannot be ignored in the development of photonic structures with stopbands in the visible range. This is because the sedimentation of those metallic CPs can outpace equilibrium and thus fail to assemble to the desired crystal structures. These aspects of progress can also be further combined with droplet microfluidics to investigate their assembly behaviors within highly controllable droplet templates and eventual properties of the assembled structures [80,81,309–311]. Secondly, microfluidics-fabrication of photonic microobjects formed from the assembly of binary deformable CPs with different diameters and their internal structures has yet to be binvestigated, despite some preliminary research regarding the use of nondeformable CPs as building blocks in a confined space or under bulk conditions having been conducted [258]. Due to gel particles' tolerance to defects and self-healing property, binary gel particles' system could form crystal structures under bulk conditions; however, how the binary gel particles assemble in a confined space and what kind of photonic properties they possess is yet to be understood [303,312,313]. This can be a promising strategy for the construction of photonic microobjects with multiple stopbands. Thirdly, some cutting-edge technologies, such as the emerging of AI, could be a good tool for the predicting and guiding of the construction of photonic microobjects with novel properties and structures. Finally, traditional colloidal photonic microobjects are mainly based on inert or stimulus-responsive colloids; photonic microobjects based on colloids with some other properties, i.e., photocatalytic or active properties, particularly the latter case that could autonomously catalyze chemical reactions coupled with the chemomechanical reactions, which eventually induce the autonomous structural color changes of the photonic microobjects, can be a big merit when being compared with conventional colloid-based photonic microobjects [314–316]. The behaviors of this kind of photonic microobjectcould be aligned with real biological species; specifically, they can directly transform out-of-equilibrium chemical reaction energy into the energy that is used for skin color change of some animals on our planet, like chameleons [21,317,318]. Eventually, the constructed photonic microobjects need to find some more practical applications; for example, it would be a big advantage when the constructed photonic crystal structures find applications in the fields of energy saving in the context of global coalition for carbon neutrality [319]. Specifically, the concept of thermal regulations via colloidal crystals has gained considerable attention [320–322]. Given their effective capability for radiative supercooling, colloidal crystal structures of this type could be emerging candidates in our endeavors in searching for ideal materials to combat global warming. Current studies on this aspect all focus on bulk structures; it would also be interesting to conduct some research to compare the efficiency difference between the bulk and microobject states of those materials. When it refers to real practical applications, the production scale from microfluidics has been the main concern, even though there have been mounting reports on the fabrication of various emulsion templates via parallelized microfluidic channels [323–329]. Despite those achievements, parallelized microfluidics has never been applied in the production of colloidal photonic microobjects. It may be worthy of exploring this aspect in future studies. In conclusion, although the development of colloid-based photonic microobjects based on droplet microfluidics and a variety of post-processing methods has been achieved in the past two decades, a lot more scientific and technological problems remain to be explored in future research efforts.

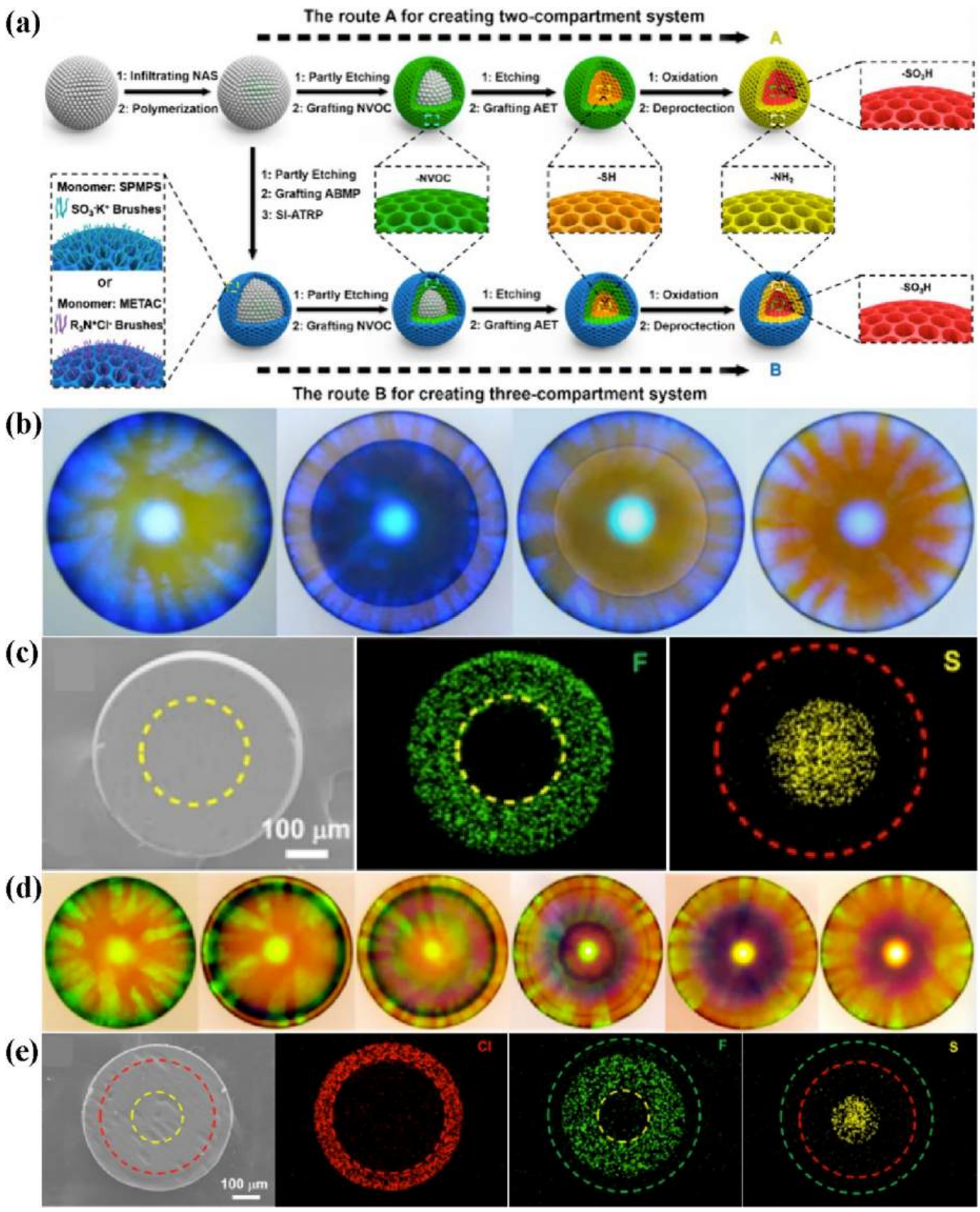


**Fig. 45.** (a) The illustration figure shows the construction of two- and three-compartment inverse opal microobjects. (b) and (d)OM images show the change of two $SiO_2$-polymer colloidal photonic composite microspheres when subjected to a two-round (b) and a three-round etching grafting process, respectively. (c) and (e) Left panels: SEM images of the two-compartment (c) and three-compartment (e) photonic microobjects; right panels: different element distributions in different regions of the corresponding individual photonic microobjects [301]. Reprinted from ref. 301 with permission from the American Chemical Society, copyright 2020.

## Declaration of generative AI in scientific writing

The authors must declare that no AI tools have been used in the preparation of the manuscript.

## CRediT authorship contribution statement

**Yuandu Hu:** Writing – original draft, Resources, Funding acquisition, Data curation, Writing – review & editing, Supervision, Investigation, Formal analysis, Conceptualization. **Arezoo Ardekani:** Writing – review & editing. **Jintao Zhu:** Writing – review & editing, Validation. **Yajiang Yang:** Writing – review & editing, Validation. **Juan Pérez-Mercader:** Writing – review & editing, Supervision.

## Declaration of competing interest

There are no conflicts to declare.

## Acknowledgements

This work is supported by the Fundamental Research Funds for the Central Universities under the grant number 2025JBZX005. Y. H. is also grateful for the open research funds support from Guangdong Provincial Key Laboratory of Technique and Equipment for Macromolecular Advanced Manufacturing under the fund number 20240518, and Fund of Key Laboratory of Advanced Materials of Ministry of Education (Tsinghua University) No. Advmat-2402.

## Appendix A. Appendix

| Types of microfluidic device | Emulsion type | Composition of the droplets | Shapes of initial droplets | Sizes of the droplets | Volume of initial droplets | Sizes of the resultant microobjects | Shapes of the resultant microobjects | References number |
|---|---|---|---|---|---|---|---|---|
| Capillary-based coflow | Single emulsion | Aqueous suspension of PMMA CPs | Spherical | Not specified | Not specified | Diameters of 74 μm, 400 μm | Microspheres | [131] |
| Micropipette injection; PDMS-based T-type device | Single emulsion | Aqueous suspension of PS CPs | Spherical | 16.7 μm | Not mentioned | Diameters of 6.4 μm, 4 μm | Microspheres | [125] |
| Capillary-based coflow microfluidic device | Single emulsion | Aqueous suspension of $SiO_2$ CPs | Spherical | Not specified | Not specified | Not specified | Microspheres | [143] |
| T-junction PDMS tube | Single emulsion | Aqueous suspension of PS-co-PAAc@PHEMA-co-PAAc core-shell CPs and CdTe NCs | Spherical | 92 to 170 μm | Not mentioned | Not specified | Microspheres | [144] |
| T-junction PDMS device | Single emulsion | Aqueous suspension of PS@PMMA-co-AAc core-shell CPs | Spherical | 120 μm | Not mentioned | 50 μm, 55 μm | Microspheres | [170] |
| Glass capillary microfluidic device | Single emulsion | Aqueous suspension of $SiO_2$ CPs | Spherical | Not specified | Not mentioned | Not specified | Microspheres | [147] |
| PDMS T-type microfluidic device | Single emulsion | Aqueous suspension of $SiO_2$ CPs and Au NPs | Spherical | Not specified | Not mentioned | 8, 15, 30, and 100 μm | Microspheres | [149] |
| PDMS microfluidic device | Single emulsion | Aqueous suspension of PS-co-pAAc CPs | Spherical | Not specified | Not mentioned | 6 μm | Spherical polyhedrons; Nonspherical; Microspheres; Deflated football-like; | [153,154] |
| Glass capillary microfluidic device | Single emulsion; Janus-type single emulsion | ETPTA resin suspensions of $SiO_2$ CPs | Spherical | 15.9, 24.5, and 53.7 μm | Not mentioned | 15.9, 24.5, and 53.7 μm | Microspheres | [109] |
| Flow focus PDMS microfluidic device | Single emulsion | Aqueous suspension of PS CPs | Spherical | 38 μm | Not mentioned | 11 μm | Spherical polyhedrons | [158] |
| PDMS microfluidic device | Single emulsion | Aqueous suspension of nonspherical MOF CPs | Spherical | Not specified | Not mentioned | 10–50 μm | Spherical and nonspherical | [20] |
| Capillary coflow microfluidic device | Single emulsion | Aqueous suspension of PS CPs and Eumelanin NPs | Spherical | 69 μm | Not mentioned | 33 μm, 26 μm | Microspheres | [169] |
| T-type microfluidic device | Single emulsion | Aqueous suspension of PS@PMMA-co-AAc CPs and PDA NPs | Spherical | 90 μm | Not mentioned | ~ 50 μm | Microspheres | [146] |
| PDMS T-junction microfluidic device | Single emulsion | PEGDA/$H_2O$ suspension of $Fe_3O_4$@ $SiO_2$ core-shell CPs | Spherical | 72 μm | Not mentioned | ~ 72 μm | Microspheres | [171] |
| Glass capillary coflow microfluidic device | Single emulsion | NIPAAm-based pregel suspension of PS CPs | Spherical | Not specified | Not mentioned | Not specified | Microspheres | [132] |
| T-junction microfluidic device | Single emulsion | AAm-based pregel suspension of PS CPs | Spherical | Not specified | Not mentioned | 247 μm | Microspheres | [173] |
| Glass capillary coflow microfluidic device | Single emulsion | PEGPEA suspension of $SiO_2$ CPs | Spherical | 146 μm, 124 μm, 117 μm, 114 μm, 108 μm | Not mentioned | 146 μm, 124 μm, 117 μm, 114 μm, 108 μm | Microspheres | [175,176] |

(continued on next page)

(*continued*)

| Types of microfluidic device | Emulsion type | Composition of the droplets | Shapes of initial droplets | Sizes of the droplets | Volume of initial droplets | Sizes of the resultant microobjects | Shapes of the resultant microobjects | References number |
|---|---|---|---|---|---|---|---|---|
| Coflow glass capillary microfluidic device; PDMS microfluidic device | Single emulsion | Aqueous suspension of $SiO_2$ CPs and $Fe_3O_4$ NPs; aqueous suspension of $Fe_3O_4$@ $SiO_2$ ellipsoidal CPs and $SiO_2$ CPs | Spherical | Not mentioned; 300 μm | Not mentioned | Not mentioned | Janus Microspheres | [178,179] |
| PDMS flow focus microfluidic device | Single emulsion | Aqueous suspension of $SiO_2$ CPs | Spherical | Not specified | Not mentioned | ~ 20 μm | Microspheres and Janus Microspheres | [180] |
| Coflow glass capillary microfluidic devices | Single emulsion with Janus or multicompartmental structures; Single emulsion | ETPTA resin suspensions of $SiO_2$ or α-$Fe_2O_3$ CPs or CB NPs | Spherical | ~ 300 μm; | Not mentioned | 300 μm; not mentioned; 400 μm | Janus Microspheres and Multicompartment microspheres | [172,181,183] |
| PDMS microfluidic devices | Single emulsion with Janus structures | Aqueous suspension of PS CPs and ETPTA resin suspension of $SiO_2$ or Fe3O4 CPs | Spherical near spherical | ~ 390 μm; 365 μm; 380 μm | Not mentioned | ~ 390 μm; 365 μm; 380 μm | Janus Microspheres | [110,185,187] |
| Theta-channel glass capillary microfluidic device | Single emulsion with Janus structures | Silicone precursor suspension of $BaFe_{12}O_{19}$ NPs and CB NPs, and ETPTA resin suspension of $SiO_2$ CPs | Spherical | ~147 μm | Not mentioned | ~147 μm | Janus Microspheres | [188] |
| Coflow microfluidic device | Single emulsion and core-shell emulsion | ETPTA suspension s of $SiO_2$ CPs | Spherical | ~ 100 μm | Not mentioned | ~ 100 μm | Microspheres, Microcapsules, and Janus microspheres | [192] |
| Coflow microfluidic device | Single emulsion with Janus structures | Aqueous dispersion of PS CPs and a stream of gas | Snowman-like Janus droplets | Not mentioned | Not mentioned | Not specified | Plate-like, bowl-like, tomato-like and microspheres | [195] |
| Glass capillary microfluidic device | Single emulsion with different geometries; multiple cores double emulsion | Aqueous suspension of PEGDA and $SiO_2$ CPs; Core: ETPTA dispersion of $SiO_2$ CPs, shell: aqueous solution of PEGDA | Plug-like single emulsions; rod-like multicore double emulsions | 700–1600 μm in length, radius ~ 60 μm, thickness ~ 200 μm for disk-like; | Not mentioned | 700–1600 μm in length, radius ~ 60 μm, thickness ~ 200 μm for disk-like | Rod-like, cuboid-like, and disk-like microobjects; multicore double rod-like microobjects | [197,198] |
| T-junction PDMS microfluidic device | Single emulsion with Janus structures | Buffer solution and an aqueous suspension of DNA-coated PS colloids | Spherical | ~ 60 μm | Not mentioned | Large nonspherical crystals | Nonspherical single crystals | [57] |
| Combining co-flow and flow focusing glass capillary microfluidic device | Single core double emulsion | Shell: 75 wt% two-part silicone rubber, 23 wt% PDMS oil and 2 wt% Dow Corning 749 surfactant; core: aqueous suspension of PS CPs | Spherical | ~ 173–180 μm | Not mentioned | ~146–152 μm | Dimpled microcapsules | [206] |
| Glass capillary microfluidic device | Single emulsion | Aqueous suspension of $SiO_2$ CPs and GO NPs | Spherical | Not specified | Not mentioned | ~ 180 μm–330 μm in radius | Microobject with a hemispherical top part and an oblate bottom part | [203] |
| T-junction microfluidic device | Single emulsion | Aqueous suspension of $Fe_3O_4$@ $SiO_2$ nano ellipsoids | Spherical | ~ 300 μm | Not mentioned | Aspect ratio from 24 μm to 300 μm | Spindle-like microobjects | [208] |
| Triphase microfluidic device | Biphasic single emulsion with different configurations | Aqueous suspension of PS-co-PHEA@PVI-co-PHEA CPs and ETPTA suspension of $Fe_3O_4$ CPs | Different shapes from double faced, triangle, tetrahedron, triangular dipyramid | Not specified | Not mentioned | The same as the droplet templates | Different shapes from double faced, triangle, tetrahedron, triangular dipyramid | [111,211] |
| Y-junction multichannel microfluidic device | Multiple-phase single emulsion | ETPTA suspensions of $SiO_2$ CPs with different diameters | Microcylinder | Diameters of 370, 368, and 362 μm; lengths of 167 to 318 and 571 μm | Not mentioned | The same as the droplet templates | Microcylinders with different photonic configurations | [212] |
| Glass capillary microfluidic device | Single core double emulsion | ETPTA resin as the shell, aqueous suspension of PS CPs or PS@PNIPAAm core-shell CPs or magnetic CPs | Microcapsules | 170 μm; 210–320 μm; Not specified | Not mentioned | 170 μm; 210–320 μm; Not specified | Microcapsules with different core compositions | [165,215,217] |
| Glass capillary microfluidic device | Single core double emulsion | Shell: ETPTA resin as the shell, Core: aqueous suspension of pNIPAAm-co-AAc gel particles or $SiO_2$ CPs or PS@pNIPAAm-co-AAc CPs | Microcapsules | ~ 200 μm; ~ 200 μm; 60–192 μm; ~100 μm | Not mentioned | ~ 200 μm; ~ 200 μm; 60–192 μm; ~100 μm; 90 μm | Microcapsules with different core compositions | [133,219,222,224,234] |

(*continued on next page*)

(*continued*)

| Types of microfluidic device | Emulsion type | Composition of the droplets | Shapes of initial droplets | Sizes of the droplets | Volume of initial droplets | Sizes of the resultant microobjects | Shapes of the resultant microobjects | References number |
|---|---|---|---|---|---|---|---|---|
| Glass capillary microfluidic device | Single core double emulsion | Shell: ETPTA or PDMS precursor suspension of $Fe_2O_3$ NPs; core: aqueous suspension of PS@ pNIPAAm core-shell CPs, linear pNIPAAm-*co*-AAc polymers, and NaCl | Microcapsules | Not specified | Not mentioned | ~ 100 μm; specified | Microcapsules with multiple crystal domains; Microcapsules with onion-like and single-crystal colloidal arrays | [241,244] |
| Glass capillary microfluidic device | Single core double emulsion | Shell: PDMS prepolymer; core: aqueous suspension of PS CPs, pAAm-*co*-AAc linear polymers, and NaCl | Microcapsules | 117 μm, 100 μm | Not mentioned | 117 μm, 100 μm | Microcapsules | [243,246] |
| Glass capillary microfluidic device | Single core double emulsion | Shell: ETPTA resin; core: aqueous suspension of PS@ PNIPAAm-co-AA CPs | Microcapsules | 80 μm in radius | Not mentioned | 80 μm in radius | Microcapsules | [245] |
| Glass capillary microfluidic device | Single core double emulsion | Core: an aqueous suspension of containing PS CPs mixtures (PS100-XA: PS ratio = 5 wt%) and 0.05 wt% SDS Shell: 75 wt% two-part silicone rubber, 23 wt% PDMS oil and 2 wt% Dow Corning 749 surfactant. | Microcapsules | Not specified | Not mentioned | Not specified | Microcapsules with dual stopbands in the core part | [258] |
| Glass capillary microfluidic devices | Single core double emulsion | Shell: prepolymer of PDMS and others Core: aqueous suspension of PS CPs, p (AAm-*co*-AAc) linear polyemrs, and NaCl | Sphericalmicrocapsules | 142 μm | Not mentioned | 142 μm | Microcapsules with dual/triple stopbands in the core part | [259] |
| Glass capillary microfluidic device | Core-shell emulsion | Shell: PS CPs in pNIPAAm hydrogel; core: PDMS oil | Spherical microcapsules | 140–160 μm | Not mentioned | 140–160 μm | Microcapsules with photonic properties in the shell part | [260] |
| Glass capillary microfluidic device | Single core double emulsion | Shell: ETPTA resin suspension of $SiO_2$ CPs; core: aqueous solution of dyes | Spherical microcapsules | 200–225 μm | Not mentioned | 200–225 μm | Microcapsules with photonic properties in the shell part | [261] |
| Glass capillary microfluidic device | Core-shell emulsion | Shell: PEGPEA resin suspension of $SiO_2$ CPs; core: aqueous solution of PVA and sucrose | Spherical microcapsules | 79 μm in radius | Not mentioned | 79 μm in radius | Microcapsules with photonic properties in the shell part | [262] |
| PDMS capillary microfluidic device | Single emulsion with a Janus structure | Aqueous suspension of PS CPs and ETPTA suspension of $SiO_2$ CPs | Spherical single emulsion with a Janus structure | 200 μm | Not mentioned | 200 μm | Microcapsules with photonic properties both in the shell and core parts | [187] |
| Glass capillary microfluidic device | Core-shell emulsion | Shell: ETPTA resin Core: aqueous suspension of PVP-decorated PS CPs or non-PVP-decorated bare PS CPs | Spherical core-shell droplets | ~ 200 μm | Not mentioned | ~130 μm | Microcapsules with photonic properties both in the shell and core parts | [274] |
| Glass capillary microfluidic device | Single emulsion | Aqueous suspension of $SiO_2$ CPs | Spherical single emulsion droplets | Not specified | Not mentioned | Not specified | Microcapsules with photonic properties both in the shell and core parts | [275] |
| Glass capillary microfluidic device | Single emulsions | ETPTA suspension of $SiO_2$ CPs; aqueous suspension of PS CPs and ultrafine $SiO_2$ NPs | Spherical single emulsion droplets | ~ 100 μm; not mentioned | Not mentioned | The same as the droplet templates; not mentioned | Inverse opal microspheres | [109,142] |
| Glass capillary microfluidic devices | Single emulsions | Aqueous suspension of $SiO_2$ CPs | Spherical single emulsion droplets | Not specified | Not mentioned | More than 300 μm; not specified | Inverse opal microspheres | [283,287] |
| Glass capillary microfluidic device | Single emulsions | An aqueous suspension of $SiO_2$ CPs | Spherical single emulsion droplets | Not mentioned | Not mentioned | Not mentioned | Inverse opal microspheres | [290] |
| Glass capillary microfluidic device | Core-shell emulsion droplets | Shell: aqueous solution of Na-alginate; core: aqueous suspension of 2 wt% sodium carboxymethylcellulose and hydrogel-based | Spherical core-shell droplet emulsion droplet contains multicores | > 100 μm for inverse opal microspheres; < 1.5 mm for microcapsules | Not mentioned | > 100 μm for inverse opal microspheres; < 1.5 mm for microcapsules | Spherical microcapsule with multicores using inverse opal microspheres | [297] |

(*continued on next page*)

(*continued*)

| Types of microfluidic device | Emulsion type | Composition of the droplets | Shapes of initial droplets | Sizes of the droplets | Volume of initial droplets | Sizes of the resultant microobjects | Shapes of the resultant microobjects | References number |
|---|---|---|---|---|---|---|---|---|
| | | inverse opal microspheres | | | | | | |
| Glass capillary T-junction microfluidic device | Single emulsion | Aqueous suspension of $SiO_2$ CPs | Spherical single emulsion droplets | 300 μm for opal microsphere templates | Not mentioned | Not mentioned | Inverse opal microspheres | [298] |
| Glass capillary T-junction microfluidic device | Single emulsion | Aqueous suspension of $SiO_2$ CPs | Spherical single emulsion droplets | 460 μm for opal microsphere templates | Not mentioned | ~ 240 μm for inverse opal in HF solution | Microcapsule with an inverse opal shell and an opal-structure core | [301] |

## Data availability

Data will be made available on request.

## References


[1] Yablonovitch E. Inhibited spontaneous emission in solid-state physics and electronics. Phys Rev Lett 1987;58:2059–62.
[2] Rayleigh LXVII. On the maintenance of vibrations by forces of double frequency, and on the propagation of waves through a medium endowed with a periodic structure. Lond Edinb Dubl Phil Mag 1887;24:145–59.
[3] Hiltner PA, Krieger IM. Diffraction of light by ordered suspensions. J Phys Chem 1969;73:2386–9.
[4] Krieger IM, Oneill FM. Diffraction of light by arrays of colloidal spheres. J Am Chem Soc 1968;90:3114–20.
[5] Clark NA, Hurd AJ, Ackerson BJ. Single colloidal crystals. Nature 1979;281:57–60.
[6] John S. Strong localization of photons in certain disordered dielectric superlattices. Phys Rev Lett 1987;58:2486–9.
[7] Miller BH, Liu H, Kolle M. Scalable optical manufacture of dynamic structural colour in stretchable materials. Nat Mater 2022;21:1014–8.
[8] Menath J, Mohammadi R, Grauer JC, Deters C, Bohm M, Liebchen B, et al. Acoustic crystallization of 2D colloidal crystals. Adv Mater 2023;35:e2206593.
[9] Li Z, Wang X, Han L, Zhu C, Xin H, Yin Y. Multicolor photonic pigments for rotation-asymmetric mechanochromic devices. Adv Mater 2022;34:e2107398.
[10] Weissman JM, Sunkara HB, Tse AS, Asher SA. Thermally switchable periodicities and diffraction from mesoscopically ordered materials. Science 1996;274:959–60.
[11] Miao S, Wang Y, Sun L, Zhao Y. Freeze-derived heterogeneous structural color films. Nat Commun 2022;13:4044.
[12] Wang Z, Li R, Zhang Y, Chan CLC, Haataja JS, Yu K, et al. Tuning the color of photonic glass pigments by thermal annealing. Adv Mater 2023;35:e2207923.
[13] He Q, Vijayamohanan H, Li J, Swager TM. Multifunctional photonic janus particles. J Am Chem Soc 2022;144:5661–7.
[14] Wijnhoven J, Vos WL. Preparation of photonic crystals made of air spheres in titania. Science 1998;281:802–4.
[15] Inan H, Poyraz M, Inci F, Lifson MA, Baday M, Cunningham BT, et al. Photonic crystals: emerging biosensors and their promise for point-of-care applications. Chem Soc Rev 2017;46:366–88.
[16] Holtz JH, Asher SA. Polymerized colloidal crystal hydrogel films as intelligent chemical sensing materials. Nature 1997;389:829–32.
[17] Sakai M, Seki T, Takeoka Y. Colorful photonic pigments prepared by using safe black and white naterials. ACS Sustain Chem Eng 2019;7:14933–40.
[18] Goerlitzer ESA, Klupp Taylor RN, Vogel N. Bioinspired photonic pigments from colloidal self-assembly. Adv Mater 2018;30:e1706654.
[19] Wang Y, Yu Y, Guo J, Zhang Z, Zhang X, Zhao Y. Bio-inspired stretchable, adhesive, and conductive structural color film for visually flexible electronics. Adv Funct Mater 2020;30:2000151.
[20] Wang JW, Liu Y, Bleyer G, Goerlitzer ESA, Englisch S, Przybilla T, et al. Coloration in supraparticles assembled from polyhedral metal-organic framework particles. Angew Chem Int Ed 2022;61:e202117455.
[21] Teyssier J, Saenko SV, van der Marel D, Milinkovitch MC. Photonic crystals cause active colour change in chameleons. Nat Commun 2015;6:6368.
[22] Yoon HH, Fernandez HA, Nigmatulin F, Cai W, Yang Z, Cui H, et al. Miniaturized spectrometers with a tunable van der Waals junction. Science 2022;378:296–9.
[23] Droguet BE, Liang HL, Frka-Petesic B, Parker RM, De Volder MFL, Baumberg JJ, et al. Large-scale fabrication of structurally coloured cellulose nanocrystal films and effect pigments. Nat Mater 2022;21:352–8.
[24] Fan W, Zeng J, Gan Q, Ji D, Song H, Liu W, et al. Iridescence-controlled and flexibly tunable retroreflective structural color film for smart displays. Sci Adv 2019;5:eaaw8755.
[25] Ye C, Liang D, Ruan Y, Lin X, Yu Y, Nan R, et al. Photonic crystal barcode: an emerging tool for cancer diagnosis. Smart Mater Med 2021;2:182–95.
[26] Takahashi S, Suzuki K, Okano M, Imada M, Nakamori T, Ota Y, et al. Direct creation of three-dimensional photonic crystals by a top-down approach. Nat Mater 2009;8:721–5.
[27] Espinha A, Dore C, Matricardi C, Alonso MI, Goni AR, Mihi A. Hydroxypropyl cellulose photonic architectures by soft nanoimprinting lithography. Nat Photonics 2018;12:343–8.
[28] Cai Z, Li Z, Ravaine S, He M, Song Y, Yin Y, et al. From colloidal particles to photonic crystals: advances in self-assembly and their emerging applications. Chem Soc Rev 2021;50:5898–951.
[29] Song DP, Zhao TH, Guidetti G, Vignolini S, Parker RM. Hierarchical photonic pigments via the confined self-assembly of bottlebrush block copolymers. ACS Nano 2019;13:1764–71.
[30] Boyle BM, French TA, Pearson RM, McCarthy BG, Miyake GM. Structural color for additive manufacturing: 3D-printed photonic crystals from block copolymers. ACS Nano 2017;11:3052–8.
[31] Zhao TH, Jacucci G, Chen X, Song DP, Vignolini S, Parker RM. Angular-independent photonic pigments via the controlled micellization of amphiphilic bottlebrush block copolymers. Adv Mater 2020;32:e2002681.
[32] Miyake GM, Piunova VA, Weitekamp RA, Grubbs RH. Precisely tunable photonic crystals from rapidly self-assembling brush block copolymer blends. Angew Chem Int Ed 2012;51:11246–8.
[33] Fang Y, Fei W, Shen X, Guo J, Wang C. Magneto-sensitive photonic crystal ink for quick printing of smart devices with structural colors. Mater Horiz 2021;8:2079–87.
[34] Galisteo-Lopez JF, Ibisate M, Sapienza R, Froufe-Perez LS, Blanco A, Lopez C. Self-assembled photonic structures. Adv Mater 2011;23:30–69.
[35] Dong Y, Ma Z, Song DP, Ma G, Li Y. Rapid responsive mechanochromic photonic pigments with alternating glassy-rubbery concentric lamellar nanostructures. ACS Nano 2021;15:8770–9.
[36] Yang Y, Kim H, Xu J, Hwang MS, Tian D, Wang K, et al. Responsive block copolymer photonicmicrospheres. Adv Mater 2018;30:e1707344.
[37] Ma X, Han Y, Zhang YS, Geng Y, Majumdar A, Lagerwall JPF. Tunable templating of photonic microparticles via liquid crystal order-guided adsorption of amphiphilic polymers in emulsions. Nat Commun 2024;15:1404.
[38] Pan YS, Xie ST, Wang HY, Huang LW, Shen ST, Deng YM, et al. Microfluidic construction of responsive photonic nicrocapsules of cholesteric liquid crystal for colorimetric temperature microsensors. Adv Opt Mater 2023;11:2202141.
[39] Chen H, Bian F, Luo Z, Zhao Y. Biomimetic anticoagulated porous particles with self-reporting structural colors. Adv Sci (Weinh) 2024;11:e2400189.
[40] Freymann GV, Kitaev V, Lotsch BV, Ozin GA. Bottom-up assembly of photonic crystals. Chem Soc Rev 2013;42:2528–54.
[41] Dumanli AG, Savin T. Recent advances in the biomimicry of structural colours. Chem Soc Rev 2016;45:6698–724.
[42] Jo S, Park H, Jun T, Kim K, Jung H, Park S, et al. Symmetry-breaking in double gyroid block copolymer films by non-affine distortion. Appl Mater Today 2021;23:101006.
[43] Park H, Jo S, Kang B, Hur K, Oh SS, Ryu DY, et al. Block copolymer gyroids for nanophotonics: significance of lattice transformations. Nanophotonics 2022;11:2583–615.
[44] Wang Z, Chan CLC, Haataja JS, Schertel L, Li R, van de Kerkhof GT, et al. Deconvoluting the optical response of biocompatible photonic pigments. Angew Chem Int Ed 2022;61:e202206562.
[45] Yang Y, Kim JB, Nam SK, Zhang M, Xu JP, Zhu JT, et al. Nanostructure-free crescent-shaped microparticles as full-color reflective pigments. Nat Commun 2023;14:793.
[46] Goodling AE, Nagelberg S, Kaehr B, Meredith CH, Cheon SI, Saunders AP, et al. Colouration by total internal reflection and interference at microscale concave interfaces. Nature 2019;566:523–7.
[47] Li KX, Li TY, Zhang TL, Li HZ, Li A, Li Z, et al. Facile full-color printing with a single transparent ink. Sci Adv 2021;7:eabh1992.
[48] Li DY, Wang W, Chu LY, Deng NN. Tunable structural coloration in eccentric water-in-oil-in-water droplets. Nano Lett 2023;23:9657–63.
[49] Parker RM, Zhao TH, Frka-Petesic B, Vignolini S. Cellulose photonic pigments. Nat Commun 2022;13:3378.

[50] Shan YW, You LQ, Bisoyi HK, Yang YJ, Ge YH, Che KJ, et al. Annular structural colors from bowl-like shriveled photonic microshells of cholesteric liquid crystals. Adv Opt Mater 2020;8:2000692.
[51] Yang DP, Ouyang C, Zhang YQ, Ma DK, Ye YM, Bu DL, et al. Simple and efficient fabrication of multi-stage color-changeable photonic prints as anti-counterfeit labels. J Colloid Interface Sci 2021;590:134–43.
[52] Qi Y, Niu W, Zhang S, Wu S, Chu L, Ma W, et al. Encoding and decoding of invisible complex information in a dual-response bilayer photonic crystal with tunable wettability. Adv Funct Mater 2019;29:1906799.
[53] Niu W, Wang X, Zheng Y, Wu S, Hua M, Wang Y, et al. Inorganic photonic microspheres with localized concentric ordering for deep pattern encoding and triple sensory microsensor. Small 2020;16:e2003638.
[54] Velev OD, Lenhoff AM, Kaler EW. A class of microstructured particles through colloidal crystallization. Science 2000;287:2240–3.
[55] Fu Q, Yu W, Bao G, Ge J. Electrically responsive photonic crystals with bistable states for low-power electrophoretic color displays. Nat Commun 2022;13:7007.
[56] Alvarez-Puebla RA, Contreras-Caceres R, Pastoriza-Santos I, Perez-Juste J, Liz-Marzan LM. Au@pNIPAM colloids as molecular traps for surface-enhanced, spectroscopic, ultra-sensitive analysis. Angew Chem Int Ed 2009;48:138–43.
[57] Hensley A, Jacobs WM, Rogers WB. Self-assembly of photonic crystals by controlling the nucleation and growth of DNA-coated colloids. Proc Natl Acad Sci USA 2022;119:e2114050118.
[58] Liu YX, Shao CM, Wang Y, Sun LY, Zhao YJ. Bio-inspired self-adhesive bright non-iridescent graphene pigments. Matter 2019;1:1581–91.
[59] Wang Y, Shang L, Bian F, Zhang X, Wang S, Zhou M, et al. Hollow colloid assembled photonic crystal clusters as suspension barcodes for multiplex bioassays. Small 2019;15:e1900056.
[60] Fonseca J, Meng L, Moronta P, Imaz I, Lopez C, Maspoch D. Assembly of covalent organic frameworks into colloidal photonic crystals. J Am Chem Soc 2023;145:20163–8.
[61] Okada T, Hosoyamada S, Takada C, Ohta C. Monodisperse clay microballs for tuning the pseudogaps by adsorption in amorphous photonic structures. Chemphotochem 2021;5:32–5.
[62] Liu Y, Wang Y, Wang Y, Shu Y, Tan H, Zhao Y. Bioinspired structural color particles with multi-layer graphene oxide encapsulated nanoparticle components. Bioact Mater 2020;5:917–23.
[63] Cheng ZD, Russell WB, Chaikin PM. Controlled growth of hard-sphere colloidal crystals. Nature 1999;401:893–5.
[64] Pusey PN, Poon WCK, Ilett SM, Bartlett P. Phase-behavior and structure of colloidal suspensions. J Phys Condensed Matter 1994;6:A29–36.
[65] Alice P, Gast YM. A new growth instability in colloidal crytalllization. Nature 1991;351:553–5.
[66] Jiang P, McFarland MJ. Wafer-scale periodic nanohole arrays templated from two-dimensional nonclose-packed colloidal crystals. J Am Chem Soc 2005;127:3710–1.
[67] Li K, Li C, Li H, Li M, Song Y. Designable structural coloration by colloidal particle assembly: from nature to artificial manufacturing. iScience 2021;24:102121.
[68] Debord JD, Lyon LA. Thermoresponsive photonic crystals. J Phys Chem B 2000;104:6327–31.
[69] Jiang P, McFarland MJ. Large-scale fabrication of wafer-size colloidal crystals, macroporous polymers and nanocomposites by spin-coating. J Am Chem Soc 2004;126:13778–86.
[70] Low J, Zhang L, Zhu B, Liu Z, Yu J. $TiO_2$ photonic crystals with localized surface photothermaleffect and enhanced photocatalytic $CO_2$ reduction activity. ACS Sustain Chem Eng 2018;6:15653–61.
[71] Chen TB, Li QN, Liu C, Hong R, Li Q, Zhu LL, et al. Hydrophobic fluorinated colloidal photonic crystals for heterogeneous aggregated cluster encoding and energy-saving applications. Chem Eng J 2021;411:128623.
[72] Sakai M, Kim H, Arai Y, Teratani T, Kawai Y, Kuwahara Y, et al. Monodisperse silica nanoparticle-carbon black composite microspheres as photonic pigments. ACS Appl Nano Mater 2020;3:7047–56.
[73] Pan GS, Tse AS, Kesavamoorthy R, Asher SA. Synthesis of highly fluorinated monodisperse colloids for low refractive index crystalline colloidal arrays. J Am Chem Soc 1998;120:6518–24.
[74] Kim H, Ge JP, Kim J, Choi S, Lee H, Lee H, et al. Structural colour printing using a magnetically tunable and lithographically fixable photonic crystal. Nat Photonics 2009;3:534–40.
[75] Huang Y, Zhou J, Su B, Shi L, Wang J, Chen S, et al. Colloidal photonic crystals with narrow stopbands assembled from low-adhesive superhydrophobic substrates. J Am Chem Soc 2012;134:17053–8.
[76] Wang J, Chen W, Yang D, Fang Z, Liu W, Xiang T, et al. Monodispersed lignin colloidal spheres with tailorable sizes for bio-photonic materials. Small 2022;18:e2200671.
[77] Hou K, Ali W, Lv JW, Guo J, Shi L, Han B, et al. Optically active inverse opal photonic crystals. J Am Chem Soc 2018;140:16446–9.
[78] Liu J, Nero M, Jansson K, Willhammar T, Sipponen MH. Photonic crystals with rainbow colors by centrifugation-assisted assembly of colloidal lignin nanoparticles. Nat Commun 2023;14:3099.
[79] Lee J, Lee SY, Lim DK, Ahn DJ, Lee S. Antifreezing gold colloids. J Am Chem Soc 2019;141:18682–93.
[80] Kim N, Huh JH, Cho Y, Park SH, Kim HH, Rho KH, et al. Achieving optical refractive index of 10-plus by colloidal self-assembly. Small 2024;20:e2404223.
[81] Huh JH, Lee J, Lee S. Soft Plasmonic assemblies exhibiting unnaturally high refractive index. Nano Lett 2020;20:4768–74.
[82] AvBaP Wiltzius. Real-space structure of colloidal hard-sphere glasses. Science 1995;270:1177–9.
[83] Zhu JX, Li M, Rogers R, Meyer W, Ottewill RH, Russell WB, et al. Crystallization of hard-sphere colloids in microgravity. Nature 1997;387:883–5.
[84] Alsayed AM, Islam MF, Zhang J, Collings PJ, Yodh AG. Premelting at defects within bulk colloidal crystals. Science 2005;309:1207–10.
[85] Wang Z, Wang F, Peng Y, Zheng Z, Han Y. Imaging the homogeneous nucleation during the melting of superheated colloidal crystals. Science 2012;338:87–90.
[86] McGrath JG, Bock RD, Cathcart JM, Lyon LA. Self-assembly of "paint-on" colloidal crystals using poly(styrene-co-N-isopropylacrylamide) spheres. Chem Mater 2007;19:1584–91.
[87] Contreras-Cáceres R, Pacifico J, Pastoriza-Santos I, Pérez-Juste J, Fernández-Barbero A, Liz-Marzán LM. Au@pNIPAM thermosensitive nanostructures: control over shell cross-linking, overall dimensions, and core growth. Adv Funct Mater 2009;19:3070–6.
[88] Hu ZB, Lu XH, Gao J. Hydrogel opals. Adv Mater 2001;13:1708–12.
[89] Cai T, Wang GN, Thompson S, Marquez M, Hu ZB. Photonic hydrogels with poly (ethylene glycol) derivative colloidal spheres as building blocks. Macromolecules 2008;41:9508–12.
[90] Sharma N, Petri C, Jonas U, Dostalek J. Reversibly tunable plasmonic bandgap by responsive hydrogel grating. Opt Express 2016;24:2457–65.
[91] Isapour G, Lattuada M. Multiresponsive photonic picrospheres formed by hierarchical assembly of colloidal nanogels for colorimetric sensors. ACS Appl Nano Mater 2021;4:3389–96.
[92] Iwata N, Koike T, Tokuhiro K, Sato R, Furumi S. Colloidal photonic crystals of reusable hydrogel microparticles for sensor and laser applications. ACS Appl Mater Interfaces 2021;13:57893–907.
[93] Isapour G, Miller BH, Kolle M. Modularassembly of mechanoresponsive color-changing materials from hydrogel-based photonic crystal microspheres. Adv Photon Res 2021;3:2100043.
[94] Ma Y, He P, Xie W, Zhang Q, Yin W, Pan J, et al. Dynamic colloidal photonic crystal hydrogels with self-recovery and injectability. Research (Wash D C) 2021;2021:9565402.
[95] Ohnuki R, Sakai M, Takeoka Y, Yoshioka S. Optical characterization of the photonic ball as a structurally colored pigment. Langmuir 2020;36:5579–87.
[96] Zhang J, Qin Y, Ou Y, Shen Y, Tang B, Zhang X, et al. Injectable granular hydrogels as colloidal assembly microreactors for customized structural colored objects. Angew Chem Int Ed 2022;61:e202206339.
[97] Sowade E, Blaudeck T, Baumann RR. Self-assembly of spherical colloidal photonic crystals inside inkjet-printed droplets. Cryst Growth Des 2016;16:1017–26.
[98] Sun J, Li W, Zhu X, Jiao S, Chang Y, Wang S, et al. A novel multiplex mycotoxin surface-enhanced raman spectroscopy immunoassay using functional gold nanotags on a silica photonic crystal microsphere biochip. J Agric Food Chem 2021;69:11494–501.
[99] Li L, Goodrich C, Yang H, Phillips KR, Jia Z, Chen H, et al. Microscopic origins of the crystallographically preferred growth in evaporation-induced colloidal crystals. Proc Natl Acad Sci USA 2021;118:e2107588118.
[100] Chu G, Chen F, Zhao B, Zhang X, Zussman E, Rojas OJ. Self-assembled nanorods and microspheres for functional photonics: retroreflector meets microlens array. Adv Opt Mater 2021;9:2002258.
[101] Ohnuki R, Kunimoto N, Takeoka Y, Yoshioka S. Optical characterization of large icosahedral colloidal clusters. Part Part Syst Charact 2022;39:2100257.
[102] Lee H, Kim J, Kim H, Kim J, Kwon S. Colour-barcoded magnetic microparticles for multiplexed bioassays. Nat Mater 2010;9:745–9.
[103] Liu W, Kappl M, Steffen W, Butt HJ. Controlling supraparticle shape and structure by tuning colloidal interactions. J Colloid Interface Sci 2022;607:1661–70.
[104] Kohri M, Yanagimoto K, Kawamura A, Hamada K, Imai Y, Watanabe T, et al. Polydopamine-based 3D colloidal photonic materials: structural color balls and fibers from melanin-like particles with polydopamine shell layers. ACS Appl Mater Interfaces 2018;10:7640–8.
[105] Giudice FD, D'Avino G, Maffettone PL. Microfluidic formation of crystal-like structures. Lab Chip 2021;21:2069–94.
[106] Lim Y, Lee SH, Li Y, Kim SH, Kang TH, Suh YD, et al. Transparent and uv-reflective photonicfilms and supraballs composed of hollow silica nanospheres. Part Part Syst Charact 2020:37.
[107] Wenderoth S, Bleyer G, Endres J, Prieschl J, Vogel N, Wintzheimer S, et al. Spray-dried photonic balls with a disordered/ordered hybrid structure for shear-stress indication. Small 2022;18:e2203068.
[108] Stephenson AB, Xiao M, Hwang V, Qu L, Odorisio PA, Burke M, et al. Predicting the structural colors of films of disordered photonic balls. ACS Photonics 2022;10:58–70.
[109] Kim SH, Jeon SJ, Yi GR, Heo CJ, Choi JH, Yang SM. Optofluidic assembly of colloidal photonic crystals with controlled sizes, shapes, and structures. Adv Mater 2008;20:1649–55.
[110] Yu Z, Wang CF, Ling L, Chen L, Chen S. Triphase microfluidic-directed self-assembly: anisotropic colloidal photonic crystal supraparticles and multicolor patterns made easy. Angew Chem Int Ed 2012;51:2375–8.
[111] Yin SN, Yang S, Wang CF, Chen S. Magnetic-directed assembly from janus building blocks to multiplex molecular-analogue photonic crystal structures. J Am Chem Soc 2016;138:566–73.
[112] Bian F, Sun L, Cai L, Wang Y, Wang Y, Zhao Y. Colloidal crystals from microfluidics. Small 2020;16:e1903931.
[113] Utada AS, Fernandez-Nieves A, Stone HA, Weitz DA. Dripping to jetting transitions in coflowing liquid streams. Phys Rev Lett 2007;99:094502.
[114] Shah RK, Shum HC, Rowat AC, Lee D, Agresti JJ, Utada AS, et al. Designer emulsions using microfluidics. Mater Today 2008;11:18–27.
[115] Dangla R, Kayi SC, Baroud CN. Droplet microfluidics driven by gradients of confinement. Proc Natl Acad Sci USA 2013;110:853–8.

[116] Delley CL, Abate AR. Microfluidic particle zipper enables controlled loading of droplets with distinct particle types. Lab Chip 2020;20:2465–72.
[117] Nunes JK. Stone HA. Introduction: microfluidics. Chem Rev 2022;122:6919–20.
[118] Utada AS, Lorenceau E, Link DR, Kaplan PD, Stone HA, Weitz DA. Monodisperse double emulsions generated from a microcapillary device. Science 2005;308:537–41.
[119] Zhao Y, Shang L, Cheng Y, Gu Z. Spherical colloidal photonic crystals. Acc Chem Res 2014;47:3632–42.
[120] Liu M, Fu J, Yang S, Wang Y, Jin L, Nah SH, et al. Janus microdroplets with tunable self-recoverable and switchable reflective structural colors. Adv Mater 2023;35:e2207985.
[121] Zhang J, Coulston RJ, Jones ST, Geng J, Scherman OA, Abell C. One-step fabrication of supramolecular microcapsules from microfluidic droplets. Science 2012;335:690–4.
[122] Jia Z, Xie R, Hu Y, Ju X, Wang W, Liu Z, et al. Thermochromic photonic crystal microspheres with uniform color display and wide coloration range. Macromol Rapid Commun 2023;44:e2200800.
[123] Wang J, Kang E, Sultan U, Merle B, Inayat A, Graczykowski B, et al. Influence of surfactant-mediated interparticle contacts on the mechanical stability of supraparticles. J Phys Chem C Nanomater Interfaces 2021;125:23445–56.
[124] Umbanhowar PB, Prasad V, Weitz DA. Monodisperse emulsion generation via drop break off in a coflowing stream. Langmuir 2000;16:347–51.
[125] Yi GR, Jeon SJ, Thorsen T, Manoharan VN, Quake SR, Pine DJ, et al. Generation of uniform photonic balls by template-assisted colloidal crystallization. Synth Met 2003;139:803–6.
[126] Suzuki N, Iwase E, Onoe H. Microfluidically patterned dome-shaped photonic colloidal crystals exhibiting structural colors with low angle dependency. Adv Opt Mater 2017;5:1600900.
[127] Shiu JY, Kuo CW, Chen P. Actively controlled self-assembly of colloidal crystals in microfluidic networks by electrocapillary forces. J Am Chem Soc 2004;126:8096–7.
[128] Hoi SK, Chen X, Kumar VS, Homhuan S, Sow CH, Bettiol AA. A microfluidic chip with integrated colloidal crystal for online optical analysis. Adv Funct Mater 2011;21:2847–53.
[129] Míguez H, Yang SM, Ozin GA. Optical properties of colloidal photonic crystals confined in rectangular microchannels. Langmuir 2003;19:3479–85.
[130] Lee SK, Yi GR, Yang SM. High-speed fabrication of patterned colloidal photonic structures in centrifugal microfluidic chips. Lab Chip 2006;6:1171–7.
[131] Zhao X, Cao Y, Ito F, Chen HH, Nagai K, Zhao YH, et al. Colloidal crystal beads as supports for biomolecular screening. Angew Chem Int Ed 2006;45:6835–8.
[132] Kanai T, Lee D, Shum HC, Weitz DA. Fabrication of tunable spherical colloidal crystals immobilized in soft hydrogels. Small 2010;6:807–10.
[133] Hu YD, Wang JY, Wang H, Wang Q, Zhu JT, Yang YJ. Microfluidic fabrication and thermoreversible response of core/shell photonic crystalline microspheres based on deformable nanogels. Langmuir 2012;28:17186–92.
[134] Jones JB, Sanders JV, Segnit ER. Structure of opal. Nature 1964;204:990–1.
[135] Ni PG, Dong P, Cheng BY, Li XY, Zhang DZ. Synthetic $SiO_2$ opals. Adv Mater 2001;13:437–41.
[136] Xu K, Xu JH, Lu YC, Luo GS. Extraction-derived self-organization of colloidal photonic crystal particles within confining aqueous droplets. Cryst Growth Des 2013;13:926–35.
[137] Hales TC. Sphere packings, I. Discrete Comput Geom 1997;17:1–51.
[138] Hales TC. Sphere packings, II. Discrete Comput Geom 1997;17:135–49.
[139] Jullien MC, Tsang Mui Ching MJ, Cohen C, Menetrier L, Tabeling P. Droplet breakup in microfluidic T-junctions at small capillary numbers. Phys Fluids 2009;21:072001.
[140] Kopnov F, Lirtsman V, Davidov D. Self-assembled colloidal photonic crystals. Synth Met 2003;137:993–5.
[141] Zhao Y, Zhao X, Sun C, Li J, Zhu R, Gu Z. Encoded silica colloidal crystal beads as supports for potential multiplex immunoassay. Anal Chem 2008;80:1598–605.
[142] Zhao Y, Zhao X, Hu J, Xu M, Zhao W, Sun L, et al. Encoded porous beads for label-free multiplex detection of tumor markers. Adv Mater 2009;21:569–72.
[143] Zhang J, Meng Z, Liu J, Chen S, Yu Z. Spherical colloidal photonic crystals with selected lattice plane exposure and enhanced color saturation for dynamic optical displays. ACS Appl Mater Interfaces 2019;11:42629–34.
[144] Yu ZY, Chen L, Chen S. Uniform fluorescent photonic crystal supraballs generated from nanocrystal-loaded hydrogel microspheres. J Mater Chem 2010;20:6182–8.
[145] Zhu Z, Liu JD, Liu C, Wu X, Li Q, Chen S, et al. Microfluidics-assisted assembly of injectable photonic hydrogels toward reflective cooling. Small 2020;16:e1903939.
[146] Areias LRP, Farinha JPS. Spherical colloidal photonic pigments with saturated structural colors through temperature-controlled polymer nanoparticle assembly. Dyes Pigments 2022;200:110153.
[147] Bian F, Sun L, Chen H, Wang Y, Wang L, Shang L, et al. Bioinspired perovskite nanocrystals-integrated photonic crystal microsphere arrays for information security. Adv Sci (Weinh) 2022;9:e2105278.
[148] Nijs BD, Dussi S, Smallenburg F, Meeldijk JD, Groenendijk DJ, Filion L, et al. Entropy-driven formation of large icosahedral colloidal clusters by spherical confinement. Nat Mater 2015;14:56–60.
[149] Vogel N, Utech S, England GT, Shirman T, Phillips KR, Koay N, et al. Color from hierarchy: diverse optical properties of micron-sized spherical colloidal assemblies. Proc Natl Acad Sci USA 2015;112:10845–50.
[150] Ohnuki R, Isoda S, Sakai M, Takeoka Y, Yoshioka S. Grating diffraction or bragg diffraction? Coloration mechanisms of the photonic ball. Adv Opt Mater 2019;7:1900227.
[151] Boles MA, Engel M, Talapin DV. Self-assembly of colloidal nanocrystals: from intricate structures to functional materials. Chem Rev 2016;116:11220–89.
[152] Engel M, Damasceno PF, Phillips CL, Glotzer SC. Computational self-assembly of a one-component icosahedral quasicrystal. Nat Mater 2015;14:109–16.
[153] Wang J, Mbah CF, Przybilla T, Zubiri BA, Spiecker E, Engel M, et al. Magic number colloidal clusters as minimum free energy structures. Nat Commun 2018;9:5259.
[154] Wang JW, Sultan U, Goerlitzer ESA, Mbah CF, Engel M, Vogel N. Structural color of colloidal clusters as a tool to investigate structure and dynamics. Adv Funct Mater 2020;30:1907730.
[155] Ohnuki R, Takeoka Y, Yoshioka S. Structural and optical characterization of decahedral-type spherical colloidal clusters. Chem Mater 2024;36:2953–62.
[156] Ohnuki R, Sakai M, Takeoka Y, Yoshioka S. Detailed analysis of peripheral reflection from a photonic ball. Adv Photon Res 2021;2:2100131.
[157] Clough JM, Guimard E, Rivet C, Sprakel J, Kodger TE. Photonic paints: structural pigments combined with water-based polymeric film-formers for structurally colored coatings. Adv Opt Mater 2019;7:1900218.
[158] Choi YH, Kim SH. Production of photonic supraballs composed of single-crystalline colloidal arrays through osmosis-induced consolidation. Chem Mater 2023;35:5562–71.
[159] Mbah CF, Wang J, Englisch S, Bommineni P, Varela-Rosales NR, Spiecker E, et al. Early-stage bifurcation of crystallization in a sphere. Nat Commun 2023;14:5299.
[160] Chen H, Miao S, Zhao Y, Luo Z, Shang L. Rotary structural color spindles from droplet confined magnetic self-assembly. Adv Sci (Weinh) 2023;10:e2207270.
[161] Avci C, De Marco ML, Byun C, Perrin J, Scheel M, Boissière C, et al. Metal-organic framework photonic balls: single object analysis for local thermal probing. Adv Mater 2021;33:e2104450.
[162] Lu Y, Yin YD, Xia YN. Three-dimensional photonic crystals with non-spherical colloids as building blocks. Adv Mater 2001;13:415–20.
[163] Wang D, Hermes M, Kotni R, Wu Y, Tasios N, Liu Y, et al. Interplay between spherical confinement and particle shape on the self-assembly of rounded cubes. Nat Commun 2018;9:2228.
[164] Zhou C, Pan M, Li S, Sun Y, Zhang H, Luo X, et al. Metal organic frameworks (MOFs) as multifunctional nanoplatform for anticorrosion surfaces and coatings. Adv Colloid Interf Sci 2022;305:102707.
[165] Kim SH, Jeon SJ, Yang SM. Optofluidic encapsulation of crystalline colloidal arrays into spherical membrane. J Am Chem Soc 2008;130:6040–6.
[166] Lee GH, Han SH, Kim JB, Kim JH, Lee JM, Kim S-H. Colloidal photonic inks for mechanochromic films and patterns with structural colors of high saturation. Chem Mater 2019;31:8154–62.
[167] Meredith P, Sarna T. The physical and chemical properties of eumelanin. Pigment Cell Res 2006;19:572–94.
[168] Shanker R, Sardar S, Chen S, Gamage S, Rossi S, Jonsson MP. Noniridescent biomimetic photonic nicrodomes by inkjet printing. Nano Lett 2020;20:7243–50.
[169] Han SH, Choi YH, Kim SH. Co-assembly of colloids and eumelanin nanoparticles in droplets for structural pigments with high saturation. Small 2022;18:e2106048.
[170] Areias LRP, Marcelo G, Farinha JPS. Polymer nanoparticle-based spherical photonic pigments for dye-free noniridescent bright coloring. ACS Appl Nano Mater 2021;4:13185–95.
[171] Kim J, Song Y, He L, Kim H, Lee H, Park W, et al. Real-time optofluidic synthesis of magnetochromatic microspheres for reversible structural color patterning. Small 2011;7:1163–8.
[172] Kim SH, Jeon SJ, Jeong WC, Park HS, Yang SM. Optofluidic synthesis of electroresponsive photonic janus balls with isotropic structural colors. Adv Mater 2008;20:4129–34.
[173] Yin SN, Wang CF, Liu SS, Chen S. Facile fabrication of tunable colloidal photonic crystal hydrogel supraballs toward a colorimetric humidity sensor. J Mater Chem C 2013;1:4685–90.
[174] Liu C, Yang L, Sun Y, Huang P, Yao Y, Tian Y, et al. Hydrogel-coated polydimethylsiloxane with reversible transparency for advanced optical switching. ACS Nano 2025;19:9017–28.
[175] Lee GH, Han SH, Kim JB, Kim DJ, Lee S, Hamonangan WM, et al. Elastic photonic microbeads as building blocks for mechanochromic materials. ACS Appl Polym Mater 2019;2:706–14.
[176] Kim JH, Kim JB, Choi YH, Park S, Kim SH. Photonic microbeads templated by oil-in-oil emulsion droplets for high saturation of structural colors. Small 2022;18:e2105225.
[177] Nam SK, Amstad E, Kim SH. Hydrogel-encased photonic microspheres with enhanced color saturation and high suspension stability. ACS Appl Mater Interfaces 2023;15:58761–9.
[178] Shang L, Shangguan F, Cheng Y, Lu J, Xie Z, Zhao Y, et al. Microfluidic generation of magnetoresponsive janus photonic crystal particles. Nanoscale 2013;5:9553–7.
[179] Xiao MQ, Liu JJ, Chen ZJ, Liu WX, Zhang CC, Yu YY, et al. Magnetic assembly and manipulation of Janus photonic crystal supraparticles from a colloidal mixture of spheres and ellipsoids. J Mater Chem C 2021;9:11788–93.
[180] Wang J, Westerbeek EY, van den Berg A, Segerink LI, Shui L, Eijkel JCT. Mass transport determined silica nanowires growth on spherical photonic crystals with nanostructure-enabled functionalities. Small 2020;16:e2001026.
[181] Zhao Y, Gu H, Xie Z, Shum HC, Wang B, Gu Z. Bioinspired multifunctional janus particles for droplet manipulation. J Am Chem Soc 2013;135:54–7.
[182] Kim SH, Lim JM, Jeong WC, Choi DG, Yang SM. Patterned colloidal photonic domes and balls derived from viscous photocurable suspensions. Adv Mater 2008;20:3211–7.

[183] Li PH, Pang HY, Zheng YF, Cui QH, Shang C, Xiao Y, et al. Composite photonic microobjects with anisotropic photonic properties from a controlled wet etching approach. Colloids Surf A Physicochem Eng Asp 2024;688:133618.
[184] Li P, Hu Y, Yang Z. Anisotropic photonic microobjects with dual stopbands formed from single photonic dispersion and their application for anticounterfeiting. ACS Appl Mater Interfaces 2025;17:15969–77.
[185] Wu X, Hong R, Meng J, Cheng R, Zhu Z, Wu G, et al. Hydrophobic poly(tert-butyl acrylate) photonic crystals towards robust energy-saving performance. Angew Chem Int Ed 2019;58:13556–64.
[186] Li GX, Qu XW, Hao LW, Li Q, Chen S. A microfluidics-dispensing-printing strategy for Janus photonic crystal microspheres towards smart patterned displays. J Polym Sci 2022;60:1710–7.
[187] Liu SS, Wang CF, Wang XQ, Zhang J, Tian Y, Yin SN, et al. Tunable janus colloidal photonic crystal supraballs with dual photonic band gaps. J Mater Chem C 2014; 2:9431–8.
[188] Nam SK, Kim JB, Han SH, Kim SH. Photonic janus balls with controlled magnetic moment and density asymmetry. ACS Nano 2020;14:15714–22.
[189] Wang J, Le-The H, Shui L, Bomer JG, Jin M, Zhou G, et al. Multilevel spherical photonic crystals with controllable structures and structure-enhanced functionalities. Adv Opt Mater 2020;8:1902164.
[190] Kristensen A, Yang JKW, Bozhevolnyi SI, Link S, Nordlander P, Halas NJ, et al. Plasmonic colour generation. Nat Rev Mater 2016;2:1–14.
[191] Cencillo-Abad P, Franklin D, Mastranzo-Ortega P, Sanchez-Mondragon J, Chanda D. Ultralight plasmonic structural color paint. Sci Adv 2023;9:eadf7207.
[192] Kim JB, Kim JW, Kim M, Kim SH. Dual-colored janus microspheres with photonic and plasmonic faces. Small 2022;18:e2201437.
[193] Latikka M, Backholm M, Baidya A, Ballesio A, Serve A, Beaune G, et al. Ferrofluid microdroplet splitting for population-based microfluidics and interfacial tensiometry. Adv Sci (Weinh) 2020;7:2000359.
[194] Cai L, Chen G, Wang Y, Zhao C, Shang L, Zhao Y. Boston ivy-inspired disc-like adhesive microparticles for drug delivery. Research (Wash D C) 2021;2021: 9895674.
[195] Xu K, Xu JH, Lu YC, Luo GS. A novel method of fabricating, adjusting, and optimizing polystyrene colloidal crystal nonspherical microparticles from gas-water janus droplets in a double coaxial microfluidic device. Cryst Growth Des 2014;14:401–5.
[196] Zhang MY, Xu K, Xu JH, Luo GS. Self-assembly kinetics of colloidal particles inside monodispersed micro-droplet and fabrication of anisotropic photonic crystal micro-particles. Crystals 2016;6:122.
[197] Zhao YJ, Xie ZY, Gu HC, Jin L, Zhao XW, Wang BP, et al. Multifunctional photonic crystal barcodes from microfluidics. Npg Asia Mater 2012;4. e25-e.
[198] Cheng Y, Zhu C, Xie Z, Gu H, Tian T, Zhao Y, et al. Anisotropic colloidal crystal particles from microfluidics. J Colloid Interface Sci 2014;421:64–70.
[199] Wang Y, Wang Y, Zheng X, Ducrot E, Lee MG, Yi GR, et al. Synthetic strategies toward DNA-coated colloids that crystallize. J Am Chem Soc 2015;137:10760–6.
[200] Wang Y, Wang Y, Zheng X, Ducrot E, Yodh JS, Weck M, et al. Crystallization of DNA-coated colloids. Nat Commun 2015;6:7253.
[201] Fang H, Hagan MF, Rogers WB. Two-step crystallization and solid-solid transitions in binary colloidal mixtures. Proc Natl Acad Sci USA 2020;117: 27927–33.
[202] Hensley A, Videbaek TE, Seyforth H, Jacobs WM, Rogers WB. Macroscopic photonic single crystals via seeded growth of DNA-coated colloids. Nat Commun 2023;14:4237.
[203] Wang H, Liu Y, Chen Z, Sun L, Zhao Y. Anisotropic structural color particles from colloidal phase separation. Sci Adv 2020;6:eaay1438.
[204] Wang H, Cai L, Zhang D, Shang L, Zhao Y. Responsive janus structural color hydrogel micromotors for label-free multiplex assays. Research (Wash D C) 2021; 2021:9829068.
[205] Datta SS, Kim SH, Paulose J, Abbaspourrad A, Nelson DR, Weitz DA. Delayed buckling and guided folding of inhomogeneous capsules. Phys Rev Lett 2012;109: 134302.
[206] Yeo SJ, Tu F, Kim SH, Yi GR, Yoo PJ, Lee D. Angle- and strain-independent coloured free-standing films incorporating non-spherical colloidal photonic crystals. Soft Matter 2015;11:1582–8.
[207] Knoche S, Kierfeld J. Osmotic buckling of spherical capsules. Soft Matter 2014;10: 8358–69.
[208] Liu JJ, Xiao MQ, Li CR, Li H, Wu ZY, Zhu QS, et al. Rugby-ball-like photonic crystal supraparticles with non-close-packed structures and multiple magneto-optical responses. J Mater Chem C 2019;7:15042–8.
[209] Li G, Cheng R, Cheng HY, Yu XQ, Ling LT, Wang CF, et al. Microfluidic synthesis of robust carbon dots-functionalized photonic crystals. Chem Eng J 2021;405: 126539.
[210] Xie AQ, Guo JZ, Zhu LL, Chen S. Carbon dots promoted photonic crystal for optical information storage and sensing. Chem Eng J 2021;415:128950.
[211] Hao LW, Liu JD, Li Q, Qing RK, He YY, Guo JZ, et al. Microfluidic-directed magnetic controlling supraballs with multi-responsive anisotropic photonic crystal structures. J Mater Sci Technol 2021;81:203–11.
[212] Sim JY, Lee GH, Kim SH. Microfluidic Design of Magnetoresponsive photonic microcylinders with multicompartments. Small 2015;11:4938–45.
[213] Sim JY, Choi JH, Lim JM, Cho S, Kim SH, Yang SM. Microfluidic molding of photonic microparticles with engraved elastomeric membranes. Small 2014;10: 3979–85.
[214] Ge XH, Geng YH, Zhang QC, Shao M, Chen J, Luo GS, et al. Four reversible and reconfigurable structures for three-phase emulsions: extended morphologies and applications. Sci Rep 2017;7:42738.
[215] Jia X, Hu Y, Wang K, Liang R, Li J, Wang J, et al. Uniform core-shell photonic crystal microbeads as microcarriers for optical encoding. Langmuir 2014;30: 11883–9.
[216] Park J-G, Benjamin Rogers W, Magkiriadou S, Kodger T, Kim S-H, Kim Y-S, et al. Photonic-crystal hydrogels with a rapidly tunable stop band and high reflectivity across the visible. Opt Mater Express 2016;7:253–63.
[217] Zhu C, Xu WY, Chen LS, Zhang WD, Xu H, Gu ZZ. Magnetochromatic microcapsule arrays for displays. Adv Funct Mater 2011;21:2043–8.
[218] Iyer AS, Lyon LA. Self-healing colloidal crystals. Angew Chem Int Ed 2009;48: 4562–6.
[219] Hu Y, Wang J, Li C, Wang Q, Wang H, Zhu J, et al. Janus photonic crystal microspheres: centrifugation-assisted generation and reversible optical property. Langmuir 2013;29:15529–34.
[220] Gong TY, Shen JY, Hu ZB, Marquez M, Cheng ZD. Nucleation rate measurement of colloidal crystallization using microfluidic emulsion droplets. Langmuir 2007;23: 2919–23.
[221] Shang L, Cheng Y, Wang J, Yu Y, Zhao Y, Chen Y, et al. Osmotic pressure-triggered cavitation in microcapsules. Lab Chip 2016;16:251–5.
[222] Shirk K, Steiner C, Kim JW, Marquez M, Martinez CJ. Assembly of colloidal silica crystals inside double emulsion drops. Langmuir 2013;29:11849–57.
[223] Kim SH, Park JG, Choi TM, Manoharan VN, Weitz DA. Osmotic-pressure-controlled concentration of colloidal particles in thin-shelled capsules. Nat Commun 2014;5:3068.
[224] Park JG, Kim SH, Magkiriadou S, Choi TM, Kim YS, Manoharan VN. Full-spectrum photonic pigments with non-iridescent structural colors through colloidal assembly. Angew Chem Int Ed 2014;53:2899–903.
[225] Choi TM, Park JG, Kim YS, Manoharan VN, Kim SH. Osmotic-pressure-mediated control of structural colors of photonic capsules. Chem Mater 2015;27:1014–20.
[226] Kim SH, Kim JW, Cho JC, Weitz DA. Double-emulsion drops with ultra-thin shells for capsule templates. Lab Chip 2011;11:3162–6.
[227] Arriaga LR, Datta SS, Kim SH, Amstad E, Kodger TE, Monroy F, et al. Ultrathin shell double emulsion templated giant unilamellar lipid vesicles with controlled microdomain formation. Small 2014;10:950–6.
[228] Li X, Zhao D, Shea KJ, Li X, Lu X. In situ formed thermogelable hydrogel photonic crystals assembled by thermosensitive IPNs. Mater Horiz 2021;8:932–8.
[229] Hu Z, Huang G. A new route to crystalline hydrogels, guided by a phase diagram. Angew Chem Int Ed 2003;42:4799–802.
[230] Lyon LA, Fernandez-Nieves A. The polymer/colloid duality of microgel suspensions. Annu Rev Phys Chem 2012;63:25–43.
[231] Chen M, Zhou L, Guan Y, Zhang Y. Polymerized microgel colloidal crystals: photonic hydrogels with tunable band gaps and fast response rates. Angew Chem Int Ed 2013;52:9961–5.
[232] Wang Y, Li M, Chang JK, Aurelio D, Li W, Kim BJ, et al. Light-activated shape morphing and light-tracking materials using biopolymer-based programmable photonic nanostructures. Nat Commun 2021;12:1651.
[233] Kolle M, Lee S. Progress and opportunities in soft photonics and biologically inspired optics. Adv Mater 2018;30:1702669.
[234] Hu YD, Li CN, Wang JY, Jia XL, Zhu JT, Wang Q, et al. Osmosis manipulable morphology and photonic property of microcapsules with colloidal nano-in-micro structure. J Colloid Interface Sci 2020;574:337–46.
[235] Meng G, Paulose J, Nelson DR, Manoharan VN. Elastic instability of a crystal growing on a curved surface. Science 2014;343:634–7.
[236] Feng L, Laderman B, Sacanna S, Chaikin P. Re-entrant solidification in polymer-colloid mixtures as a consequence of competing entropic and enthalpic attractions. Nat Mater 2015;14:61–5.
[237] Fernandes GE, Beltran-Villegas DJ, Bevan MA. Interfacial colloidal crystallization via tunable hydrogel depletants. Langmuir 2008;24:10776–85.
[238] Xing XC, Li ZF, Ngai T. pH-controllable depletion attraction induced by microgel particles. Macromolecules 2009;42:7271–4.
[239] Irvine WT, Bowick MJ, Chaikin PM. Fractionalization of interstitials in curved colloidal crystals. Nat Mater 2012;11:948–51.
[240] Rossi L, Sacanna S, Irvine WTM, Chaikin PM, Pine DJ, Philipse AP. Cubic crystals from cubic colloids. Soft Matter 2011;7:4139–42.
[241] Choi TM, Je K, Park JG, Lee GH, Kim SH. Photonic capsule sensors with built-in colloidal crystallites. Adv Mater 2018;30:e1803387.
[242] Manoharan VN. Colloidal matter: packing, geometry, and entropy. Science 2015; 349:1253751.
[243] Kim YG, Park S, Choi YH, Han SH, Kim SH. Elastic photonic microcapsules containing colloidal crystallites as building blocks for macroscopic photonic surfaces. ACS Nano 2021;15:12438–48.
[244] Choi TM, Lee GH, Kim YS, Park JG, Hwang H, Kim SH. Photonic microcapsules containing single-crystal colloidal arrays with optical anisotropy. Adv Mater 2019;31:e1900693.
[245] Kim DE, Park S, Choi YH, Han SH, Kim SH. Crystallization and melting of thermoresponsive colloids confined in microcapsules. Chem Mater 2022;34: 3509–17.
[246] Kim YG, Park S, Kim SH. Centrifugation-assisted growth of single-crystalline grains in microcapsules. ACS Nano 2023;17:2782–91.
[247] Chen H, Zhang W, Ren S, Zhao X, Jiao Y, Wang Y, et al. Temperature-triggered supramolecular assembly of organic semiconductors. Adv Mater 2022;34: e2101487.
[248] Singh G, Pillai S, Arpanaei A, Kingshott P. Multicomponent colloidal crystals that are tunable over large areas. Soft Matter 2011;7:3290–4.
[249] Xiao M, Hu Z, Wang Z, Li Y, Tormo AD, Le Thomas N, et al. Bioinspired bright noniridescent photonic melanin supraballs. Sci Adv 2017;3:e1701151.

[250] Shevchenko EV, Talapin DV, Kotov NA, O'Brien S, Murray CB. Structural diversity in binary nanoparticle superlattices. Nature 2006;439:55–9.
[251] Nozawa J, Uda S, Toyotama A, Yamanaka J, Niinomi H, Okada J. Heteroepitaxial fabrication of binary colloidal crystals by a balance of interparticle interaction and lattice spacing. J Colloid Interface Sci 2022;608:873–81.
[252] Nho HW, Yoon TH. Structural colour of unary and binary colloidal crystals probed by scanning transmission X-ray microscopy and optical microscopy. Sci Rep 2017;7:12424.
[253] Yu J, Yan Q, Shen D. Co-self-assembly of binary colloidal crystals at the air-water interface. ACS Appl Mater Interfaces 2010;2:1922–6.
[254] Bartlett P, Campbell AI. Three-dimensional binary superlattices of oppositely charged colloids. Phys Rev Lett 2005;95:128302.
[255] Cai Z, Liu YJ, Lu X, Teng J. Fabrication of well-ordered binary colloidal crystals with extended size ratios for broadband reflectance. ACS Appl Mater Interfaces 2014;6:10265–73.
[256] Velikov KP, Christova CG, Dullens RP, van Blaaderen A. Layer-by-layer growth of binary colloidal crystals. Science 2002;296:106–9.
[257] de Folter JWJ, Liu P, Jiang L, Kuijk A, Bakker HE, Imhof A, et al. Self-organization of anisotropic and binary colloids in thermo-switchable 1D microconfinement. Part Syst Charact 2014;32:313–20.
[258] Lin Z, Gong Z, Bower DQ, Lee D, Deravi LF. Bidispersed colloidal assemblies containing xanthommatin produce angle-independent photonic structures. Adv Opt Mater 2021;9:2100416.
[259] Yang S, Kim YG, Park S, Kim SH. Structural color mixing in microcapsules through exclusive crystallization of binary and ternary colloids. Adv Mater 2023;35:e2302750.
[260] Kanai T, Lee D, Shum HC, Shah RK, Weitz DA. Gel-immobilized colloidal crystal shell with enhanced thermal sensitivity at photonic wavelengths. Adv Mater 2010;22:4998–5002.
[261] Wang JY, Hu YD, Deng RH, Xu WJ, Liu SQ, Liang RJ, et al. Construction of multifunctional photonic crystal microcapsules with tunable shell structures by combining microfluidic and controlled photopolymerization. Lab Chip 2012;12:2795–8.
[262] Kim JH, Hamonangan WM, Kim SH. Color-tunable elastic photonic shells with high color saturation and deformability. Adv Opt Mater 2023;11:2300085.
[263] Takeoka Y, Seki T. Biform structural colored hydrogel for observation of subchain conformations. Macromolecules 2007;40:5513–8.
[264] Jiang P, Ostojic GN, Narat R, Mittleman DM, Colvin VL. The fabrication and bandgap engineering of photonic multilayers. Adv Mater 2001;13:389–93.
[265] Tian Y, Chen M, Zhang J, Tong YL, Wang CF, Wiederrecht GP, et al. Highly enhanced luminescence performance of LEDs via controllable layer-structured 3D photonic crystals and photonic crystal beads. Small Methods 2018;2:1800104.
[266] Wang C, Lin X, Schäfer CG, Hirsemann S, Ge J. Spray synthesis of photonic crystal based automotive coatings with bright and angular-dependent structural colors. Adv Funct Mater 2020;31:2008601.
[267] Fu Y, Zhao H, Wang Y, Chen D, Yu Z, Zheng J, et al. Reversible photochromic photonic crystal device with dual structural colors. ACS Appl Mater Interfaces 2022;14:29070–6.
[268] Hu HB, Chen QW, Tang J, Hu XY, Zhou XH. Photonic anti-counterfeiting using structural colors derived from magnetic-responsive photonic crystals with double photonic bandgap heterostructures. J Mater Chem 2012;22:11048–53.
[269] Qi Y, Chu L, Niu WB, Tang BT, Wu SL, Ma W, et al. New encryption strategy of photonic crystals with bilayer inverse heterostructure guided from transparency response. Adv Funct Mater 2019;29:1903743.
[270] Wu S, Liu T, Tang B, Li L, Zhang S. Different structural colors or patterns on the front and back sides of a multilayer photonic structure. ACS Appl Mater Interfaces 2019;11:27210–5.
[271] Romanov SG, Yates HM, Pemble ME, DeLa Rue RM. Opal-based photonic crystal with double photonic bandgap structure. J Phys Condens Matter 2020;12:8221–9.
[272] Torza S, Mason SG. Coalescence of two immiscible liquid drops. Science 1969;163:813–4.
[273] Zhou C, Zhang S, Hui T, Cui Q, Hu Y. Microfluidics-assisted fabrication of dual stopband photonic microcapsules and their applications for anticounterfeiting. Polymers (Basel) 2022;14:3954.
[274] Lee JH, Choi GH, Park KJ, Kim D, Park J, Lee S, et al. Dual-colour generation from layered colloidal photonic crystals harnessing "core hatching" in double emulsions. J Mater Chem C 2019;7:6924–31.
[275] Ye B, Ding H, Cheng Y, Gu H, Zhao Y, Xie Z, et al. Photonic crystal microcapsules for label-free multiplex detection. Adv Mater 2014;26:3270–4.
[276] Fu F, Shang L, Zheng F, Chen Z, Wang H, Wang J, et al. Cells cultured on core-shell photonic crystal barcodes for drug screening. ACS Appl Mater Interfaces 2016;8:13840–8.
[277] Du X, Li C, Wang J, Li Z, Zhu J, Yang Y, et al. Multifunctional photonic microobjects with asymmetric response in radial direction and their anticounterfeiting performance. J Colloid Interface Sci 2024;671:457–68.
[278] Honda M, Seki T, Takeoka Y. Dual tuning of the photonic band-gap structure in soft photonic crystals. Adv Mater 2009;21:1801–4.
[279] Meng F, Ju B, Wang Z, Han R, Zhang Y, Zhang S, et al. Bioinspired polypeptide photonic films with tunable structural color. J Am Chem Soc 2022;144:7610–5.
[280] Du X, Zhang S, Zhou J, Chi H, Sheng Z, Hu Y, et al. Inverse opal torus-shaped photonic microobjects with superior stimulus-responsive properties to their spherical equivalents. Small 2025;21:e2412117.
[281] Chen C, Liu Y, Wang H, Chen G, Wu X, Ren J, et al. Multifunctional chitosan inverse opal particles for wound healing. ACS Nano 2018;12:10493–500.
[282] Shinohara S, Seki T, Sakai T, Yoshida R, Takeoka Y. Photoregulated wormlike motion of a gel. Angew Chem Int Ed 2008;47:9039–43.
[283] Wang JY, Hu YD, Deng RH, Liang RJ, Li WK, Liu SQ, et al. Multiresponsive hydrogel photonic crystal microparticles with inverse-opal structure. Langmuir 2013;29:8825–34.
[284] Cui Q, Ward Muscatello MM, Asher SA. Photonic crystal borax competitive binding carbohydrate sensing motif. Analyst 2009;134:875–80.
[285] Zhang B, Cheng Y, Wang H, Ye B, Shang L, Zhao Y, et al. Multifunctional inverse opal particles for drug delivery and monitoring. Nanoscale 2015;7:10590–4.
[286] Couturier JP, Sutterlin M, Laschewsky A, Hettrich C, Wischerhoff E. Responsive inverse opal hydrogels for the sensing of macromolecules. Angew Chem Int Ed 2015;54:6641–4.
[287] Sun X, Liu L, Zou H, Yao C, Yan Z, Ye B. Intelligent drug delivery microparticles with visual stimuli-responsive structural color changes. Int J Nanomedicine 2020;15:4959–67.
[288] Jurewicz I, King AAK, Shanker R, Large MJ, Smith RJ, Maspero R, et al. Mechanochromic and thermochromic sensors based on graphene infused polymer opals. Adv Funct Mater 2020;30:2002473.
[289] Fu F, Chen Z, Wang H, Liu C, Liu Y, Zhao Y. Graphene hybrid colloidal crystal arrays with photo-controllable structural colors. Nanoscale 2019;11:10846–51.
[290] Wang YT, Zhang DG, Zhang H, Shang LR, Zhao YJ. Responsive photonic alginate hydrogel particles for the quantitative detection of alkaline phosphatase. Npg Asia Mater 2022;14:54.
[291] Pan M, Wang C, Hu Y, Wang X, Pan L, Lin Y, et al. Dual optical information-encrypted/decrypted invisible photonic patterns based on controlled wettability. Adv Opt Mater 2021;10:2101268.
[292] Zhou CT, Qi Y, Zhang SF, Niu WB, Wu SL, Ma W, et al. Fast water-response double-inverse opal films with brilliant structural color. Chem Eng J 2021;426:131213.
[293] Kim JH, Moon JH, Lee SY, Park J. Biologically inspired humidity sensor based on three-dimensional photonic crystals. Appl Phys Lett 2010;97:103701.
[294] Chen Z, Zhang H, Yang S, Wei J. Multiangle patterned photonic films based on CdS and $SiO_2$ nanoparticles for bar code applications. ACS Appl Nano Mater 2021;4:14026–34.
[295] Chen Z, Wu J, Wang Y, Shao C, Chi J, Li Z, et al. Photocontrolled healable structural color hydrogels. Small 2019;15:e1903104.
[296] Wang L, Chen G, Fan L, Chen H, Zhao Y, Lu L, et al. Biomimetic enzyme cascade structural color hydrogel microparticles for diabetic wound healing management. Adv Sci (Weinh) 2023;10:e2206900.
[297] Wang H, Zhao Z, Liu Y, Shao C, Bian F, Zhao Y. Biomimetic enzyme cascade reaction system in microfluidic electrospray microcapsules. Sci Adv 2018;4:eaat2816.
[298] Cui J, Zhu W, Gao N, Li J, Yang H, Jiang Y, et al. Inverse opal spheres based on polyionic liquids as functional microspheres with tunable optical properties and molecular recognition capabilities. Angew Chem Int Ed 2014;53:3844–8.
[299] Zhang W, Li Y, Liang Y, Gao N, Liu C, Wang S, et al. Poly(ionic liquid)s as a distinct receptor material to create a highly-integrated sensing platform for efficiently identifying numerous saccharides. Chem Sci 2019;10:6617–23.
[300] Liu C, Zhang W, Zhao Y, Lin C, Zhou K, Li Y, et al. Urea-functionalized poly(ionic liquid) photonic spheres for visual identification of explosives with a smartphone. ACS Appl Mater Interfaces 2019;11:21078–85.
[301] Zhou K, Tian T, Wang C, Zhao H, Gao N, Yin H, et al. Multifunctional integrated compartment systems for incompatible cascade reactions based on onion-like photonic spheres. J Am Chem Soc 2020;142:20605–15.
[302] Brijitta J, Schurtenberger P. Responsive hydrogel colloids: structure, interactions, phase behavior, and equilibrium and nonequilibrium transitions of microgel dispersions. Curr Opin Colloid Interface Sci 2019;40:87–103.
[303] Scotti A, Gasser U, Herman ES, Han J, Menzel A, Lyon LA, et al. Phase behavior of binary and polydisperse suspensions of compressible microgels controlled by selective particle deswelling. Phys Rev E 2017;96:032609.
[304] Park SH, Park H, Hur K, Lee S. Design of DNA origami diamond photonic crystals. ACS Appl Bio Mater 2020;3:747–56.
[305] Posnjak G, Yin X, Butler P, Bienek O, Dass M, Lee S, et al. Diamond-lattice photonic crystals assembled from DNA origami. Science 2024;384:781–5.
[306] Liu H, Matthies M, Russo J, Rovigatti L, Narayanan RP, Diep T, et al. Inverse design of a pyrochlore lattice of DNA origami through model-driven experiments. Science 2024;384:776–81.
[307] Li Y, Zhou W, Tanriover I, Hadibrata W, Partridge BE, Lin H, et al. Open-channel metal particle superlattices. Nature 2022;611:695–701.
[308] Zhou S, Li J, Lu J, Liu H, Kim JY, Kim A, et al. Chiral assemblies of pinwheel superlattices on substrates. Nature 2022;612:259–65.
[309] Lee S. Colloidal superlattices for unnaturally high-index metamaterials at broadband optical frequencies. Opt Express 2015;23:28170–81.
[310] Kim K, Yoo S, Huh J-H, Park QH, Lee S. Limitations and opportunities for optical metafluids to achieve an unnatural refractive index. ACS Photonics 2017;4:2298–311.
[311] Kim S, Zheng CY, Schatz GC, Aydin K, Kim KH, Mirkin CA. Mie-resonant three-dimensional metacrystals. Nano Lett 2020;20:8096–101.
[312] Chen M, Zhang YP, Jia SY, Zhou L, Guan Y, Zhang YJ. Photonic crystals with a reversibly inducible and erasable defect state using external stimuli. Angew Chem Int Ed 2015;54:9257–61.
[313] Immink JN, Bergman MJ, Maris JJE, Stenhammar J, Schurtenberger P. Crystal-to-crystal transitions in binary mixtures of soft colloids. ACS Nano 2020;14:14861–8.
[314] Li QJ, Deng Y, Dai SJ, Wu YX, Li W, Zhuo SQ, et al. Microfluidic assembly synthesis of magnetic $TiO_2$@$SiO_2$ hybrid photonic crystal microspheres for photocatalytic degradation of deoxynivalenol. J Inorg Organomet Polym 2021;31:2360–7.

[315] Sakai T, Yoshida R. Self-oscillating nanogel particles. Langmuir 2004;20:1036–8.
[316] Zhou L, He H, Tao M, Muhammad Y, Gong W, Liu Q, et al. Chloroplast-inspired microenvironment engineering of inverse opal structured IO-$TiO_2$/Chl/IL for highly efficient $CO_2$ photolytic reduction to $CH_4$. Chem Eng J 2023;464:142685.
[317] Heuser T, Merindol R, Loescher S, Klaus A, Walther A. Photonic devices out of equilibrium: transient memory, signal propagation, and sensing. Adv Mater 2017; 29:1606842.
[318] Takeoka Y, Watanabe M, Yoshida R. Self-sustaining peristaltic motion on the surface of a porous gel. J Am Chem Soc 2003;125:13320–1.
[319] Wang T, Wu Y, Shi L, Hu X, Chen M, Wu L. A structural polymer for highly efficient all-day passive radiative cooling. Nat Commun 2021;12:365.
[320] Yu XQ, Wu J, Wang JW, Zhang NX, Qing RK, Li GX, et al. Facile access to high solid content monodispersed microspheres via dual-component surfactants regulation toward high-performance colloidal photonic crystals. Adv Mater 2024; 36:e2312879.
[321] Kim HH, Im E, Lee S. Colloidal photonic assemblies for colorful radiative cooling. Langmuir 2020;36:6589–96.
[322] Kim HH, Kwak S, Lee J, Im E, Raman AP, Lee S. Structured fluids as colorful paintable radiative coolers. Cell Rep Phys Sci 2024;5:102068.
[323] Kim HH, Cho Y, Baek D, Rho KH, Park SH, Lee S. Parallelization of microfluidic droplet junctions for ultraviscous fluids. Small 2022;18:2205001.
[324] Arriaga LR, Amstad E, Weitz DA. Scalable single-step microfluidic production of single-core double emulsions with ultra-thin shells. Lab Chip 2015;15:3335–40.
[325] Perez-Mercader J, Hu Y. Anti-clogging microfluidic multichannel device. Google Patents. 2020.
[326] Abate AR, Weitz DA. Faster multiple emulsification with drop splitting. Lab Chip 2011;11:1911–5.
[327] Gelin P, Bihi I, Ziemecka I, Thienpont B, Christiaens J, Hellemans K, et al. Microfluidic device for high-throughput production of monodisperse droplets. Ind Eng Chem Res 2020;59:12784–91.
[328] Eberhardt A, Bošković D, Loebbecke S, Panić S, Winter Y. Customized design of scalable microfluidic droplet generators using step-emulsification methods. Chem Eng Technol 2019;42:2195–201.
[329] Mashiyama S, Hemmi R, Sato T, Kato A, Taniguchi T, Yamada M. Pushing the limits of microfluidic droplet production efficiency: engineering microchannels with seamlessly implemented 3D inverse colloidal crystals. Lab Chip 2024;24: 171–81.